Master thesis

Re-design of a polymer oil wiper for reciprocating compressors

by

Bernhard Radler, BSc.

Montanuniversitaet Leoben
Department of Polymer Engineering and Science

Chair of Polymer Processing
Head of the Chair: Univ.-Prof. Dipl.-Ing. Dr.mont. Clemens Holzer

Supervision: assoz.Prof. Dr. Thomas Lucyshyn

May 2017

Affidavit

I declare in lieu of oath, that I wrote this thesis and performed the associated research myself, using only literature cited in this volume.

Eidesstattliche Erklärung

Ich erkläre an Eides statt, dass ich diese Arbeit selbstständig verfasst, andere als die angegebenen Quellen und Hilfsmittel nicht benutzt und mich auch sonst keiner unerlaubten Hilfsmittel bedient habe.

Date	Bernhard Radler, BSc.

Acknowledgement

This thesis was developed in close cooperation with the R&D team of Hoerbiger Ventilwerke GmbH. I want to express my sincere gratitude to Dr. Marian Janko for his support throughout the whole time of us working together. Also DI Andreas Kaufmann, Martin Lagler and Alexander Jandl provided valuable input for the present thesis. My sincere thanks also go to assoz.Prof. Thomas Lucyshyn and Prof. Clemens Holzer from the Chair of Polymer Processing at Montanuniversitaet Leoben for enabling this thesis.
Last but not the least, I would like to thank my loved ones for constant support and encouragement!

Abstract

The present thesis discusses the potential of re-designing an existing oil wiper ring, which is a vital part of any reciprocating compressor. Its function is the prevention of oil loss from the crankcase of a compressor and thereby causing high operational costs and pollution of the compressed gas. Furthermore, the product is designed to compensate occurring wear to enhance its lifetime.
The project was initialised by field reports of performance problems particularly in application of compressors in the PET blow moulding industry. These compressors are characterised by high rotational speeds and small spaces between crankcase and cylinder. An additional reason for a product re-design are the high manufacturing costs.
The first part of the work was an investigation of the product requirements. To start a focused redesign of the product it was necessary to evaluate the performance of the current product. Therefore an application like test scenario was designed. It enables to measure the oil wiping performance of the oil wiper ring during its operation in a reciprocating compressor.
The current product consists of a polymer ring with four parts, a metallic garter spring and a metallic lug spring. One part of the product optimisation was found in replacing the metallic lug spring by a polymer spring to reduce the high manufacturing costs and to prevent damage of the piston rod surface. With prototypes of this concept a thorough evaluation of the mechanical behaviour was done. The result is that a replacement with the selected material and design is feasible but further investigation is necessary to gain a marketable product.
The geometry of the current polymer ring design bears the potential of reducing the production costs and improving the oil wiping performance. Several concepts addressing these problems are shown. The new ring designs follow different approaches like reducing the number of single parts (up to one-body uncut ring), enhancing the number of wiping edges or different approaches of wear compensation. To determine the best concept further evaluation of the oil wiping performance is necessary.

Kurzfassung

Die vorliegende Arbeit behandelt das Potential einer Produktverbesserung eines Ölabstreifrings, eines wichtigen Bauteils in Hubkolbenverdichtern. Seine Funktion ist die Vermeidung von Ölverlust aus dem Kurbelkasten und einer Verschmutzung des zu verdichtenden Gases. Desweiteren erlaubt das Design des Ringes einen Ausgleich von auftretendem Verschleiß, um die Lebensdauer zu verlängern.
Das Projekt wurde initialisiert durch Berichte von Anwendungsproblemen vor allem im Einsatz in Kompressoren der PET-Blasform Industrie. Diese Kompressoren sind charakterisiert durch hohe Drehzahlen und kleine Bauräume zwischen Kurbelkasten und Zylinder. Ein weiterer Grund für die Neukonstruktion des Produkts sind die hohen Herstellkosten.
Der erste Teil der Arbeit bestand aus der Untersuchung der Produktanforderungen. Um eine gezielte Verbesserung des Produktes durchzuführen, war es nötig die Leistungsfähigkeit des bestehenden Produktes zu evaluieren. Dazu wurde ein anwendungsnahes Testszenario erstellt. Es ermöglicht die Ölverlustmessung während des Einsatzes in einem Hubkolbenverdichter.
Das derzeitige Produkt besteht aus einem Kunststoffring mit vier Teilen, einer Metallfeder am Umfang, sowie einer axialen Metallfeder. Ein Teil der Produktoptimierung bestand aus dem Ersatz der metallischen Axialfeder durch eine Kunststofffeder, um die hohen Herstellkosten zu reduzieren und Schäden an der Kolbenstangenoberfläche zu verhindern. Das mechanische Verhalten dieses Konzeptes wurde genau charakterisiert. Es wurde festgestellt, dass das Konzept mit dem ausgewählten Material sowie der gewählten Konstruktion machbar ist. Dennoch ist weitere Entwicklungsarbeit notwendig, um das Konzept einer Kunststofffeder zur Marktreife zu bringen.
Die Form des bestehenden Produktes bietet Potential um die Produktionskosten zu senken und die Ölabstreifleistung zu verbessern. Mehrere Konzepte zur Verbesserung dieser Probleme werden vorgestellt. Diese verfolgten mehrere Ansätze wie die Reduzierung der Teileanzahl (bis zu einteiligem Ring), die Erhöhung der Anzahl von Ölabstreifkanten oder verschiedene Verschleißausgleichsmechanismen. Um das beste Konzept zu eruieren sind weitere Messungen zur Ölabstreifleistung notwendig.

Contents

1 Introduction

The constant improvement of the product portfolio is essential for companies to either gain new markets or defend their position within the market. Therefore a lot of effort is taken to develop new products or improve existing products. The present thesis was developed together with Hoerbiger Ventilwerke GmbH, Vienna (HOERBIGER) as a feasibility study. Its purpose is to present ideas and concepts to improve an existing product. To focus all activities of the research and development activities, it is necessary to thoroughly understand the underlying problem. The first chapter of the thesis outlines the current product and its application in reciprocating compressors.

1.1 Principle of operation of reciprocating compressors

Reciprocating compressors are widely used in the oil and gas processing industry. They have a similar structure according to Fig. 1.1, but vary in terms of capacity, medium to be compressed and design details. The drive is usually an electric or gas motor, which rotates the crank shaft. The rotation movement is translated via a connecting rod and the cross head to the axial movement of the piston rod. This primary components are separated. The crankcase contains crankshaft, connecting rod and crosshead. The piston rod (see Fig. 1.2) reaches into the crankcase and transmits the energy to the piston, which is placed in the cylinder. In the cylinder the gas is either sucked into the expanding volume or compressed and exhausted. The space between cylinder and crankcase is used for packings of rings which fulfil different functions. The rings next to the crankcase should ensure that the oil necessary for lubrication stays within the crankcase. The rings next to the cylinder are installed in a so-called pressure packing and seal the pressure from the cylinder.

The product in focus is a so-called oil wiper ring. These rings are the first after the crankcase and wipe the lubrication oil from the piston rod. Usually two wiper rings are placed in a wiper packing attached to the crankcase (see Fig. 1.3). Pressure rings are added in the second cup, to prevent the entering of possible gas pressure impulses to the crankcase which could cause explosions.

The main function is to prevent oil loss from the crankcase. The oil loss causes two main problems. The first is an economic problem for operators of reciprocating compressors. The costs for refilling the lubrication oil can be up to several thousands of Euros per year per compressor. The other problem is the pollution of the compressed gas. It has to be cleaned with additional methods (like oil separators) if an oil free gas is demanded (e.g. for the production of food and beverage packaging).

The functions of the oil wiper ring can be defined as:

Oil wiping The lubrication system within the crankcase spreads the lubricating oil over all moving parts via several attached injectors. This ensures constant lubrication of the crankshaft and crosshead bearings. As a result the oil also wets the piston rod. The oil wiper ring forms a geometric barrier on the surface of the piston rod. The function of this barrier is to wipe off the oil from the rod. The oil stays at the crankcase side of the wiper.

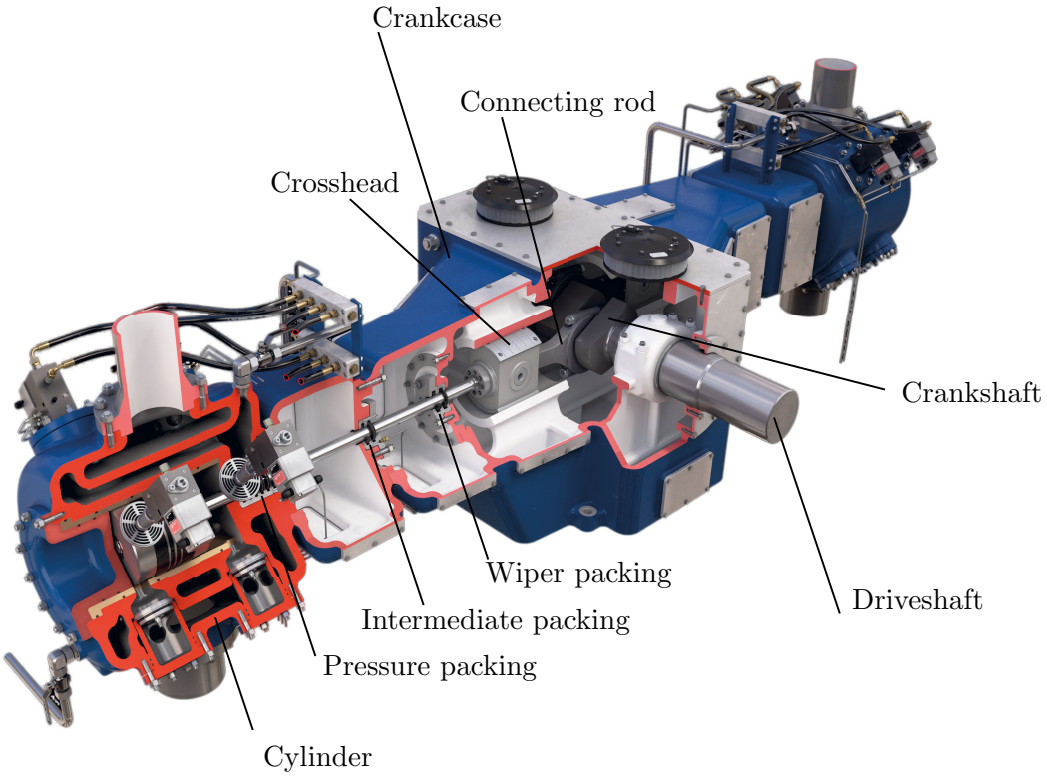

Figure 1.1: Typical structure of a reciprocating compressor [9]

Wear compensation The geometric barrier inhibits contact between the surface of the rod and the oil wiper ring. This contact is supported by a contact pressure between those surfaces. The ring is pressed onto the surface of the rod by a prestressed garter spring. The reciprocating movement of the rod in combination with the contact pressure leads to a significant amount of wear on the oil wiper's rod faced surface. To maintain the contact of the wiper surface on the rod, the wear is compensated by readjusting of the inner diameter of the contact surface.

Radial movement compensation The rod is on one side supported in the crosshead, on the other side in the piston. Both supports do not suppress radial movement of the piston rod, the rod can float up to 1 mm (depending on compressor size) from its initial position. Thus the oil wiper ring has to float within the cup to compensate these movements without generating a leak path for the oil. This function is generated by sufficient space between the outer diameter of the oil wiper ring an the inner diameter of the oil wiper cup.

The wiper packing has a vent hole which is connected to the crankcase. Therefore oil, which is gathered in the wiper cup, can flow back into the crankcase.

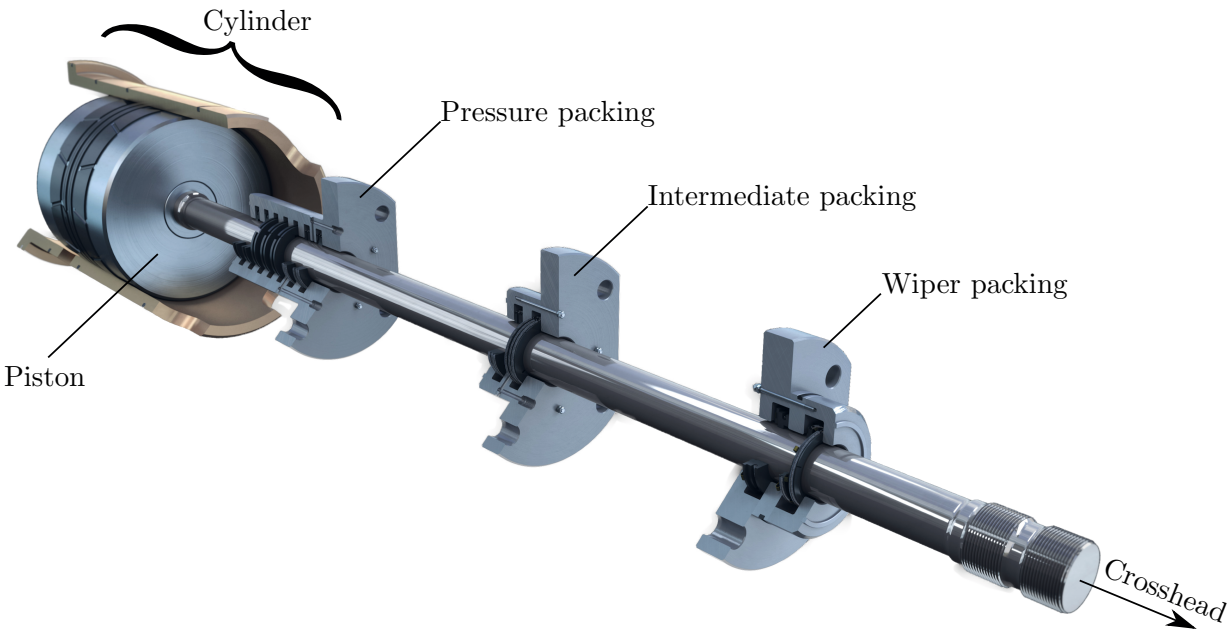

Figure 1.2: Compressor rod with packings [9]

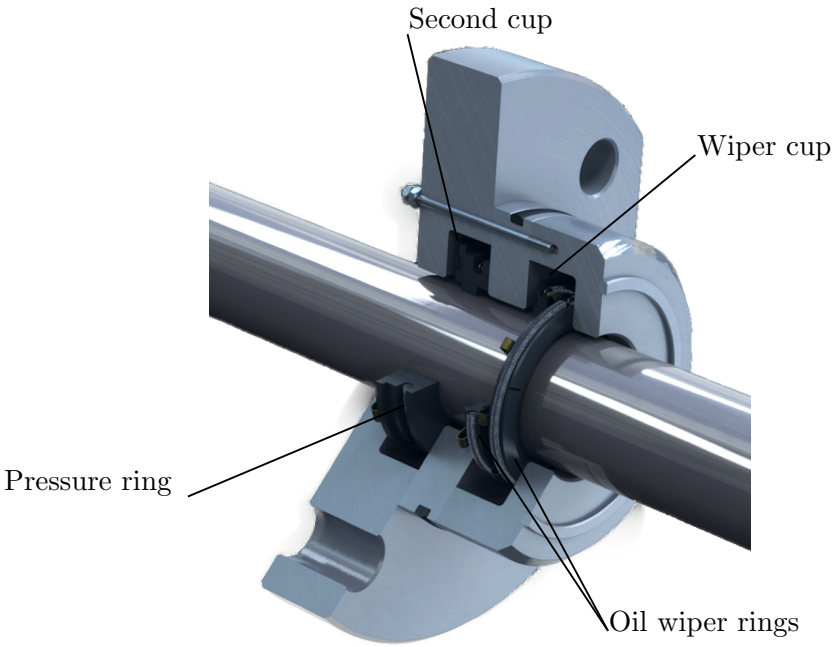

Figure 1.3: Detail of a wiper packing with the wiper cup, containing the wiper packing [9]

1.2 Current situation

The present solution of HOERBIGER is the OFD wiper (Oil film dynamic, see Fig. 1.4). This polymeric wiper ring design consists of four parts made of polytetrafluoroethylene (PTFE), a metallic garter spring for radial contact pressure and a metallic lug spring for axial contact pressure. The used PTFE is a special material for tribological applications and is highly filled with additives such as glass fibres and graphite. The wiper ring consists of two inner ring segments and two cover ring segments. Each pair of segments is separated by a defined gap. This space allows to shrink the inner diameter and therefore compensate the wear of the wiping surface. The four PTFE parts are manufactured of

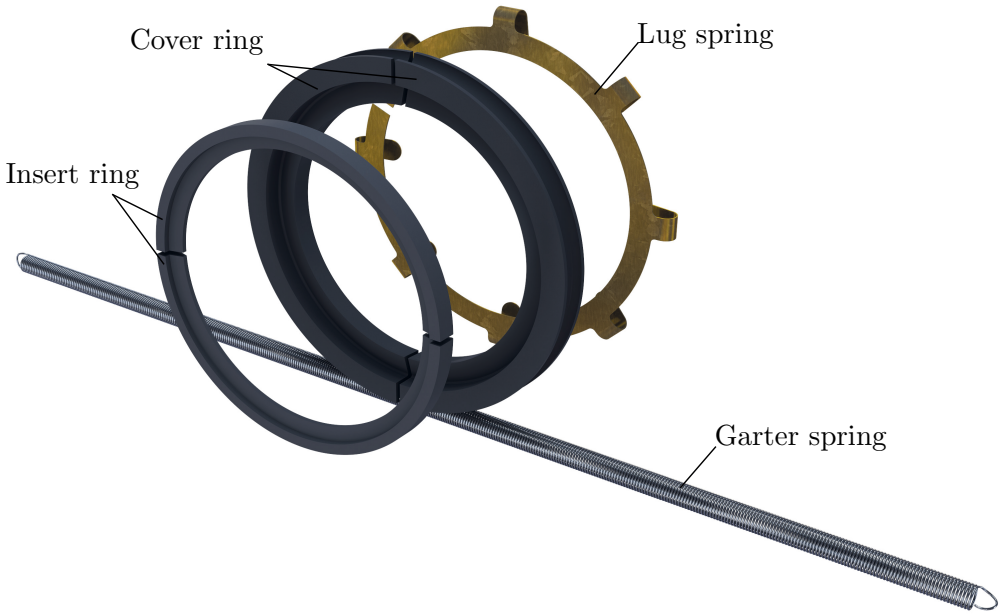

Figure 1.4: Structure of the OFD wiper assembly showing the manufacturing components

cylindrical semi-finished parts. First the cover ring and the insert ring are produced on a CNC lathe. Then the insert ring is placed in the cover ring and the wiping geometry is turned in one go for both parts. Afterwards the two rings are cut in half to generate the gap for the wear compensation. The four parts are then assembled with the cutting sides of the inner and outer pair of rings with a 90° offset. A detailed drawing is shown in Appendix, Sec. 7.1. The metallic lug spring is laser cut out of a flat sheet metal and bent into the final shape. A heat treatment is appended after the manufacturing. The garter spring is fabricated of an endless tube, which is cut to size and provided with spring eyes at both ends.

Economic situation

The complex manufacturing process results in high costs per piece. The cost structure is shown in Tab. 1.1. The listed fixed costs inhibit the set-up costs. The variable costs inhibit the material costs (including material overhead costs), machining costs and personnel costs. The production costs are highly depending on the batch size, but even at a batch size of 100 pieces the costs are more than € 30. This results in the claim of an effective reduction of manufacturing costs.

Table 1.1: Cost calculation of OFD for 1.25" rod diameter (according to [10])

	Batch Size	1	5	10	50	100
Wiper ring	Fix / pc.	€ 20.07	€ 4.01	€ 2.01	€ 0.40	€ 0.20
	Var. / pc.	€ 25.74	€ 25.74	€ 25.74	€ 25.74	€ 25.74
		€ 45.81	**€ 29.76**	**€ 27.75**	**€ 26.14**	**€ 25.94**
Lug spring	Fix / pc.	€ 138.78	€ 27.76	€ 13.88	€ 2.78	€ 1.39
	Var. / pc.	€ 9.37	€ 7.59	€ 6.10	€ 4.91	€ 4.76
		€ 148.15	**€ 35.34**	**€ 19.98**	**€ 7.68**	**€ 6.15**
Garter spring	Fix / pc.	€ 3.48	€ 0.70	€ 0.35	€ 0.07	€ 0.03
	Var. / pc.	€ 0.52	€ 0.52	€ 0.52	€ 0.52	€ 0.52
		€ 4.00	**€ 1.22**	**€ 0.87**	**€ 0.59**	**€ 0.55**
Complete wiper/pc.		**€ 197.96**	**€ 66.32**	**€ 48.59**	**€ 34.42**	**€ 32.64**

Technical situation

Compressors are distinguished by aspects like compressed medium and capacity. With this, many requirements concerning the oil wiper vary (e.g. rod diameter), but have to be met with the same product. The current oil wiper ring has known performance issues (high oil loss) in applications in the compressed natural gas (CNG) and PET (polyethylene terephthalate) blow moulding industry. Typical characteristics for these compressors are a small form factor (pressure packing directly attached to the wiper packing), high rotational speed and a high overall temperature level. For a straight forward development process it is necessary to determine these aspects as exactly as possible. Therefore a product requirements document [10] was generated, containing all information about the product. A summary of the most important technical requirements is shown in Tab. 1.2.

Table 1.2: List of most important requirements for oil wiper rings according to [10]

Requirement	**Specification**
Rod diameter	from 1" to 2.25"
Rod displacement	up to 5"
Rotational speed	up to 1800 rpm
Mounting situations	various
Surrounding conditions	Short time rod temperature: up to 300 °C Long time rod temperature: 60 °C to 180 °C H_2S - sour gas atmosphere Mineral oil ISO 100-250 class
Lifetime	two years, up to three years

For this project it was specified to maintain the used material of the oil wiper ring. It is a custom-made PTFE compound with various fillers. The material is tailor made for tribological applications and also used for pressure rings. A general overview of its properties is shown in the following section.

1.3 Polytetrafluoroethylene (PTFE)

PTFE is a thermoplastic polymer with a linear, nearly un-branched molecular chain with the monomeric unit shown in Fig. 1.5. The high bonding energy of fluorine and carbon leads to very unique properties. It is the polymer with the best chemical resistance. Only dilutions of alkali metals can separate the bonding between fluorine and carbon (see [5]). Another unique property is the very low friction coefficient, especially with PTFE itself as friction combination.

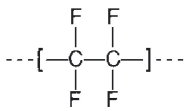

Figure 1.5: Monomeric unit of PTFE (see [4])

Polymerisation of PTFE

PTFE is radically polymerised from tetrafluoroethylene ($CF_2 = CF_2$). It is, besides the polymerisation of ethylene, the second industrially used pressure polymerisation. The polymerisation mechanism according to [5] takes place as follows:

The initiator is formed by degradation of a persulfate under heat:

$$K_2S_2O_8 + heat \rightarrow 2SO_4^{\bullet} + 2K^+$$

The persulfate fragments form new radicals with the tetrafluoroethylene:

$$SO_4^{\bullet} + F_2C = CF_2 \rightarrow SO_4(F_2C - CF_2)^{\bullet}$$

The chain propagation takes place by adding further monomers to the radical:

$$SO_4(F_2C - CF_2)^{\bullet} + n\ F_2C = CF_2 \rightarrow SO_4(F_2C - CF_2)_n - (F_2C - CF_2)^{\bullet}$$

As the polymerisation is done in an aqueous suspension the free radicals undergo a hydrolysis, replacing the sulfate end group:

$$SO_4(F_2C - CF_2)_n - (F_2C - CF_2)^{\bullet} + H_2O \rightarrow HO(F_2C - CF_2)_n - (F_2C - CF_2)^{\bullet} + H^+ + HSO_4$$

$$HO(F_2C - CF_2)_n - (F_2C - CF_2)^{\bullet} + H_2O \rightarrow COOHCF_2(F_2C - CF_2)_n^{\bullet} + 2HF$$

The last step is the termination by recombination of two radicals:

$$COOHCF_2(F_2C - CF_2)_n^{\bullet} + COOHCF_2(F_2C - CF_2)_m^{\bullet} \rightarrow COOH - (F_2C - CF_2)_{n+m} - COOH$$

The fluorine atoms are effectively shielding the carbon chain of the macromolecules. Therefore a combination of free radicals with a saturated macromolecule is not favoured. The result is a polymer chain with no detectable branches.

Fillers of PTFE

Contrary to other polymers PTFE is not supported with any additives enhancing chemical properties. Due to the low mechanical properties it is, according to the specific application, compounded with various fillers. They enhance the mechanical performance (Young's modulus, tensile strength, creep behaviour) and thermal conductivity. The fillers shown in Tab. 1.3 are commonly used.

Table 1.3: Common fillers for PTFE (see [4] and [3])

Filler	**Enhancement**
Graphite	Abrasion resistance and self lubrication properties
Bronze	Creep strength, thermal conductivity and abrasion resistance
MoS_2	Lubrication properties
Glass fibres	Creep strength and Young's modulus

The currently used material will be maintained and is a compound of PTFE with graphite and glass fibres as fillers.

The schedule of this product re-design is to evaluate the performance of the current product, as a basis of a focused improvement. Furthermore, the metallic and expensive lug spring should be replaced. The final step is to develop new wiper ring designs and compare their performance with the current product.

2 Evaluation of the current product

A vital part of every product development process is the exact knowledge about the performance of the current product. The re-design was, among other things, initialised by reports from performance issues in field applications. Those were gathered under varying circumstances. Therefore it was necessary to investigate the performance on a known and repeatable basis. The main indicator of the product performance is the oil loss from the crankcase during operation of the oil wiper ring on a compressor.

2.1 Oil loss measurement on multi purpose test compressor (MPTC)

A simulation of the product application was not possible with off-the-shelf test equipment. HOERBIGER operates an enhanced test compressor with lots of possibilities for modifications. Therefore a test set-up, attached to this compressor was developed. The test set-up allowed continuous measurement of the oil loss along with several influencing environmental conditions during operation. The concept is based on [18] and was further developed. The technical specifications of the MPTC are shown in Tab. 2.1.

Table 2.1: Specifications of the multi purpose test compressor

Specification	**Value**
Drive unit	Ariel JGM/2
Speed	Variable, up to 1500 rpm
Rod diameter	28.58 mm (1.25 ”)
Stroke	89 mm
Capacity	90 kW
Compressed gases	Air, N_2, He

The measurement set-up consisted of a measurement cup, directly attached to the crankcase of the drive unit of the compressor (see Fig. 2.1). At the MPTC a distance piece is placed between crankcase and cylinder. This means the wiper packing and the pressure packing are separated. Compressors used in the PET blow moulding industry usually do not have this distance piece, the wiper packing and pressure packing are attached to each other. The direct attachment of the pressure packing was simulated via a section of high pressure on the rod. The pressure was sealed with two balanced cup design rings (BCD rings) at each end. This allowed to vary the cylinder pressure, which would not be possible with a directly attached pressure packing. Between wiper cup and pressure cup a side-loaded BCD ring (SL BCD ring) was placed to prevent pressure waves from entering the crankcase. The addition of this ring is very common for the design of wiper packings. During the oil loss measurements no gas was compressed. The piston was installed to support the piston rod in the cylinder.

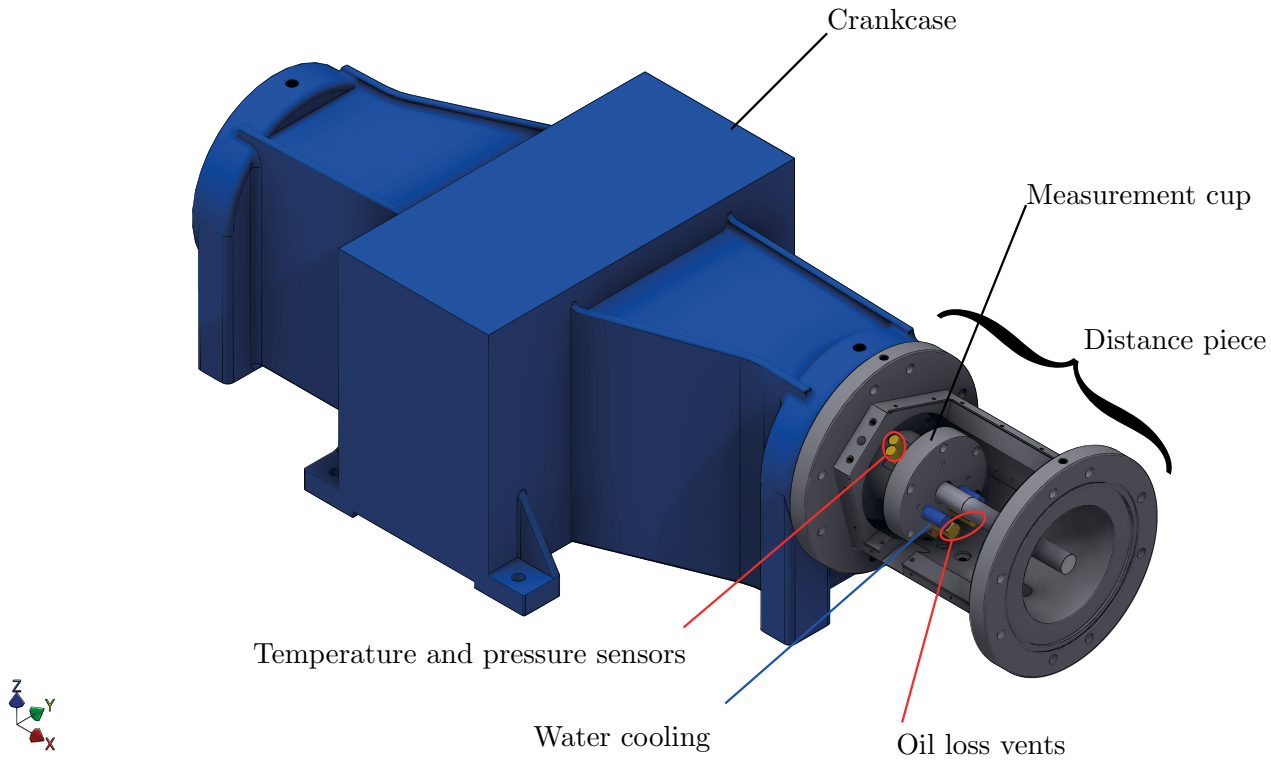

Figure 2.1: Measurement set-up attached to the crankcase of the test compressor

Oil loss measurement

The oil loss was gathered and measured at three locations. The first location was the oil wiper cup. The oil gathered in this cup has flown through the first oil wiper ring, but was wiped off by the second oil wiper ring. It is guided back into the crankcase in normal compressors. The second location was the SL BCD cup. Oil lost in this cup is indicating an oil flow through the wiper cup. The third location was in the pressure section. Oil gathered in this section is polluting the compressed gas. The three locations are shown in Fig. 2.2. The oil loss in the oil wiper cup and SL BCD cup was guided via vent pipes into two containers. A pressure transducer at the bottom of the container measured the amount of oil by the increasing hydrostatic pressure on it. It was calibrated by filling the cup with a known amount of oil to calculate the volumetric amount of oil loss. The oil loss in the pressure section was guided with a vent pipe into a pressure vessel. Here, a hydrostatic pressure measurement was not accurate, because the applied pressure level shifted the measurement to higher absolute values. This would lower the resulting accuracy. Thus the pressure vessel was attached to a weight measuring system and the oil loss was measured by the weight increase of it. The principle of the measurement procedure is also shown in Fig. 2.2. The gathered data was recorded with a Dewetron data-acquisition system (Dewe-801). To limit the amount of acquired data, a trigger started a recording at 5 kHz for 0.3 s every minute. This enabled to observe fast events like shuttling movements and the axial distribution of rod temperature. The other data is averaged over this 0.3 s long period. The evaluation of the data was done in Matlab 2016.

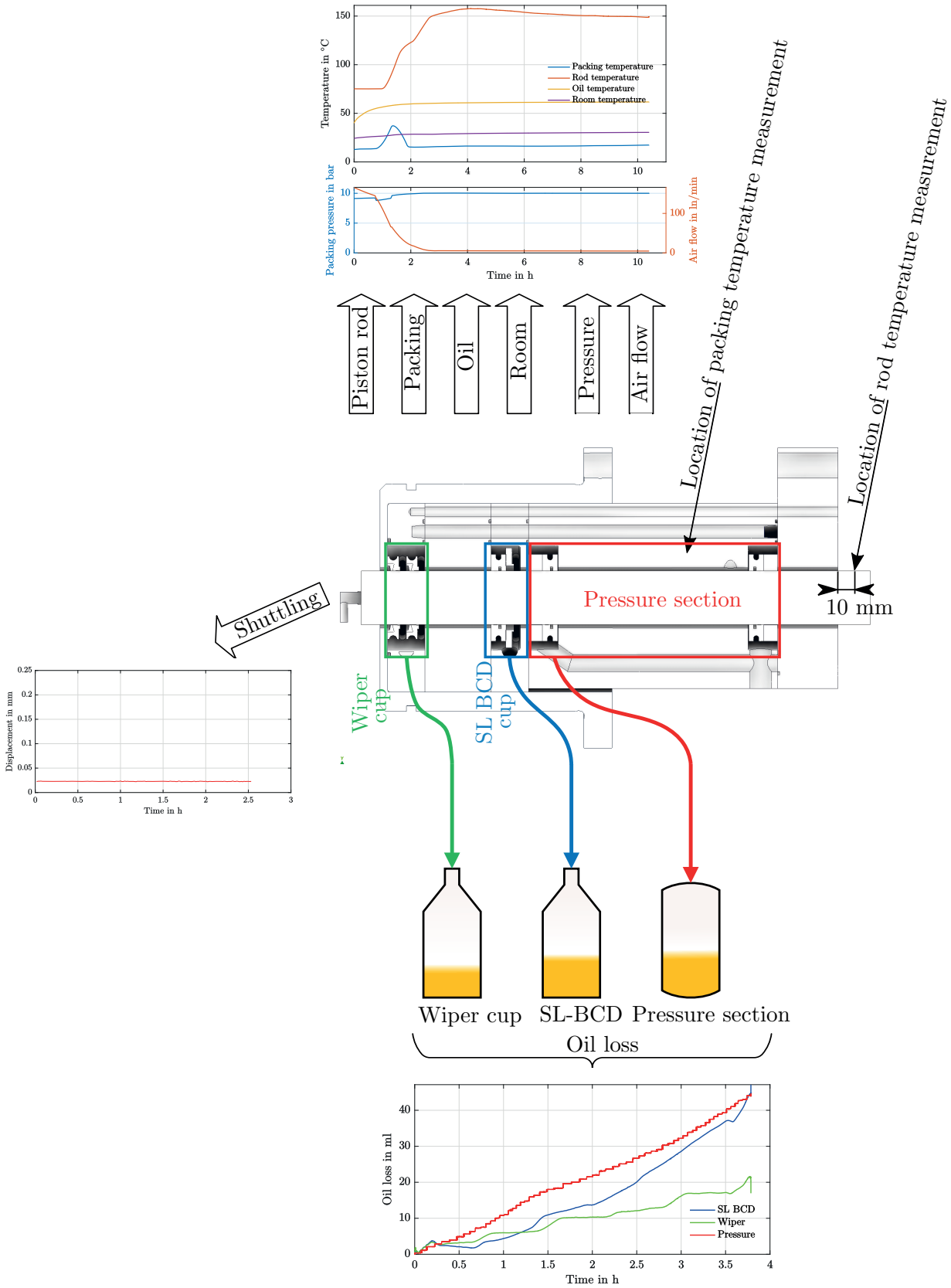

Figure 2.2: Overview of the measurement procedure with the gathered data and configuration of the test packing

Surrounding conditions measurement

The measurement procedure was very sensitive to changes in environmental conditions. The reason for this can be found in the dependency of the oil viscosity on its temperature. Therefore the parameters shown in Tab. 2.2 were measured continuously. To measure the packing, oil and room temperature,

Table 2.2: Surrounding parameters measured during test runs

Parameter	**Detail**
Temperature	Piston rod
	Packing
	Oil
	Room
Pressure	Pressure section
Air flow	Air pressure pipe
Displacement	First wiper ring

three thermocouple sensors (Type K) were used. The packing temperature sensor was placed inside a hole in the test packing, to measure the temperature in the pressure section. The oil temperature sensor was placed on a pipe of the oil circuit of the crank case. The room temperature sensor was placed about 10 cm above the test packing. The piston rod temperature was measured remotely with a Impac140 pyrometer. Due to the high spectral emissivity of metallic surfaces, the temperature measurement range begins at 75 °C. It was focused to a point 10 mm off the test packing. As the rod temperature was varying along the piston rod, the recorded temperature showed a cyclic profile. For the evaluation this temperature profile was averaged to one temperature value for each measurement period. The air pressure in the pressure section was measured at the air supply pipe. Additionally, the air flow was measured with a gas flow-meter (Bronkhorst F115). This enabled to observe the sealing of the pressure section.

Displacement measurement (shuttling)

Besides the oil loss, the sealing function of the oil wiper ring was in the focus of interest. To ensure the sealing function, the wiper has to maintain its axial position. The axial position was measured with a capacitive displacement sensor (shown in Fig. 2.3). It was expected that the displacement of a possible shuttling is very small. Therefore a sensor with a measurement range of 0 µm to 200 µm was used (MICRO-EPSILON capaNCDT CS02). A capacitive displacement sensor requires a conductive sensor target. The oil wiper rings are made of carbon filled PTFE, therefore the requirement was fulfilled. The oil wiper was not an even, plate-shaped target, therefore the displacement measurement was expected to be slightly non-linear. This was accepted because the measurement system had the advantage of a very fast measurement rate. This enabled to detect highly frequent shuttling movements. They were expected to occur with the same frequency as the compressor's drive speed which is up to 25 Hz at 1500 rpm.

This measurement set-up enabled to record the oil loss and therefore oil wiper performance evaluation as a function of compressor speed and applied pressure in the pressure section. The next step was to define the experimental design.

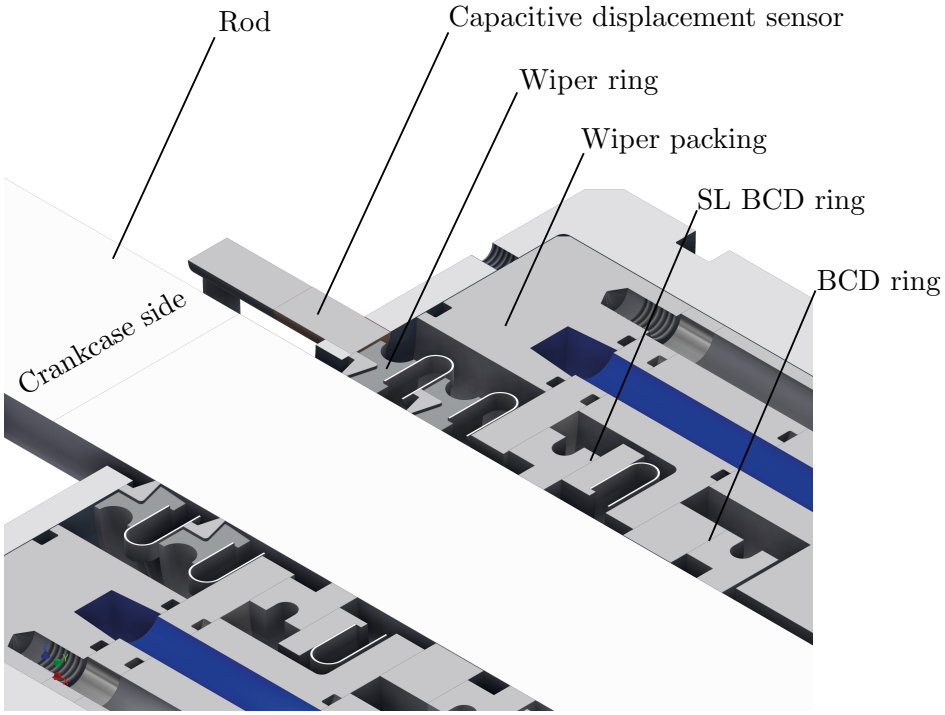

Figure 2.3: Assembly of the capacitive displacement (shuttling) sensor

2.2 Experimental design

As mentioned before the two factors "speed" and "pressure" were variable. To look for any non-linear effects it was desired to vary on three different levels. To execute the evaluation properly it was necessary to determine the levels which are stable during each experiment. The levels of the factor "speed" were defined according to the capability of the compressor. The upper limit of the drive unit was given with 1500 rpm (see Sec. 7.3). The lowest speed relevant for compressors in the PET processing industry is 700 rpm. With equidistant steps between the levels it was easier to analyse the gathered data, therefore the middle level was chosen with 1100 rpm. Those levels were also within the product specification.

To determine the levels of the factor "pressure" it was first necessary to find out the upper limit of the pressure leading to valid results. A high applied pressure on the pressure section leads to high friction between the pressure sealing rings of the section and the piston rod, which was expected to result in a constant heat-up of all parts. This means the viscosity of the oil is continuously changing during the experiment. The results of such a measurement would not be valid, the monitored temperatures should be on a constant level.

2.2.1 Implementation of measurement on MPTC

Before the test set-up was used to determine the performance of the current product, as well as the evaluation of new designs, it was necessary to understand all processes which take place during the measurement.

Start-up phase

The results of the experiment at 10 bar and 1100 rpm showed exemplary various changes of the surrounding conditions during the experiment in Fig. 2.4. At the beginning the two pressure sealing rings of the pressure section did not seal the applied pressure. This resulted in an air flow of 145 ln/min (ln = standard litres) and no increase of the rod temperature. A manual shut-down of the packing cooling for 30 min led to a general temperature increase and after approximately 2.5 h the rings provided a sealing effect. The maximum average rod temperature of 157 °C was reached after 4 h. After the peak the temperature was decreasing again. This may have been caused by the build-up of a transfer-film of the PTFE on the rod surface (see [3]). This mechanism lowers the friction and influences the generated heat and thereby the rod temperature. A stable condition was reached after approximately 8 h, which led to very long measurement times. This start-up process occurred on all measurements with a variatio ɔout 3 h.

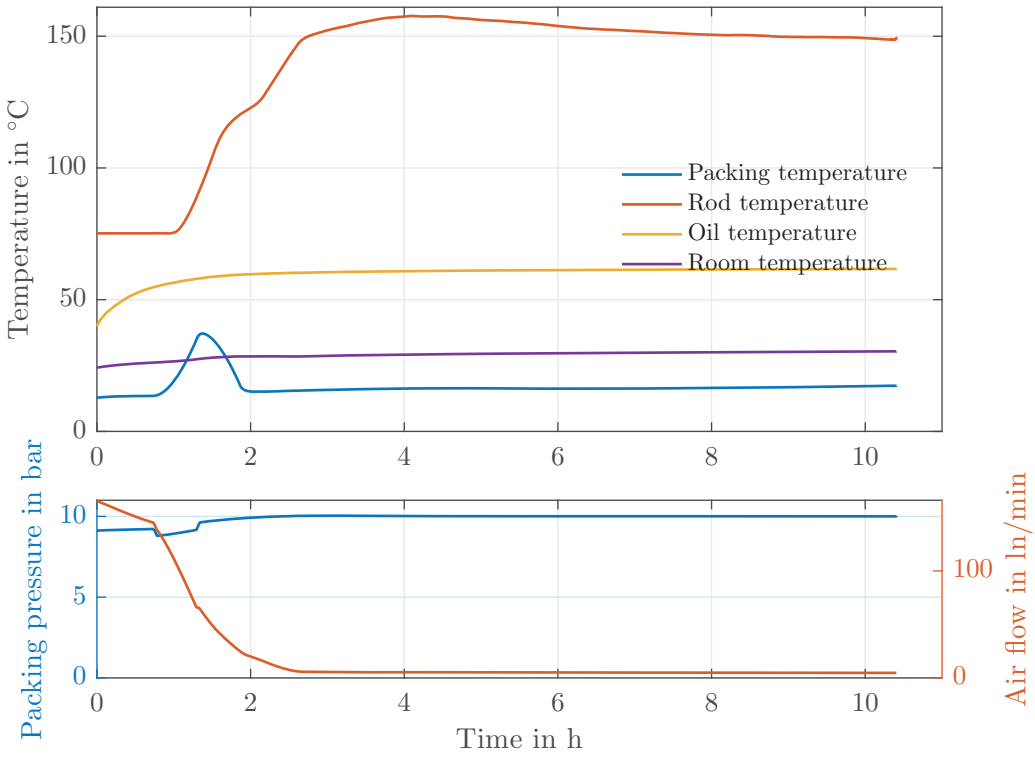

Figure 2.4: Surrounding conditions of experiment at 1100 rpm and 10 bar

Oil loss measurement

In Fig. 2.5 the corresponding oil loss measurement to Fig. 2.4 is shown. The three measurement curves show various characteristics. The hydrostatic oil loss measurements of the oil loss at the wiper cup and the SL BCD cup were fluctuating very strongly. Although there was an overall oil loss detectable, the signal (especially of the SL BCD) was even decreasing during the measurement. This would suggest a back-flow of oil into the compressor, which is not possible. It seemed, that the measurement was overlapped by ambient disturbances. This could have been caused by the sensitivity of the pressure transducers. They have a full scale of 50 mbar, so the change of the ambient air pressure could have been measured. The ambient air pressure depends e.g. on varying weather conditions or the air conditioning system. The weight measurement of the oil loss in the pressure section showed an unstable signal during the first two hours. This corresponds with the unstable surrounding conditions

shown in Fig. 2.4. As the air flow decreased (indicating a sealing effect of the BCD rings at the ends of the pressure section) the oil loss stabilised. This underlined the importance of stable surrounding conditions.
In general, the recorded data showed that the measurement of the oil loss was very sensitive to varying surrounding conditions. To gather reliable data for a valid evaluation of the current product, further investigation of the measurement process itself was necessary.

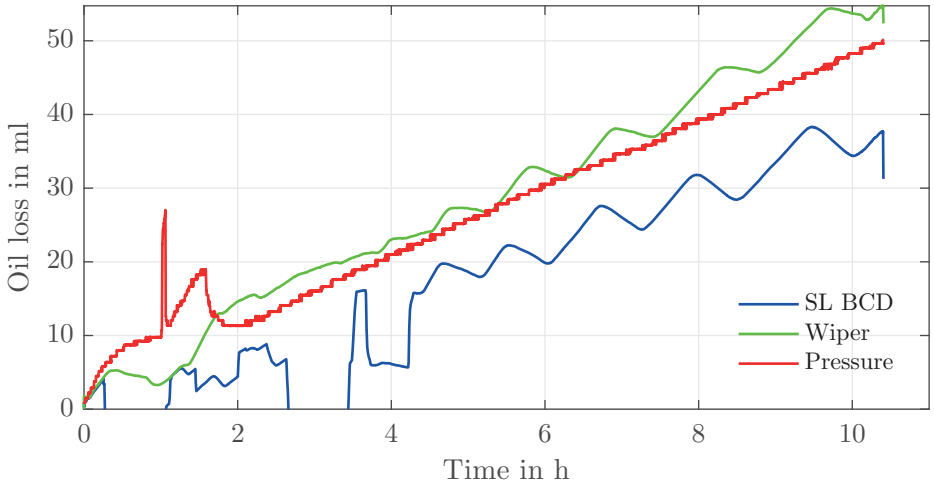

Figure 2.5: Oil loss of experiment at 1100 rpm and 10 bar

Rod temperature

To ensure the function of the polymeric sealing rings at the pressure section (BCD rings), the rod temperature must be below 200 °C. The rod temperature shown in Fig. 2.4 is an average of subsequent cycles. In Fig. 2.6 the axial distribution during six subsequent reciprocating movements is shown. The detail was gathered at the maximum averaged temperature shown in Fig. 2.4 (after 4.05 h). The peak temperature was at 217 °C, which was significantly above the temperature limit of the BCD rings. It was expected that this is the highest temperature of the rod, because the BCD rings used to seal the pressure section generate the most friction. Furthermore, the smallest amount of oil on the rod was at the second ring. As a consequence, a measurement at a static pressure of 10 bar was not possible with the used BCD rings.

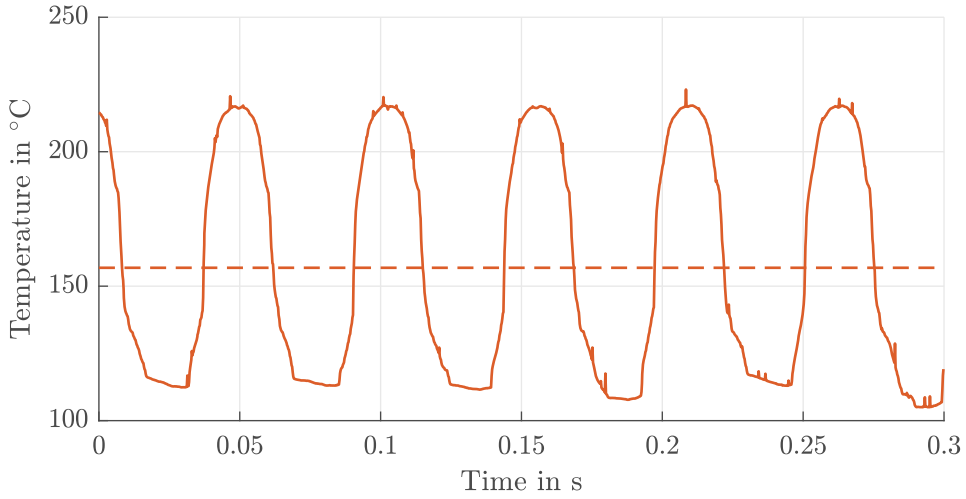

Figure 2.6: Axial distribution of rod temperature during six reciprocating movements and averaged rod temperature (dotted line)

Repeatability of the oil loss measurement

For a reliable evaluation of the product performance and comparison of new designs, it was important to know how accurate the measurement of the performance is. Therefore the same experiment was measured several times. In Fig. 2.7 four measurements at 1500 rpm and 5 bar are shown. In contrast to the measurement previously shown in Fig. 2.5, the oil loss measurement in the wiper and the SL BCD cup were very smooth, because the air conditioning system was turned off. The experiments have been recorded on four subsequent days, starting at the same time in the morning. There have been no modifications of the set-up during the four measurements. At the first measurement the oil loss at the three measured locations was very similar. There seems to be a kink after 3.5 h. At the second measurement the largest amount of oil loss was measured in the pressure section. This means the performance of the oil wiper has worsened, because more oil was let through. At the third measurement the amount of oil measured at the wiper cup and the pressure section were roughly equal, half of this amount was measured at the SL BCD cup. At the fourth measurement the wiper cup and the pressure section again gathered the most oil, in the SL BCD cup almost no oil loss was detected.

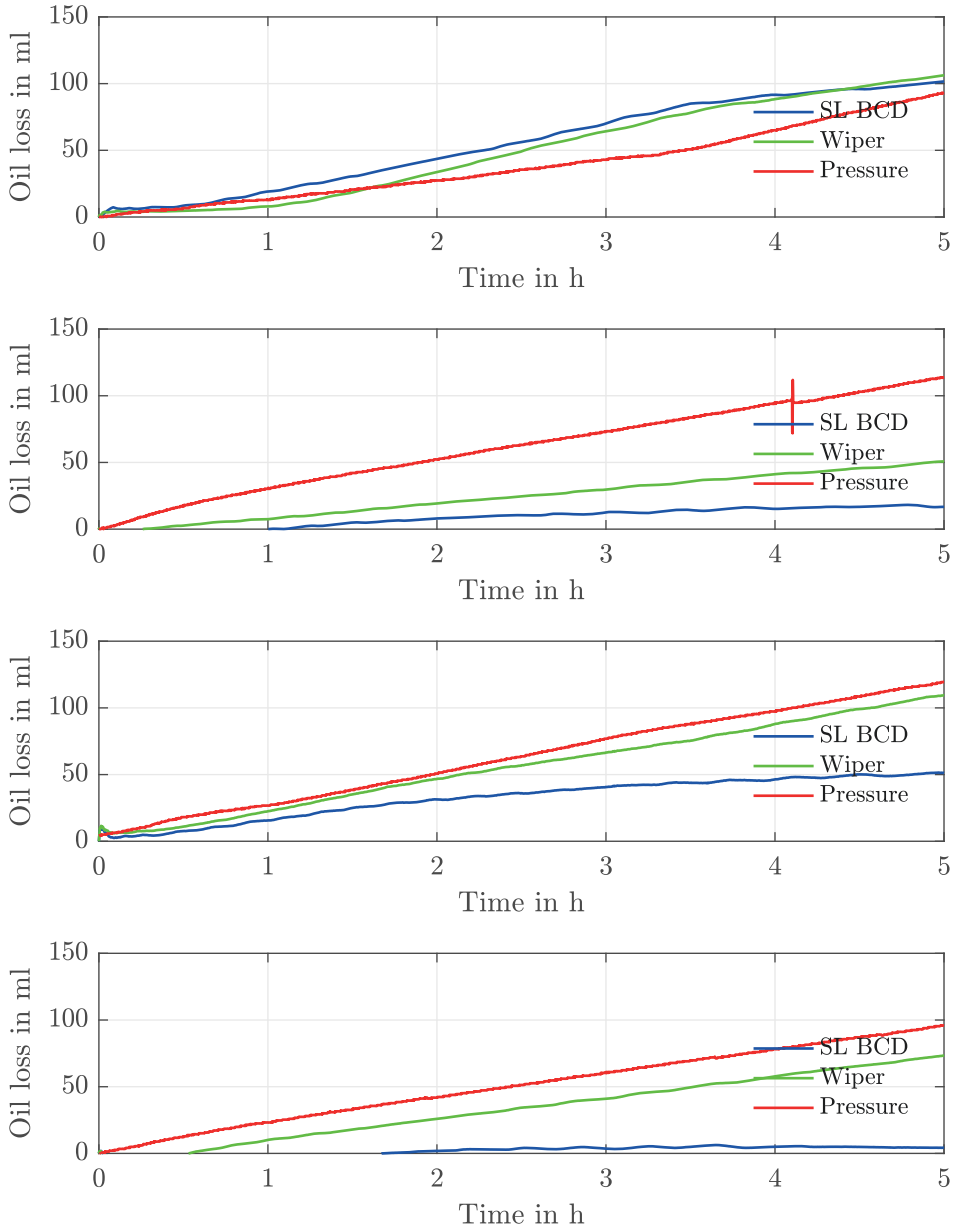

Figure 2.7: Subsequent repeat of four measurements at 1500 rpm and 5 bar

In Tab. 2.3 and Fig. 2.8 the overall oil loss after 5 h (sum of all measured oil losses) is shown. This indicates how much oil left the crankcase. At measurement 1 and 3, as well as 2 and 4, a similar amount of oil was measured. The difference within these measurements is about 50 %, indicating a low repeatability. As the low oil loss and high oil loss appeared irregularly, there was an unidentified influence on the measurement. This was also shown by the performance of the oil wiper (oil loss in wiper section). At the first measurement, the oil loss in the wiper cup was equal to the other two oil losses. At the second measurement, the oil loss in the wiper cup was greatly reduced. At the third it was increased again and at the fourth the amount of oil measured in the wiper cup was the lowest. The oil loss measured at the SL BCD cup was similarly fluctuating but at a higher level of overall oil loss. The oil loss gathered in the pressure section was roughly constant. The varying oil loss measurements did not enable a conclusion of the oil loss mechanism. Under the assumption of a constant oil spill from the crankcase on the piston rod, the fluctuating overall oil loss was raising questions.

Table 2.3: Summarised oil loss of four subsequent measurements at 1500 rpm and 5 bar after 5 h

Measurement	**Oil loss in wiper cup in ml**	**Oil loss in SL BCD cup in ml**	**Oil loss in pressure section in ml**	**Overall oil loss in ml**
1	106	102	93	301
2	51	17	114	182
3	109	52	119	280
4	73	4	96	173

The measured surrounding conditions did not indicate any variations during the four measurements, except the rod temperature. The rod temperature has a strong influence on the oil viscosity (see [8]), therefore a stable rod temperature level is very important. In Fig. 2.9 the average rod temperatures of the four measurements are shown. The temperature increase at the first, second and fourth measurement was similar. The temperature increase at measurement three was delayed, but they were all resulting in a rod temperature of 125 °C to 145 °C. The highest peak temperature of measurement two is 195 °C, which was permissible for the BCD ring. This behaviour was not corresponding with the oil loss measurements and did not explain the oil loss mechanism. It was suspected that there is an interaction between the oil wiper package in the oil wiper cup, the SL BCD cup and the pressure section. The exact mechanism of that interaction was not detectable with the present measurement set-up. As a next step, the complexity of the measurement procedure was reduced.

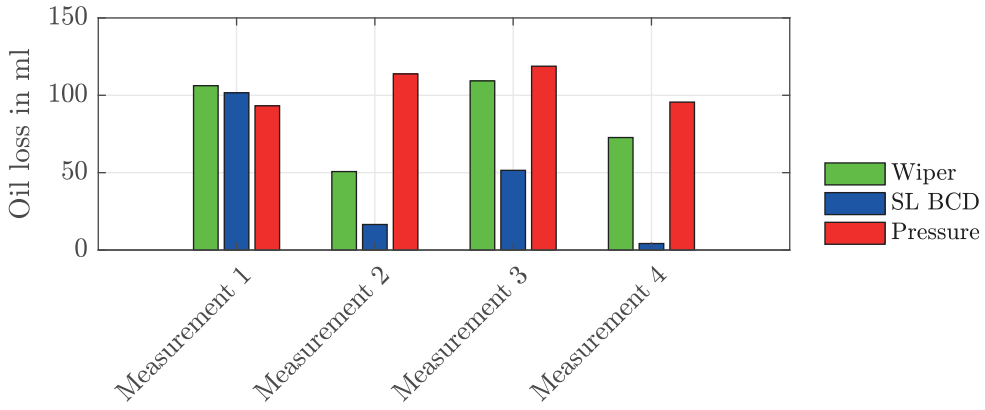

Figure 2.8: Bar chart of oil loss from four subsequent measurements at 1500 rpm and 5 bar

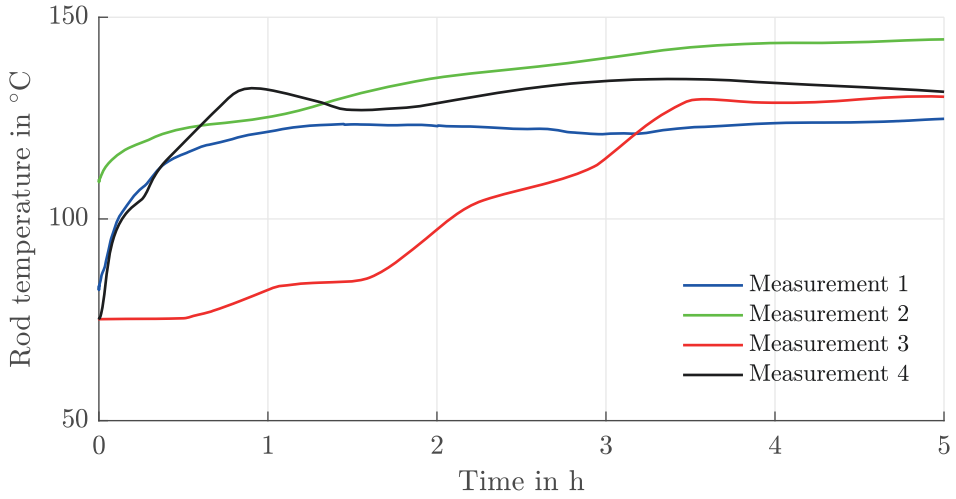

Figure 2.9: Average rod temperature of four subsequent measurements at 1500 rpm and 5 bar

2.2.2 Simplifying the measurement set-up

As mentioned above, the measurement set-up did not allow a reliable investigation of the oil loss, occurring in a combined packing. The interaction of the directly attached pressure section to the wiper cup was not comprehensible. As the evaluation of the oil loss performance of the wiper design was the primary goal of the investigation, the influencing factor "pressure" was eliminated. This led to a new configuration of the set-up shown in Fig. 2.10. The wiper cup was mounted in the same configuration as in the previous set-up. The second cup, containing the SL BCD ring, was left empty. The third cup was equipped with a wiper system known to be effective, removing almost all oil from the rod and leading it into the pressure section. It is a classic metallic wiper design, but implemented as polymeric wiper. This wiper concept is called radial scraper and further described in Sec. 4.1.4. The oil loss gathered in this section indicated the amount of oil passing through the wiper cup with its two wiper rings. The amount of oil measured in the wiper cup was the amount of oil wiped off by the second ring in the wiper cup. If there is no leakage of oil detectable along the piston rod (outside the test packing), the oil loss can be exactly allocated. Additionally, the hydrostatic measurement principle of the oil loss in the wiper and the SL BCD cup has been replaced by a weight measuring system. It was calibrated with a known amount of oil to calculate the volumetric oil loss. This resulted in a smoother measurement signal.

The remaining factor "speed" was varied again at 700 rpm, 1100 rpm and 1500 rpm. In Fig. 2.11 the measurement at 700 rpm is shown. As expected, there was no oil gathered in the SL BCD cup. At a measurement time of 17.5 h a kink occured in the measured curves. This was not corresponding with any change in the surrounding conditions (shown in Appendix, Fig. 7.8).

To evaluate the strength of the effect, the slope of the oil loss versus time was calculated for four sections of the measurement period (see black dash-dotted lines in Fig. 2.11a). With four sections it was possible to detect changes without generating too much data. The result was the oil loss per hour. Additionally, to evaluate the influence of the factor "speed", the result was normalised to the amount of oil lost per stroke. In Fig. 2.11b the results of this analysis are shown. This analysis was used for the evaluation of all further measurements, to make experiments of different durations comparable. It was recognisable that the amount of oil lost in the pressure section was higher than the amount of oil wiped off by the second oil wiper ring in the wiper cup.

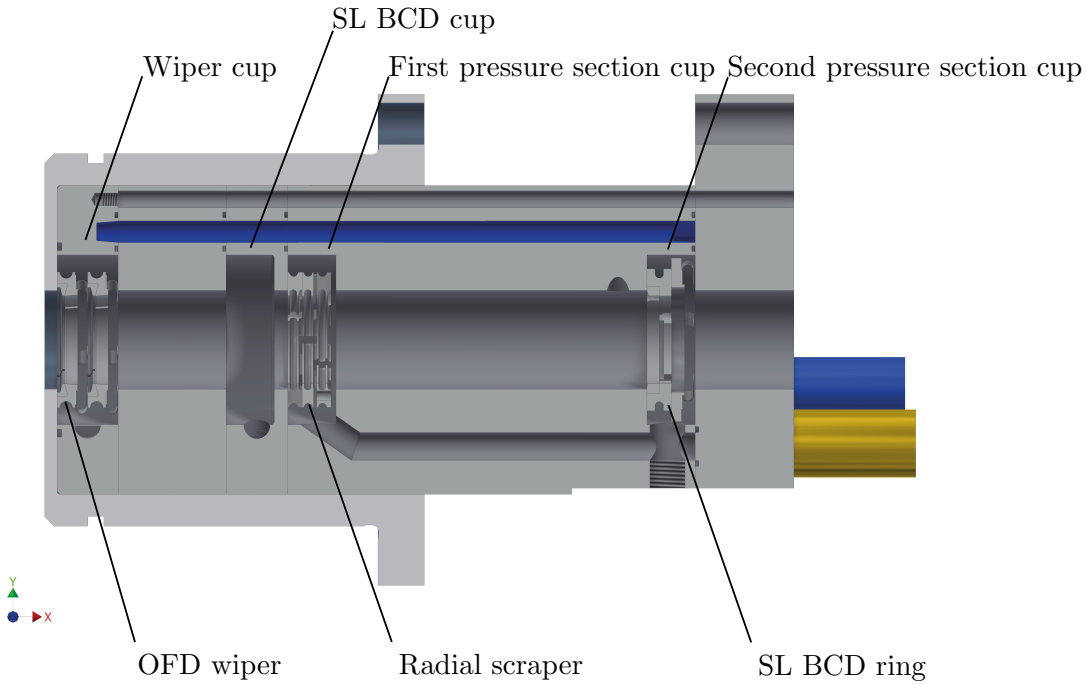

Figure 2.10: Simplified configuration of the test set-up with OFD wiper in the wiper cup, empty SL BCD cup and radial scraper in the first pressure section cup

The simplified measurement set-up was also investigated in terms of repeatability. A repeat of the experiment at 700 rpm is shown in Fig. 2.12. The oil loss versus time was very constant, with just a small variance during the start-up phase. Again more oil loss was measured in the pressure section than in the wiper cup. But the absolute values showed a strong variance between the two experiments at 700 rpm. In the first experiment an overall oil loss of 1.7×10^{-4} ml/stroke in the wiper cup and 3.0×10^{-4} ml/stroke in the pressure section has been measured. In the repeat of the experiment, the amounts were 2.5×10^{-4} ml/stroke in the wiper cup and 6.3×10^{-4} ml/stroke in the pressure section. This is a variation of 50 %, only the characteristic of more oil in the pressure section was constant. As the oil loss rates during the experiments were very stable, it is assumed that the results are valid. The difference in the absolute values was accepted, due to the fact that the goal of the project was to develop new wiper ring designs. Furthermore, it could not be excluded that the variation was caused by the OFD wiper design. The defined levels of the experimental design to evaluate the performance of the common OFD and the new designed wipers are shown in Tab. 2.4. It was planned to do at least one repeat of each experiment, which enabled to detect serious variations in the characteristic of the oil wiper performance with an acceptable experimental effort. A full measurement of an oil wiper design took approximately one and a half weeks (six 24 h runs).

Table 2.4: Definition of levels in rpm

Factor	**Level 1**	**Level 2**	**Level 3**
Speed	700	1100	1500

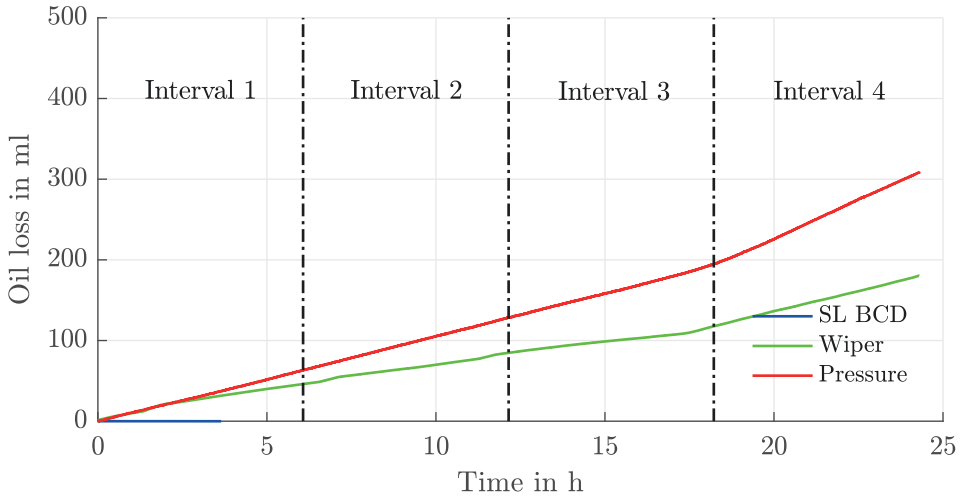

(a) Oil loss of experiment at 700 rpm with indication of evaluation intervals (black dash-dotted line)

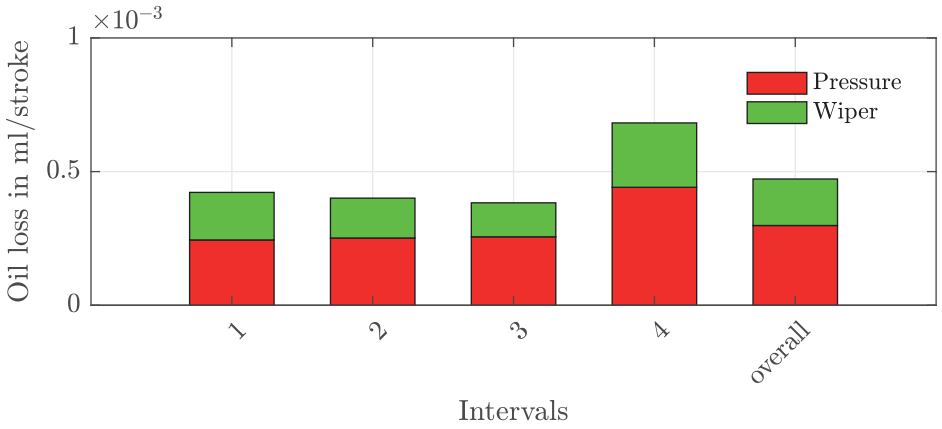

(b) Oil loss per stroke at 700 rpm

Figure 2.11: Measurement results and analysis of experiment at 700 rpm for 24 h

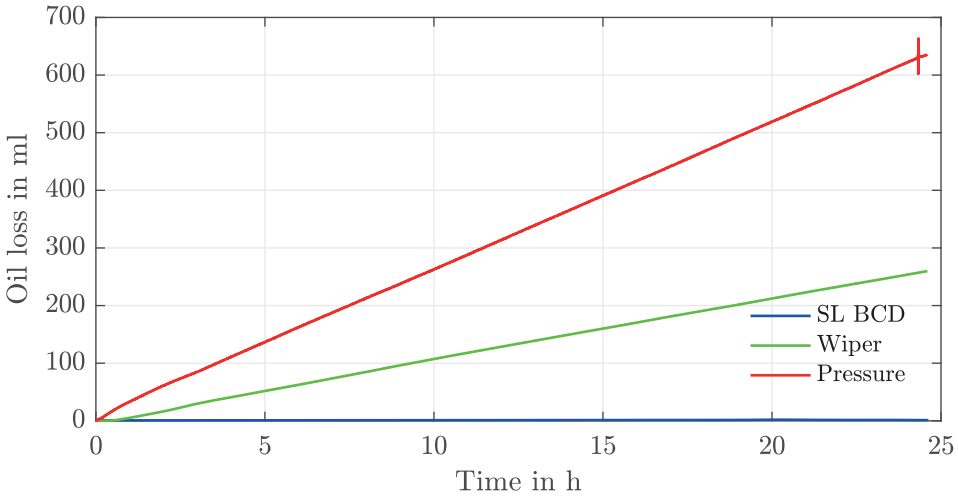

(a) Oil loss of the repeat of experiment at 700 rpm

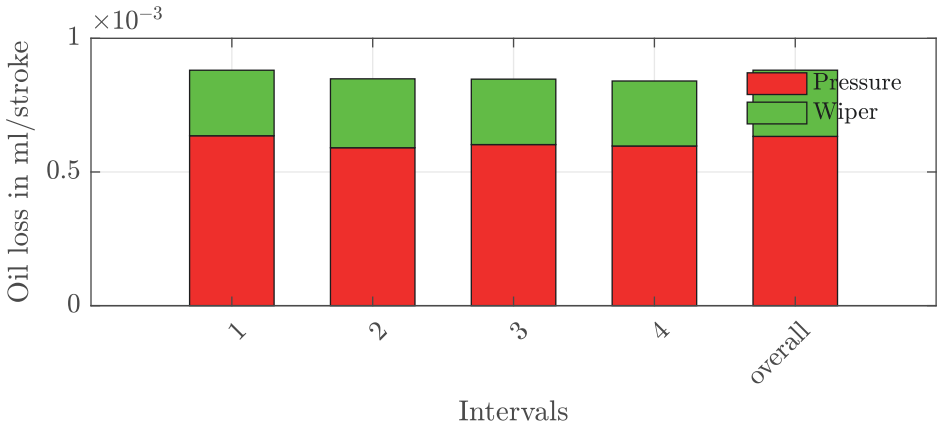

(b) Oil loss per stroke at 700 rpm

Figure 2.12: Measurement results and analysis of the repeat of experiment at 700 rpm for 24 h

2.3 Oil loss measurement of the current oil wiper (OFD wiper)

The experiments have been performed according to Sec. 2.2.2. Two subsequent measurement rows have been done, beginning each at 700 rpm. The summarised results are shown in Fig. 2.13, detailed results are shown in Sec. 7.5. In addition to the oil loss per stroke, the oil loss per hour was evaluated. This output is more significant for the operational application of the oil wiper. In Fig. 2.13a it is shown, that there is a significant variation in the overall oil loss between the two single runs. The overall oil loss at run 2 is higher in every level of speed. The difference is between 30% (at 1100 rpm) and 50% (at 700 rpm and 1500 rpm). This variation did not allow a reliable conclusion. The reasons for this difference have not been found. It is possible, that the deviation between run 1 and run 2 were either caused by the measurement set-up or the OFD wiper itself. The assumption, that more reciprocating movements of the piston rod lead to more oil loss was not confirmed, because as shown in Fig. 2.13a the overall oil loss at 1500 rpm is less than at 1100 rpm. An explanation could be the changing viscosity of the oil. According to [8] the relation between oil viscosity and temperature is logarithmic. A temperature increase of 10 K leads to half of the initial oil viscosity. As shown in Sec. 7.5 the rod temperature level at 1500 rpm was about 15 K higher than at 1100 rpm. The temperature increase of the oil with increasing drive speed could not be compensated, because there was no temperature control available. Neglecting the absolute difference from run 1 and run 2 the overall oil loss was rising from 700 rpm to 1100 rpm. This trend did not continue with 1500 rpm drive speed. This disagreed with the assumption that more reciprocating movements deliver more oil from the crankcase. This could have been either caused by the lower oil viscosity (caused by the higher temperature) or inertia effects led to a different mechanism in the build-up of the oil film on the rod. Furthermore, it was not ruled out that the variation was caused by the performance of the OFD wiper itself. With this and the fact that the measurement procedure is very time consuming it was decided to abandon a detailed characterisation of the oil wiping performance of the OFD wiper and to use the results as benchmarks for further investigations.

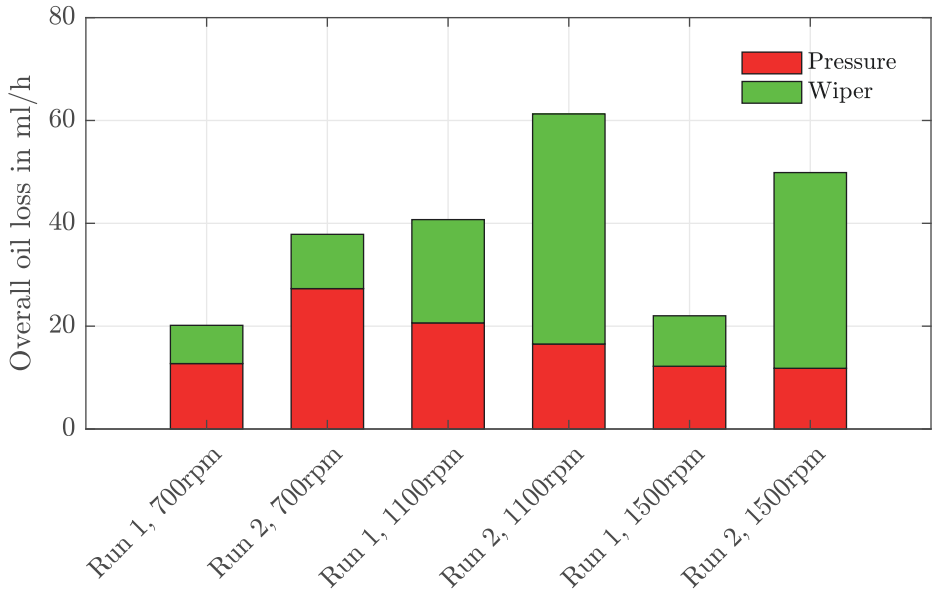

(a) Overall oil loss of the OFD wiper

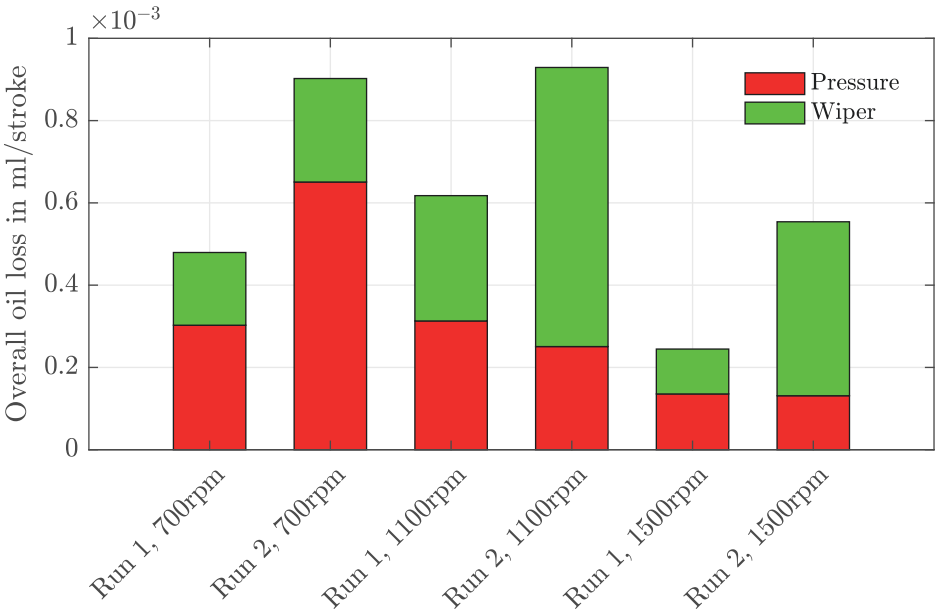

(b) Normalised oil loss of the OFD wiper

Figure 2.13: Summary of the oil loss measurement of the OFD wiper at three levels of speed

2.4 Conclusion

In this chapter it was shown how the performance evaluation of an oil wiper ring was implemented. The presented measurement set-up was very application oriented. This had the benefit of results gathered on realistic conditions. A clear disadvantage is shown in Sec. 2.2.1 regarding the repeatability of the measurement procedure. The circumstances at the direct implementation were not fully clarified and controllable, thus leading to strong variations of the absolute results. Contrary, the single measurements seemed to be very stable, as the oil loss versus time was linear. The simplification of the measurement set-up shown in Sec. 2.2.2 enhanced the stability of the single measurement processes. But there was still a huge absolute variation in terms of the oil wiping performance (see Fig. 2.13b). An exact value for the performance of the OFD wiper could not be given. It was not possible to derive a comprehensible characteristic of the oil wiping performance. It was decided to forego a further time intensive enhancement of the measurement set-up in order to test new concepts. It could not be ruled out, that the strong variation of the performance was caused by the design of the OFD wiper or the result of the complex interaction between drive speed, oil temperature and viscosity.

A possibility to improve the variation of the results is to build a set-up detached of the compressor and the crankcase. An oil film with an adjustable temperature could be spread on a reciprocating rod in a more controllable way, to stabilise the input conditions of the oil wiper function.

3 Elastomer spring

As shown in Sec. 1.2 the lug spring is a very expensive part of the oil wiper group. Another issue is the usage of metal as spring material because it has the potential of scraping the piston surface. In case of a fraction of the spring, splitters get between the moving piston rod and stationary rings and cause significant damage. Therefore it was desired to change the material of the spring to a polymer material which does not bear the potential of damaging the piston rod. This chapter is about replacing a metal spring by a polymer spring element.

3.1 Concept

The easiest way to realise an elastic spring element is to deform an elastic body. The material can be strained in tension/compression, bending or torsion. As the resulting geometry should be easily predictable and manufacturable, a compression spring was designed. The concept shown in Fig. 3.1 consists of several cylinders arranged on a ring. The high number of cylinders on the ring provide an even distribution of the obtained force during compression of the spring. This concept is adjustable by varying the number of cylinders on the ring, cross-sectional area of the cylinders and height of cylinders.

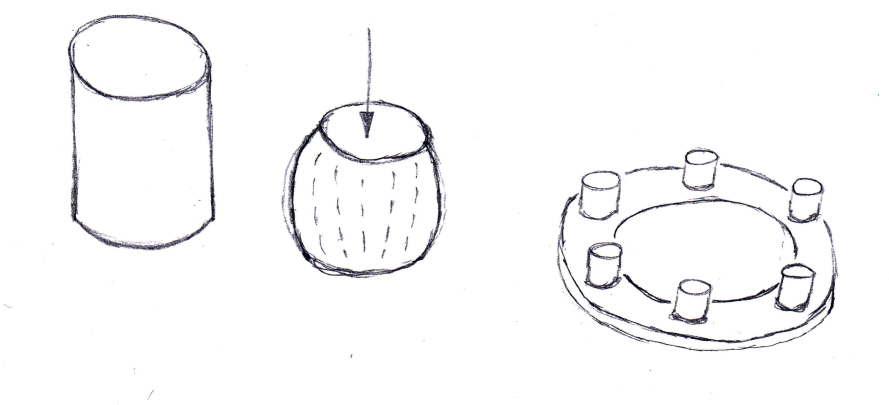

Figure 3.1: Concept of elastomer spring with deformable cylinders

3.1.1 Functional requirement

The function of the lug spring is:

Axial force The lug spring applies axial pressure on the oil wiper ring. It prevents the ring from axial movement during each stroke of the piston rod.

The function of the lug spring inhibits, that all axial forces occurring during each stroke must be compensated. These axial forces are caused by friction between the surface of the oil wiper ring and

the piston rod. For a proper prediction of the required axial force of the lug spring, it was necessary to measure the friction force.

3.1.2 Determination of friction force

The free body diagram in Fig. 3.2 shows that the axial force of the lug spring must be higher than the friction force to maintain the axial position in the cup. In the case of an equilibrium between friction force and axial force, during the positive rod displacement, the contact pressure p_c between wiper ring and the front surface of the cup disappears. Thus there is no sealing effect. During the negative rod displacement (rod moving towards the crankcase) the friction force is enhancing the contact pressure p_c. A sealing effect is therefore guaranteed, if the sealing during the positive displacement is enough.

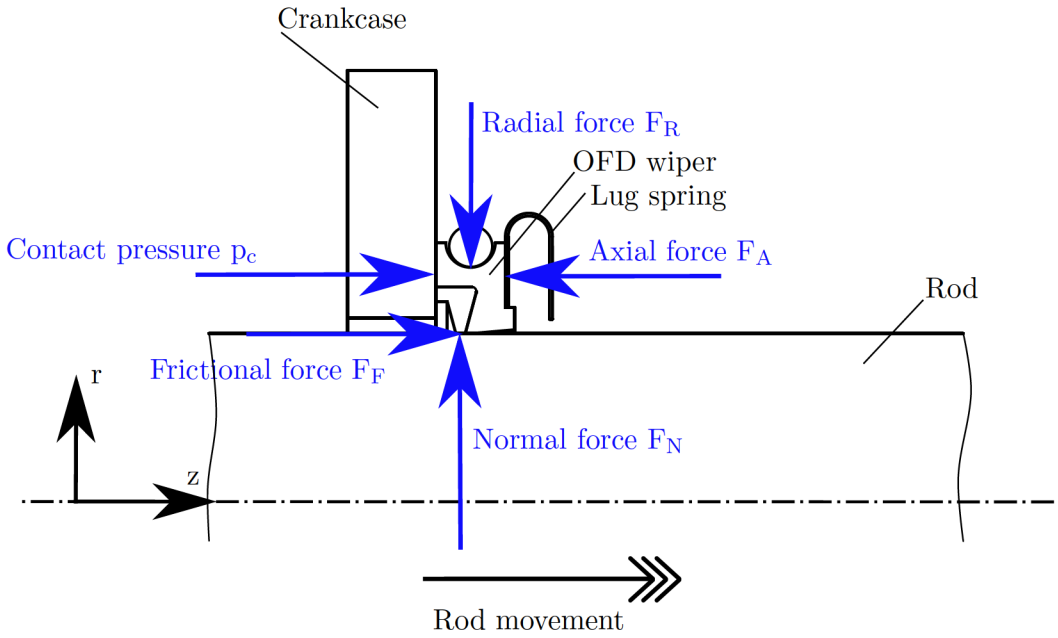

Figure 3.2: Free body diagram of OFD wiper during positive rod displacement

$$\sum F_z = p_c \cdot A - F_A + F_F = 0 \tag{3.1}$$

$$\sum F_r = F_N - F_R = 0 \tag{3.2}$$

During the negative rod displacement, the direction of the friction force F_F is in the same direction as the axial force F_A and therefore supports the lug spring in maintaining the position of the wiper ring.

To determine the occuring frictional forces a special test set-up was implemented. The measurement set-up (see Fig. 3.3) used a Zwick tensile testing machine as a basis. The force transducer was extended with a rod dummy. This dummy had the same surface finish (hardening and grinding) as a rod used in a reciprocating compressor. The oil wiper ring was mounted in a cup with space for radial flotation. The cup could be filled with oil to ensure same friction conditions as occurring during operation in a reciprocating compressor. The limitation of the test was the maximum displacement speed of 1 m/s, whereas average rod displacement speeds are around 15 m/s.

During the operation of a reciprocating compressor different situations regarding the friction conditions occur. In the power-up phase there is no oil present on the surface of the piston rod. This means there is a dry friction between the oil wiper and the piston rod. With advancing time, the piston rod

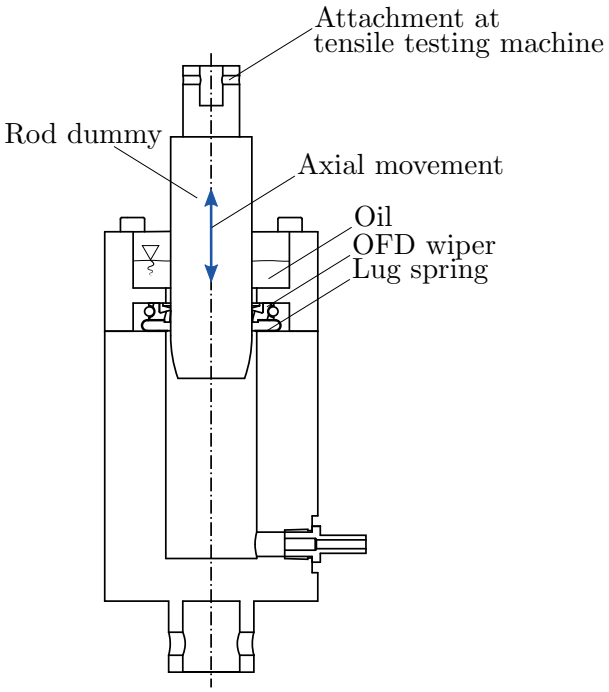

Figure 3.3: Set-up of friction force measurement

is increasingly wetted and an oil film is changing the friction behaviour between the wiper ring and the piston rod. Depending on the design of the crankcase, it is also possible that huge amounts of oil are directly spilled onto the wiper cup. This situation is measured by filling the wiper cup completely with oil. The three different situations are summarised in Tab. 3.1.

Table 3.1: Conditions of friction force measurement

Measurement	**Condition**
Dry rod	No use of oil
Lightly wet rod	Oil film on rod
Heavily wet rod	Cup filled with oil

The measurements were recorded consecutively, beginning with the dry rod measurement and ending with the heavily wet measurement. With this, residuals of oil on the piston rod were excluded. The measurement process was a cycle with two reciprocating strokes. Doing so, occurring pre-loads caused by the assembly and positioning of the rod dummy were eliminated. For evaluation of the influence of the displacement speed, it was varied from 100 mm/min to 1000 mm/min (limit of the tensile testing machine).Every measurement was repeated twice after the full set of first measurements to verify the precision. The measurement results were highly repeatable, therefore only one set is shown in Fig. 3.4. Only the measurement with a lightly wet piston rod shows variations during the positive stroke (rod diving into the cup, curves on the positive scale of the graph), because the oil film distribution along the rod was not perfectly even. The highest friction force occurred on a dry rod and from standstill to movement (static friction) during power-up of the compressor. The lug spring has to resist the frictional forces in this situation and keep the wiper ring in its position. A wiper movement is not allowed, because a sudden oil swell could fill the wiper cup with oil. Such a wetting of the cup increases the oil flow through the cup. The maximum force was 14.7 N at a displacement of 0 mm and an acceleration to a speed of 100 mm/min. A thin oil film (Fig. 3.4b) reduced the maximum force only marginally to 14.2 N. Also a heavily wet piston rod showed a maximum friction force of 14.2 N. The dynamic friction was more influenced by the friction conditions. On a dry rod the friction force was

between 13.6 N and 11.6 N during a stroke. On a lightly wet rod the average dynamic friction during a reciprocating movement was reduced from 10.5 N to 6.8 N. The heavily wet piston rod reduces the friction force further from 10.2 N to 5.5 N.

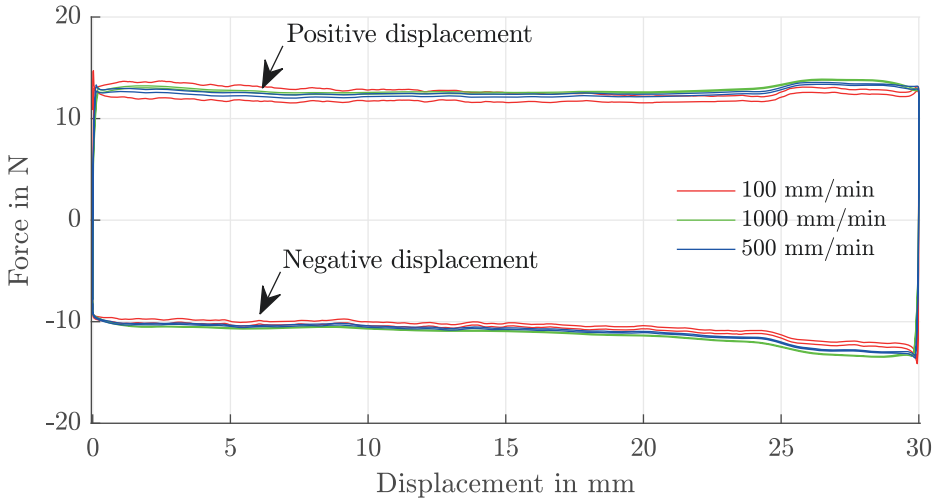

(a) Dry rod

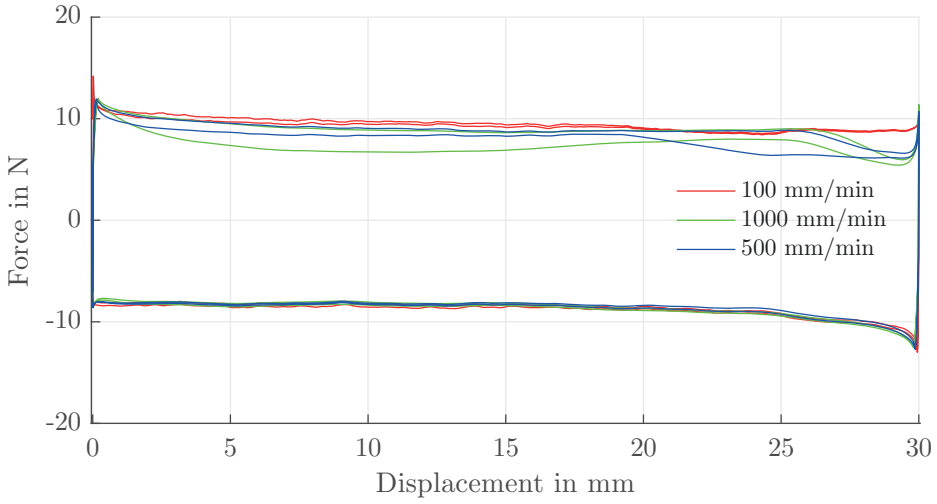

(b) Lightly wet rod

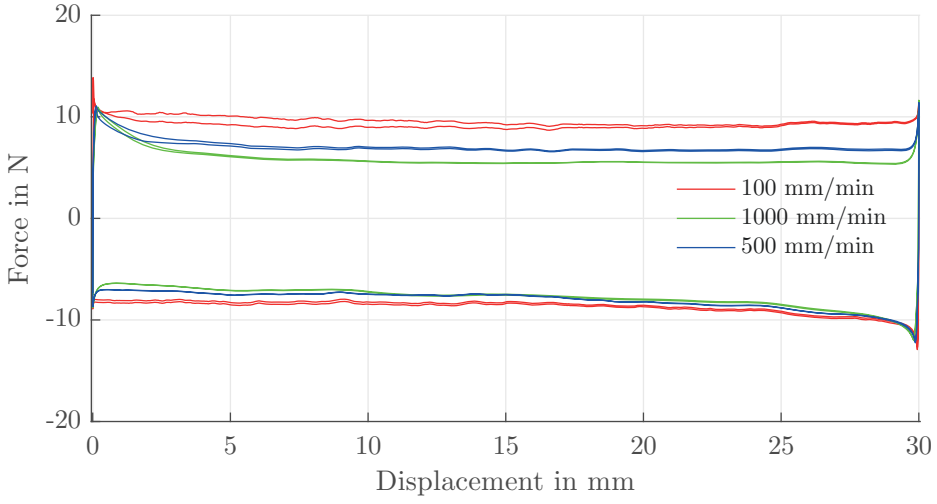

(c) Heavily wet rod

Figure 3.4: Friction measurement with varying conditions and varying displacement speed

The results are summarised in Tab. 3.2:

Table 3.2: Results of friction force F_F measurement of the OFD wiper

Measurement	**Static friction in N**	**Dynamic friction in N**
Dry rod	14.7	13.6-11.6
Lightly wet rod	14.2	10.5-6.8
Heavily wet rod	14.2	10.2-5.5

The installation process was measured separately. This delivered information about loads occurring during the mounting process. The oil wiper ring must be mountable without additional tools and heavy forces to prevent damages of the wiping geometry (see [10]). The friction force during the mounting of the rod was measured by recording the force of the dummy generating contact to the wiper and move on for further 30 mm. This routine was repeated, to recognise any variable influences. The measurement shown in Fig. 3.5 was very stable. The highest forces occured at the beginning, because the inner diameter of the OFD wiper was compressed by the radial spring (wear compensation). Thus the four ring segments were expanded under enhanced axial friction force. The maximum friction force of 32.5 N was satisfying the claim of a tool-free installation process (according to [10]).

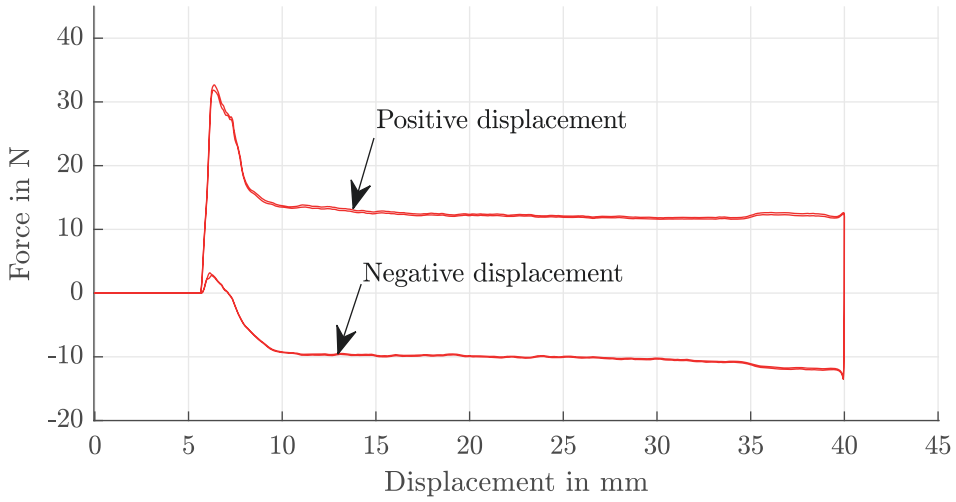

Figure 3.5: Friction force measurement during mounting of the rod

3.1.3 Characterisation of current lug spring

The current lug spring is a metallic spring with eight deformable arms. The shape is laser cut from high quality steel sheets. After that, the eight single ends are bent into the final shape. As the laser cutting changes the inter-metallic structure at the cutting edges, it is necessary to append a heat treatment. The current design of the OFD wiper compresses the lug spring in the cup for 1.5 mm. The characteristic force-displacement-curve is shown in Fig. 3.6. The spring provides an axial force of $F_A = 22.5 \pm 0.5\,\mathrm{N}$. According to (3.1), the minimum remaining force for sealing the wiper cup with the OFD wiper is:

$$p_c \cdot A = F_A - F_F = 7.8N$$

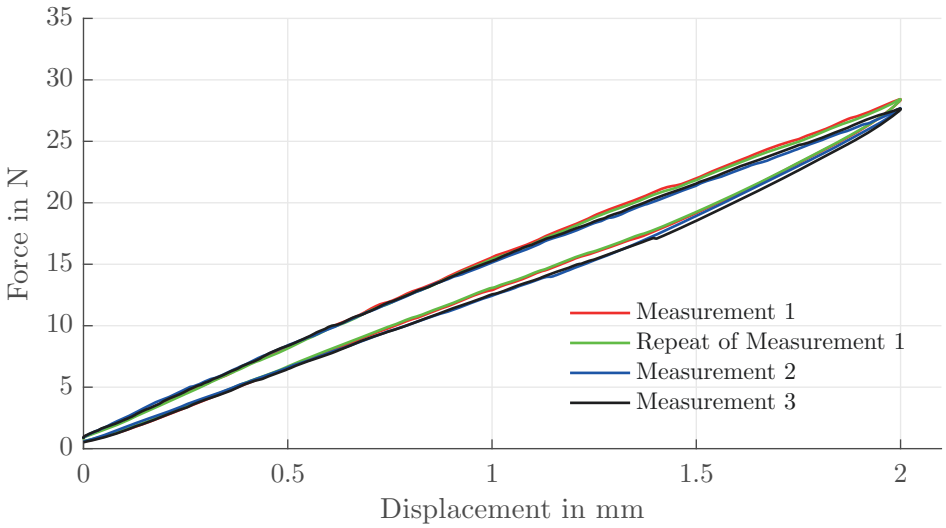

Figure 3.6: Characteristic force-displacement-curve of three metallic lug springs

3.2 Material selection

The material selection was very crucial in terms of successfully replacing a metallic component. The surrounding conditions are very demanding and the most critical are summarised in Tab. 3.3.

Table 3.3: Requirements regarding the material selection of the lug spring

Requirement	**Value**
Temperature stability	up to 150 °C
Chemical stability	H_2S-sour gas Mineral oil
Mechanical stability	Lifetime of more than two years

The mechanical load leads to a long-term compression stress of the material. Therefore a low relaxation rate is very important to ensure a proper function of the spring element. Additionally, a low Young's modulus is required. Thus the material class of elastomer polymers was selected. Although thermoplastic elastomers or thermoplastic urethanes could also provide the required mechanical function, they have commonly a faster relaxation rate, a lower chemical resistance against oil and a lower temperature stability ([6]).

The selection of a specific elastomer was done with focus on the requirements regarding operational temperature and chemical resistance. According to Fig. 3.7 the elastomers in Tab. 3.4 are fulfilling the requirements. Although the claim of a low volume change in ASTM oil does not include a full chemical resistance, it is clearly indicating which elastomers are less influenced than others.

Table 3.4: Elastomers fulfilling the requiurements of temperature and chemical resistance

Fluoro rubber (FKM)
Perfluoro rubber (FFKM)
Fluorosilicone rubber (FVMQ)
Acrylate rubber (ACM)
Hydrogenated nitrile butadiene rubber (H-NBR)

From the elastomers listed, several were excluded: FFKM is a high performance material with chemical

resistance similar to polytetrafluorethylene (PTFE). It is only used where the high material price is reasonable because of no other options. The FVMQ is a silicone based rubber and is challenging in processing. The ACM is less stable against diluted acids like H_2S than H-NBR and FKM.

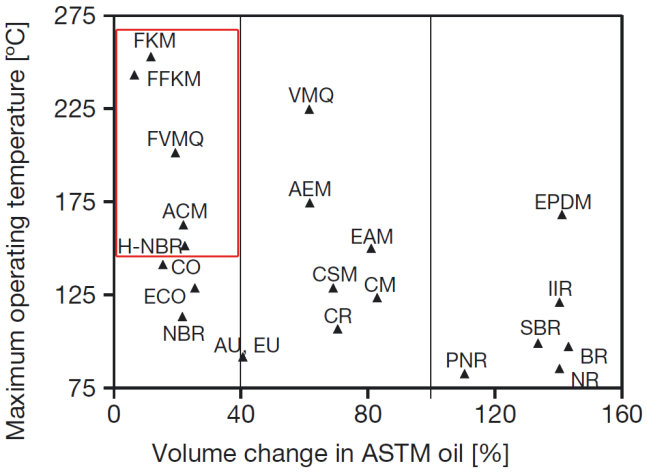

Figure 3.7: Chemical resistance and maximum operational temperature of elastomers [6]

3.2.1 Fluoro rubber (FKM)

Fluoro rubbers are gained by polymerisation of different fluoro monomers. Depending on the type of monomers, co-, ter- and tetrapolymere fluoro rubbers are distinguished. The content of fluorine is between 65 % and 71 %. The high bending energy between fluorine and carbon leads to high temperature and chemical resistance. Typical applications are environments demanding these qualities (see [4]). Fig. 3.8 shows different structures of FKM rubbers.

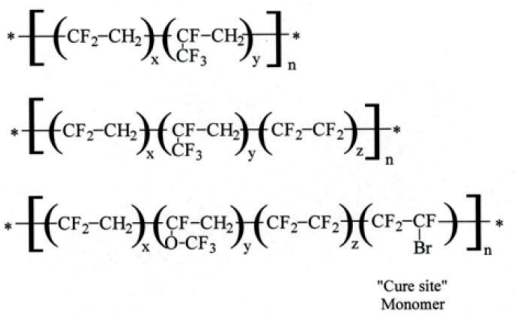

Figure 3.8: Co-, ter- and tetrapolymere molecular structures of FKM rubbers (see [4])

3.2.2 Hydrogenated nitrile butadiene rubber (H-NBR)

Hydrogenated nitrile butadiene rubber is gained by hydrogenation of the double bond of butadiene in nitrile butadiene rubber (NBR). This saturation leads to improved weather-, ozone- and heat-resistance. Usual applications are in heat-, oil-, chemical- and weather-resistance demanding environments (see [4]). Fig. 3.9 shows the structure of an H-NBR molecule.

Gummiwerk KRAIBURG GmbH is a supplier of elastomer rubber materials. After consultation about

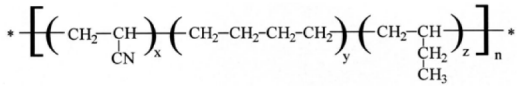

Figure 3.9: Structure of an H-NBR molecule (see [4])

the specific requirements, an FKM and an H-NBR rubber as a laboratory sample have been provided (see [13] and [14]). The samples are rubber compounds, ready for manufacturing. They consist the rubber, fillers and the cross-linking agent.

3.3 Preliminary design

To estimate the dimensions and number of the cylinders a preliminary design was made. The goal was to develop three designs for a prototyping thereof. The designs were developed with focus on the application in the MPTC and the OFD wiper, as well as new wiper designs.

The OFD wiper has a contact area of $A = 628.3\,\text{mm}^2$ (see [10]). With the measured axial force $F_A = 22.5\,\text{N}$ of the lug spring the resulting contact pressure p_c is

$$p_c = 0.0124\,\text{MPa}.$$

This is a very low pressure to provide a sealing effect because it is only about a tenth of the atmospheric pressure. The desired maximum contact pressure which should be evaluated is 0.05 MPa, to determine if a too low level of contact pressure influences the oil loss of the wiper ring. Thus the axial force F_A of the lug spring is

$$F_A = F_F + p_c \cdot A = 46.1\,\text{N}.$$

This is the axial force F_A, the new lug spring should provide over its complete lifetime. Additionally, for test runs on the same contact pressure level as the current metallic lug spring, single cylinders could be removed to vary the axial force. The OFD wiper design has space at its spring sided face for cylinders with a diameter of $d = 5.175\,\text{mm}$. For an even distribution of the axial force at least eight cylinders are necessary. An approximation of the resulting force can be done with Hooke's law (uniaxial compression, see [16]):

$$\sigma = \epsilon \cdot E$$

$$F = \sigma \cdot A = \epsilon \cdot E \cdot A$$

With Young's modulus $E_{FKM} = 2.1\,\text{MPa}$ and $E_{H-NBR} = 4.2\,\text{MPa}$ (see [13] and [14]) and a cylinder diameter $d = 4.5\,\text{mm}$ the forces in Tab. 3.5 were expected. This approximation was neglecting the fact, that the used Young's modulus is given for tensile stress and could deviate from Young's modulus of compression. This difference had to be evaluated by a material characterisation, because there was no data available for the selected materials. Another limitation was the assumption of an uniaxial compression, which might not be given in a cylinder with diameter/height ratio of approximately 1 (further annotations are given in Sec. 3.7). To have a variety of options during the evaluation of the concept, it was decided to design three prototypes with varying number of cylinders and deformation height. One design is shown in Fig. 3.10. The resulting axial forces of the three designs are shown in Tab. 3.5.

Table 3.5: Approximation of resulting forces for different spring designs and materials

# Cylinders	Height in mm	Deformation in mm / %	Resulting force of FKM in N	Resulting force of H-NBR in N
12	4.5	0.5 / 11.1	44.5	89.1
12	5	0.5 / 10	40.1	80.2
8	4.5	0.5 / 11.1	29.7	59.4

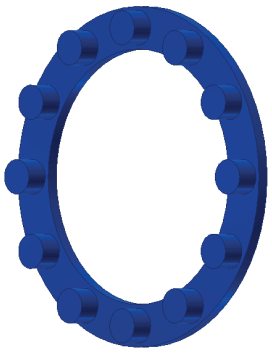

Figure 3.10: ElastoSpring design with 12 cylinders and height h=4.5 mm

3.4 Manufacturing concept

The manufacturing of rubber parts from uncured rubber blends is a semi-continuous process. According to [15], the three common methods are:

- Compression moulding
- Transfer moulding
- Injection moulding

Compression and transfer moulding are mostly used for small quantities. The uncured rubber is placed in the cavity of a two-part tool, which is heated to the cross-linking temperature. In the injection moulding process, after closing the tool, the cavity is filled with rubber and the cross-linking begins. After the part is fully cross-linked, the tool opens and the part is removed. As the desired quantity of the ElastoSpring design is suitable for an injection moulding process (see [10]), it was decided to investigate this process for manufacturing. Main advantages are the shorter cycle time and higher automation grade, which significantly influences the part price. The main components are shown in Fig. 3.11. In the injection moulding process, the uncured rubber is plasticised in a cylinder containing a screw feeder (see Fig. 3.11a). The cylinder is heated to temperature T_Z, the uncured rubber is transported by the rotating screw into the variable volume of plasticising with feeding pressure p_{St} and heated by dissipated frictional heat to curing temperature T_V. During the injection phase (see Fig. 3.11b), the screw is moved axially by the hydraulic pressure p_{HE} and the uncured rubber is injected into the cavity of the closed tool with pressure p_E and temperature T_V. These two parameters influence the temperature of the uncured rubber T_E at the beginning of the cross-linking phase by increasing it with dissipated frictional heat. Additionally, the wall temperature of the cavity T_W is heating the rubber. During the cross-linking time of the part in the cavity, the dosing for the next shot begins. At the end of the cross-linking phase, the mould is opened and the part removed from the cavity. With the closure of the mould the next cycle begins.

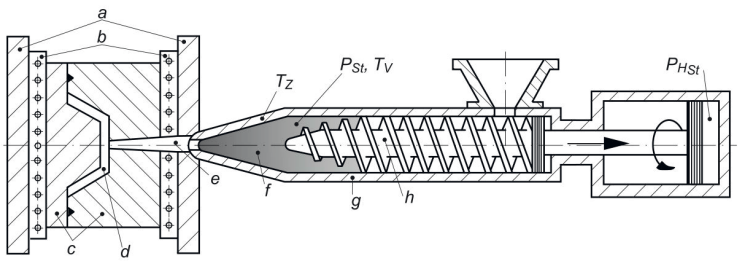

(a) Dosing phase of the rubber injection moulding process

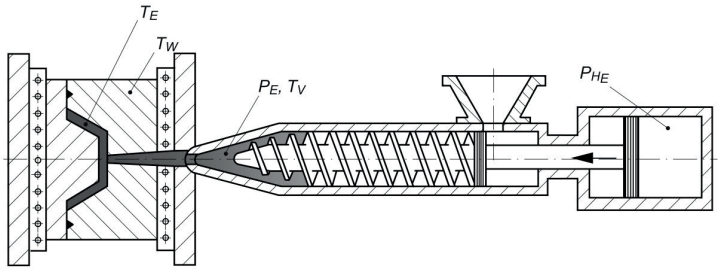

(b) Injection phase of the rubber injection moulding process

Figure 3.11: Components of a rubber injection process with: a mould support plates, b heating plates, c mould plates, d cavity, e runner, f variable volume of plasticising, g cylinder, h screw [15]

A test mould (see Fig. 3.12) was designed to enable the production of various prototypes at low cost of the mould itself. Therefore, no automatic ejector system is included. The nozzle side (Fig. 3.12a) contains the runner and the guide bushing. The cavity side (Fig. 3.12b) contains the guiding pins and a milled pocket for exchangeable inserts. The mould does not contain any heating system, it must be provided by the clamping plates of the injection moulding machine. The drawings of the mould are shown in the Appendix, Sec. 7.6.

For the three different designs of the ElastoSpring three exchangeable inserts were milled. As mentioned in Sec. 3.3, it is necessary to make a dedicated material characterisation. Therefore an additional exchangeable insert was designed to mould various test specimens (see Sec. 7.6). It consisted of one cavity to mould a tensile test specimen (according to DIN 53504) and two types of compression test specimens with three cavities each. The first type of compression test specimen was a cylinder with diameter $d = 6\,\text{mm}$ and height $h = 6\,\text{mm}$, the second was a cylinder with diameter $d = 10\,\text{mm}$ and height $h = 10\,\text{mm}$. This enabled the investigation of size depending effects on the mechanical properties of the material.

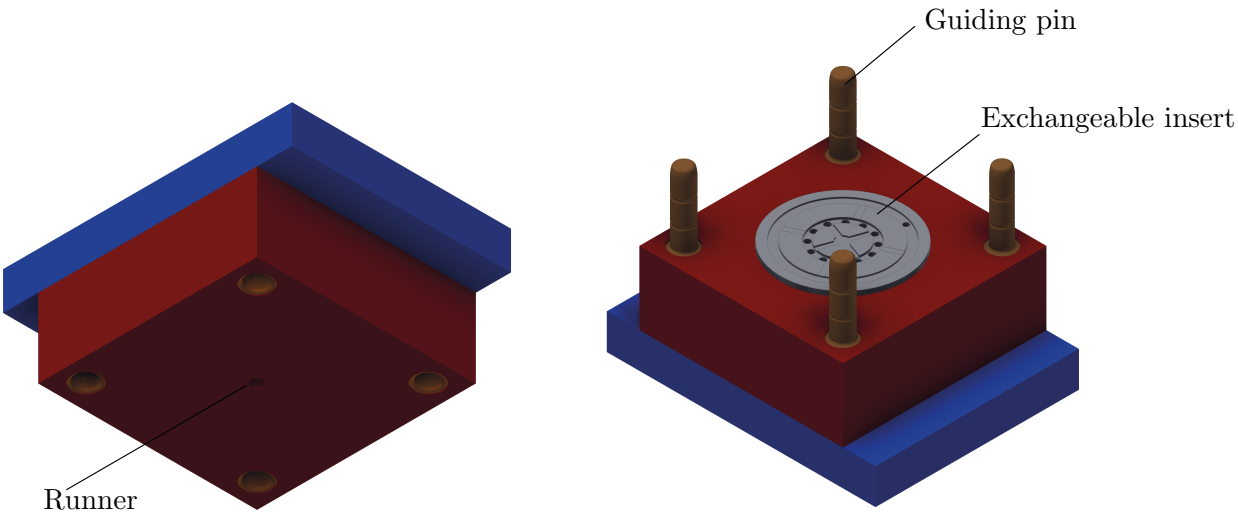

(a) Nozzle side (b) Cavity side

Figure 3.12: Test mould for concept of the elastomer spring

3.5 Sampling of the test mould

For the sampling process a Maplan MTF750/160 (see Fig. 3.13) rubber injection moulding machine was available. The machine has a vertical clamping and injection unit. The clamping unit is powered by a hydraulic drive system. General technical information is summarised in Tab. 3.6.

Figure 3.13: Maplan MTF 750/160 injection moulding machine [7]

The test mould fitted the size of the heating plates and the minimum mould height, thus the installation process was unproblematic.

Table 3.6: Specifications of the Maplan MTF 750/160 rubber injection moulding machine

Specification	**Value**
Opening stroke	450 mm
Heating plates (width × depth)	450 mm × 510 mm
Minimum mould height	150 mm
Clamping force	1590 kN
Injection volume	750 cm^3

3.5.1 Sampling of the H-NBR rubber

The laboratory sample of the provided rubber was delivered as sheet material. The sheet was cut into stripes, to fit in the feeder of the machine. According to [12] the processing parameters in Tab. 3.7 were set. The temperature of the heating plates was raised to get a constant temperature of 170 °C on the surface of the cavity. For this material a vulcanisation time for 90% cross linking (according to DIN 53529) of 2.21 min is given. The vulcanisation times of the three different ElastoSpring prototypes and the test specimen insert were expected to be longer, because the measurement of vulcanisation time is done with a thinner sample on a rotary vulcanometer. The cavities have much thicker wall sections, therefore the heating time was set to 5 min, to ensure a high level of cross linking. A visual check of the cross sectional texture of the cylinders (cut in half with a knife) showed no evidence of uncured areas, therefore the heating time of 5 min was accepted.

Table 3.7: Processing parameters for sampling of the H-NBR rubber

Parameter	**Value**
Temperature heating plate closing side T_W	195 °C
Temperature heating plate fixed side T_W	195 °C
Temperature feeder	60 °C
Temperature cylinder T_Z	70 °C
Temperature nozzle	80 °C
Clamping force	450 kN
Injection speed	2 mm/s
Heating time	5 min
Shot volume	11 cm^3

Problems during the sampling process

For a proper function of the machine's dosing cycle a minimum dosing volume of 150 cm^3 was necessary. This resulted in a huge amount of material (more than 10 shots) which was already exposed to higher temperatures within the cylinder. It was also necessary to vary and tune the injection speed concerning machine internal control parameters, to avoid short shots or overfilled parts.

Another problem occurred during the demoulding process (see Fig. 3.14). During the opening movement of the tool, the runner stuck in the runner hole. This caused a fracture of the part at the four runner gates. The resulting axial force partially demoulded single cylinders next to the runner gates and fractured the combining ring. The stuck runner had to be removed manually with a pair of pliers. Although the hole is shaped conical, the runner could not be demoulded without a significant level of axial force. The reason of the stuck runner can be found in the surface of the runner hole. It was

drilled by milling with a cylindrical tool. Therefore the machining was done with a helical pattern, which roughens the surface and prevents an easy demoulding.

(a) Stuck and fractured part in the fixed side

(b) Stuck and fractured runner in the moving side

Figure 3.14: Fracture of part during the demoulding process

3.5.2 Sampling of the FKM rubber

The sampling of the FKM rubber was done analogously to the sampling of the H-NBR rubber. The machine parameters (see Tab. 3.8) were adjusted to the required higher temperature. To reach a surface temperature of 180 °C (according to [11]), a heating temperature of 210 °C at the moving side and 220 °C at the fixed side was necessary. Although the same shot volume as mentioned in Tab. 3.7 was required, a setting of 7 cm^3 led to the best results. The heating time was adjusted to 3 min, because of the faster cross-linking mechanism of the FKM rubber. A visual check of the cross sectional texture of the cylinders showed no evidence of uncured areas, so the heating time of 3 min was accepted.

Table 3.8: Processing parameters for sampling of the FKM rubber

Parameter	**Value**
Temperature heating plate closing side T_W	210 °C
Temperature heating plate fixed side T_W	220 °C
Temperature feeder	60 °C
Temperature cylinder T_Z	70 °C
Temperature nozzle	80 °C
Clamping force	450 kN
Injection speed	2 mm/s
Heating time	3 min
Shot volume	7 cm^3

Problems during the sampling process

Again, the small amount of material, compared to the size of the injection unit was problematic. As the melt compressibility differs from H-NBR, the best value for the shot size was different.

The demoulding process led again to fractured parts (see Fig. 3.15). The result was less problematic, because the fractures were always at the runner gates and not at the combining ring. The runner had to be demoulded manually with a pair of pliers.

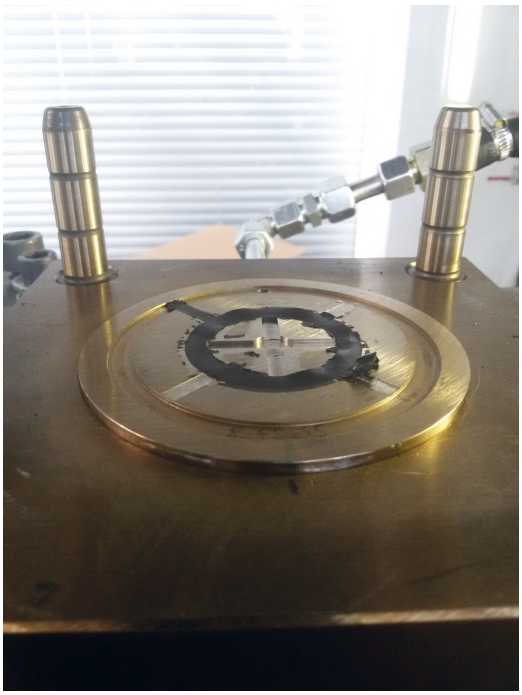

Figure 3.15: Demoulding of the FKM rubber caused fractures at the runner gates

3.5.3 Results of the sampling process

The goal of the sampling process was to produce prototypes of the ElastoSpring concept. It was possible to produce at least ten shots of every insert and material. During the sampling process the following problems occurred:

- Short shots
- Fractured parts during the demoulding

The short shots were a result of the dosing and filling parameters. It was necessary to vary the injection speed and shot volume to fill the part properly. The reason for this problems can be found at the injection machine itself. The positioning and filling movement of the injection unit is driven by a servo-hydraulic system. This system is designed for shot volumes up to 750 cm^3. The necessary shot volume of (see Fig. 3.11a, f) about 10 cm^3 is at the lowest level possible for the machine to produce. The usage of a smaller machine, appropriate to the shot size, would solve this problem.

The demoulding problem was caused by the test mould. The surface of the runner was too rough to enable a safe release of the rubber material from the mould. The problem was enhanced by a manufacturing error of the exchangeable inserts. As shown in the corresponding drawings (see Appendix, Sec. 7.6, drawing number VE10712-VE10714), the cavity is shaped as a hole through the complete steel plate. Unfortunately the back side was deburred, causing an undercut. Thus the part

had to be demoulded very carefully, pushing all cylinders outwards nearly simultaneously.

3.6 Material characterisation

In the provided data of the material supplier (see [13] and [14]) important material parameters were missing. For a reliable design of the ElastoSpring concept additional information was necessary. The goal of the material characterisation was to measure the material behaviour under application-like conditions and derive data concerning the long-term behaviour from short-term measurements at elevated temperatures. Additionally, it was planned to measure the resulting axial forces of the different prototypes and compare them with the preliminary design.

3.6.1 Compression stress measurement

The technical data sheets provide the tensile strength and elongation at break (see [14] and [13]), as well as tensile stress at 100% elongation (see [13]). For elastomers usually the stress-strain behaviour for tension and compression stress differs. The missing information was gathered by compression test measurement using the moulded compression test specimen with diameter $d = 10\,\text{mm}$ and height $h = 10\,\text{mm}$. The used equipment is shown in Tab. 3.9. To apply a uni-axial compression stress, two flat compression plates were used.

Table 3.9: Test equipment for compression test measurement

Equipment	**Name**
Universal tensile testing machine	Zwick/Roell Z010
Force transducer	Zwick/Roell KAP-TC, 500 N
Test specimen mounting	Flat compression plate

The measurement set-up is shown in Fig 3.16. The lower compression plate is mounted stationary. On the moving cross bar the force transducer and the upper compression plate is mounted. The Zwick Z010 is equipped with a displacement measurement system at the moveable cross bar, as well as with extension sensors for small displacements. The accuracy of the extension sensor is significantly higher, because it is not affected by deformations of the cross bar and the force transducer. The sensor is also adjusted to small displacements, thus offering a higher resolution. As the distance between the two compression plate surfaces is too small to attach the two arms of the sensor, they are positioned above, respectively below the plates. The deformation of the compression plates themselves was neglected, because they are made of steel and therefore have a higher stiffness (approximately factor 10^5 higher) compared to the rubber materials.

The measurement cycle started with the application of a pre-load (1 N). Then the test specimen was compressed for 1.5 mm, this equals a strain of 15 %. Compression speed was set to 1 mm/min to achieve a strain rate of 10 %/min. After this cycle, a short-time relaxation cycle was added with a compression strain of 10 % for 15 min.

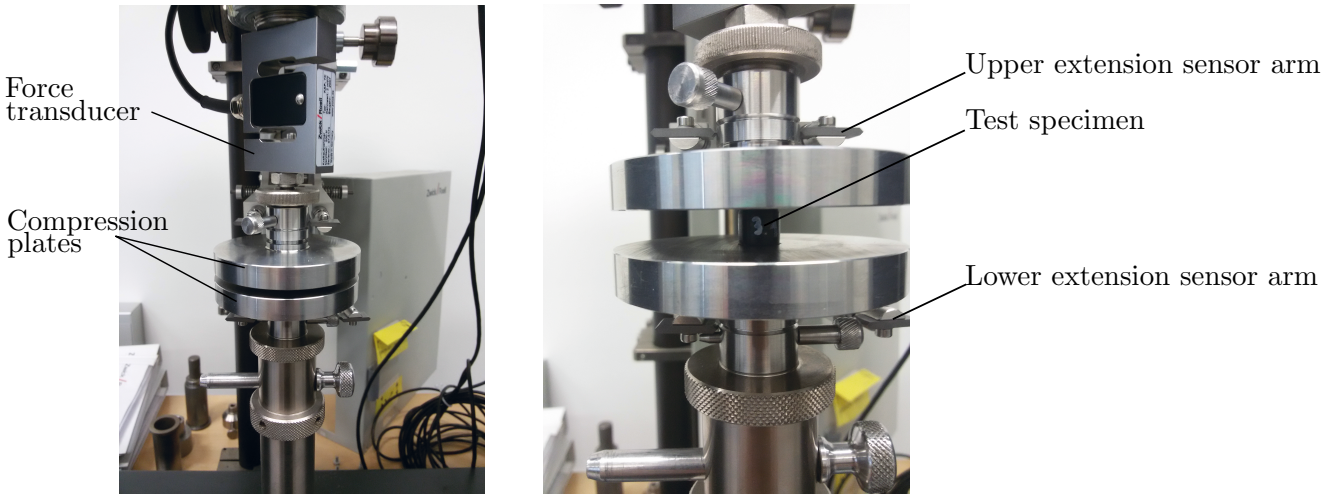

(a) Force transducer and compression plates

(b) Displacement measurement with the extension sensors

Figure 3.16: Set-up of the compression test measurement on a universal tensile testing machine

Compression stress measurement of the H-NBR rubber

In Fig. 3.17 the results of three consecutive measurements of the H-NBR rubber are shown. The load curves (see Fig. 3.17a) are very linear and congruent, thus the assumption of a low variation of the mechanical properties within the sample and a linear material behaviour up to a strain of 15 % is valid. The unloading curve differs from the load curve, because of relaxation mechanisms. The resulting hysteresis is caused by the visco-elastic material behaviour of the rubber. This is demonstrated with a short-time relaxation measurement. In Fig. 3.17b a measurement at a compression strain of 10 % is shown. In particular at the beginning (first minute) the fastest relaxation rate occurred. This mechanism is overlaying the compression stress measurement and causing the observed hysteresis.

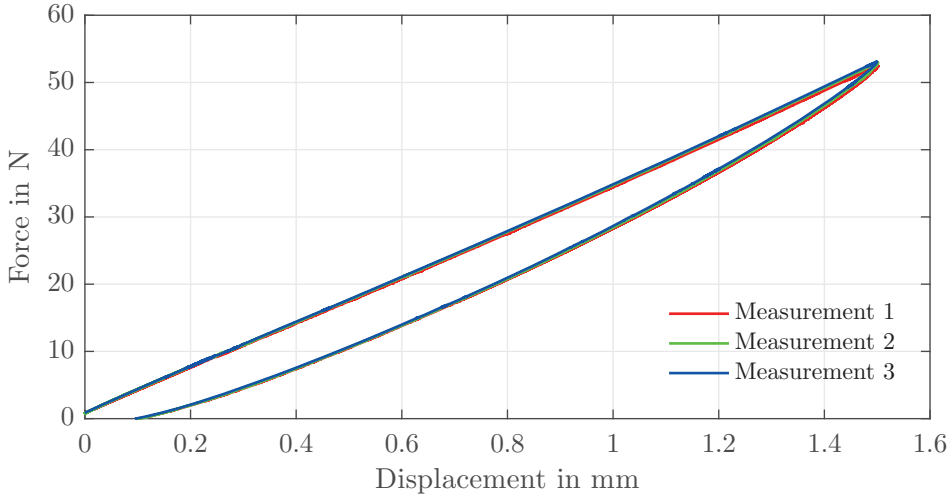

(a) Compression stress measurement

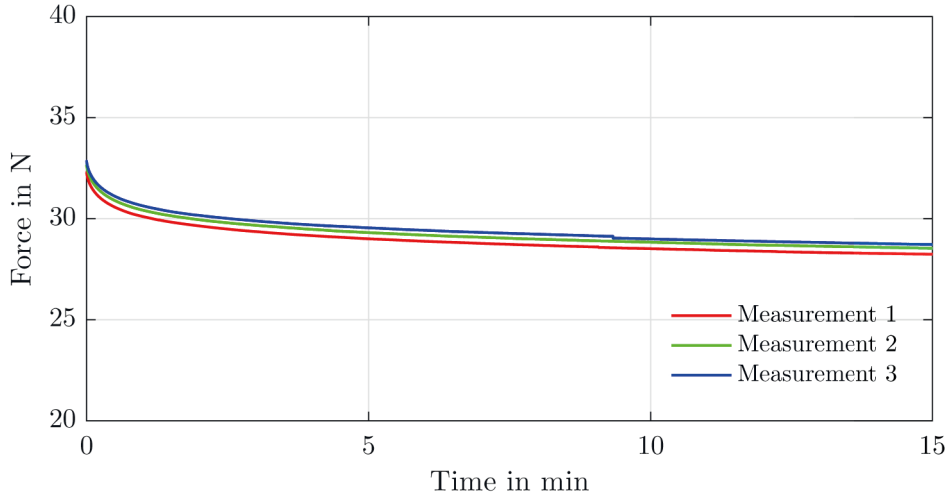

(b) Relaxation of compression stress at a strain of 10 %

Figure 3.17: Material characterisation of H-NBR rubber on the tensile testing machine

Compression stress measurement of the FKM rubber

The results of corresponding measurements of the FKM rubber are shown in Fig. 3.18. The curves are very congruent, indicating again a low variability of the mechanical properties within the sample. The load curve of the compression stress measurement (see Fig. 3.18a) is very linear, thus the material behaviour can be assumed as linear within a strain of 15 %. The unloading curve differs a little bit less compared to Fig. 3.17a, indicating the relaxation mechanisms of the FKM rubber being slower. This is confirmed by the short-time relaxation measurement (shown in Fig. 3.18b). The relaxation force of the H-NBR rubber decreases below 30 N within approximately 1.5 min to 2.5 min compared with more than 14 min at the FKM rubber.

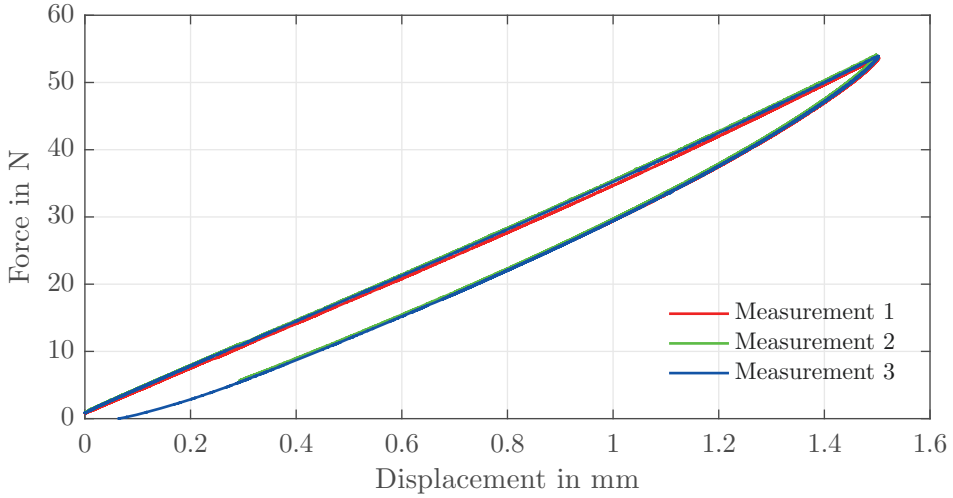

(a) Compression stress measurement

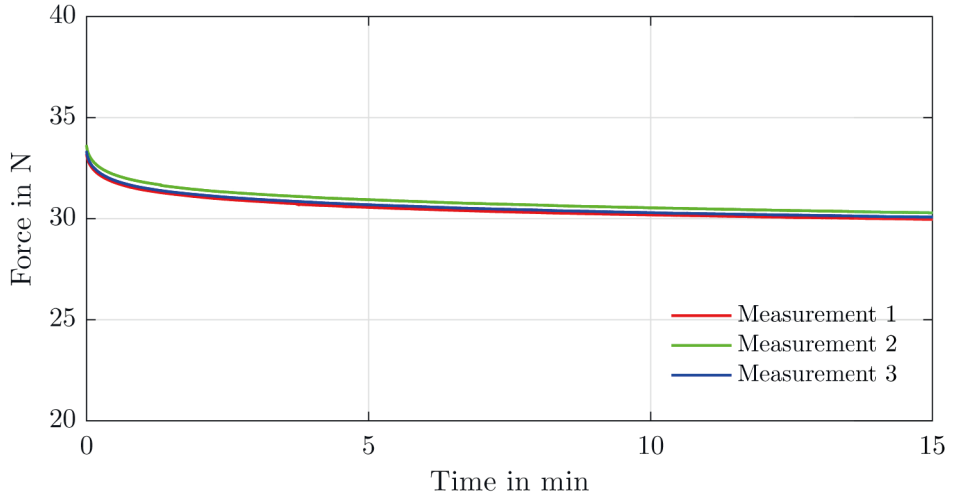

(b) Relaxation of compression stress at a strain of 10 %

Figure 3.18: Material characterisation of FKM rubber on the tensile testing machine

Results of the compression stress measurement

Both materials showed a linear compression stress curve up to 15 % strain. From these results material data for further calculations could be derived. The results of the short-time relaxation measurement indicated a significant relaxation at a strain of 10 %. As this was the determined strain of the ElastoSpring prototypes further evaluation was necessary. Additionally, the influence of higher temperatures on the observed material behaviour had to be measured.

3.6.2 Long-time relaxation of compression stress measurement

The observed relaxation behaviour demanded further investigation, due to the long and constant load of the ElastoSpring during its lifetime. Therefore a long-time relaxation measurement at a specific strain level and various higher temperatures was desired. For this purpose a custom-made measurement device was available. The measurement system (see Fig. 3.19) was initially developed to measure creep of PTFE compounds at specific compression stress levels (see [2]). The pneumatic cylinders ap-

ply the stress on the compression test specimen. The force transducer measures the resulting force and controls the applied pressure. The creep displacement is measured by three displacement sensors. This set-up could be modified to measure relaxation. To do so two displacement limiters were added. By applying enough pressure to deform the compression test specimen to the distance limiter, the force transducer recorded the relaxation of the resulting force. As the whole set-up was mounted in a hot-air oven, the measurement could run at higher temperatures (up to 250 °C). The initial set-up is determined to measure the creep behaviour of PTFE, thus the full scale of the force transducer is 5 kN. The expected resulting forces during the relaxation measurement of the rubber materials were far lower. Therefore six test specimens have been measured together at one pneumatic cylinder to shift the resulting forces to a higher level. This was necessary to achieve a higher accuracy with the force transducer, because it was measuring at the lower limit of the measurement range (below 1 % of the full scale). The results were divided by six to compare them to the results shown in Fig. 3.17.

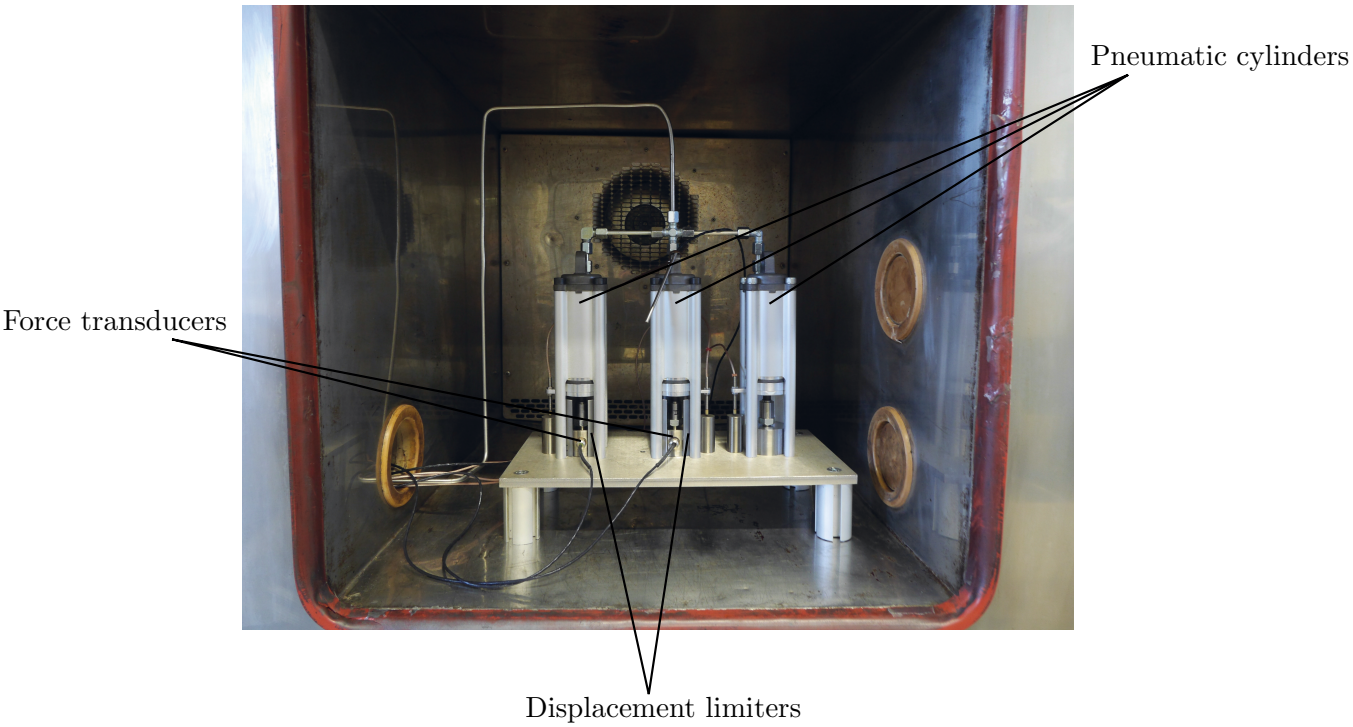

Figure 3.19: Set-up for long-time relaxation measurement

Due to the operational conditions of the ElastoSpring, measurements at temperatures of 26 °C, 80 °C and 160 °C have been planned. For each temperature level the same six test specimens have been used. The results are shown in Fig. 3.20. The first measurement (see Fig. 3.20a) was stopped after 16 h, because the relaxation rate was very slow. The maximum value (peak at the beginning) differs from the measurement on the Zwick tensile testing machine. This is caused by the higher accuracy of the force transducer used in the tensile testing machine (full scale: 500 N) compared with the force transducers in the relaxation measurement set-up (full scale: 5 kN). Also the surrounding temperature was slightly higher, influencing the stiffness of the material. Both materials show the same relaxation rate. The measurement at 80 °C (see Fig. 3.20b) starts at a significantly higher force. The H-NBR sample has about the same relaxation rate as at 26 °C. After approximately 40 h the measured force is nearly constant. The relaxation rate of the FKM sample is higher than at 26 °C and is not constant after 96 h. The measurement at 160 °C is starting again at higher force levels. The H-NBR sample has a higher relaxation rate than at 80 °C and is not constant after 96 h. The FKM sample shows an unexpected fast relaxation. This indicates a material failure, because according to [13] it should show a higher temperature stability than the H-NBR rubber.

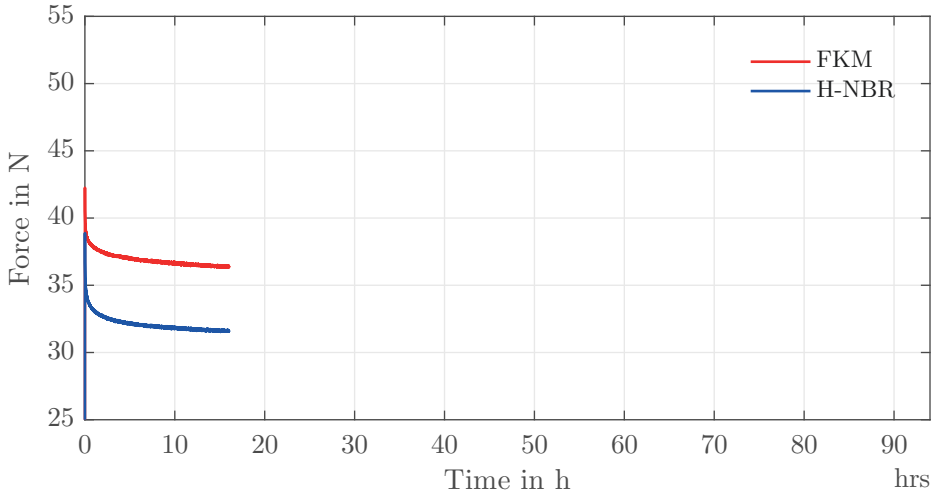

(a) Relaxation at 26 °C for 16 h

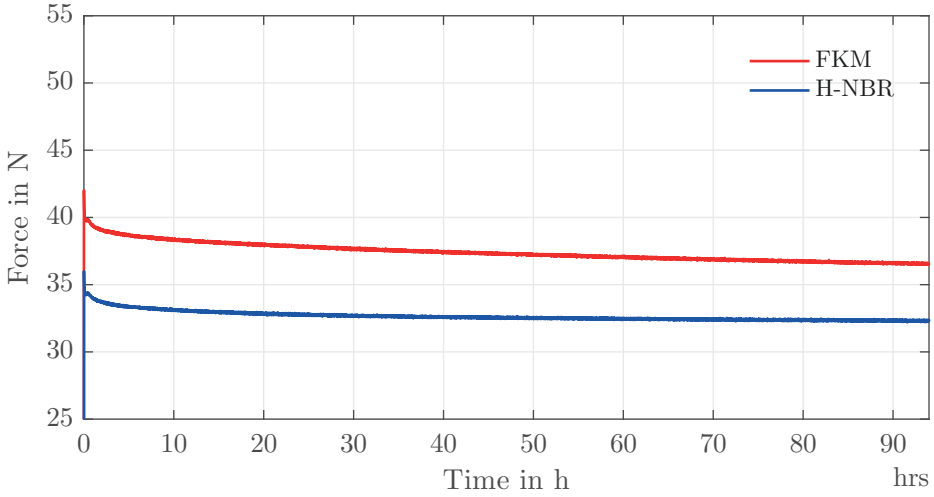

(b) Relaxation at 80 °C for 96 h

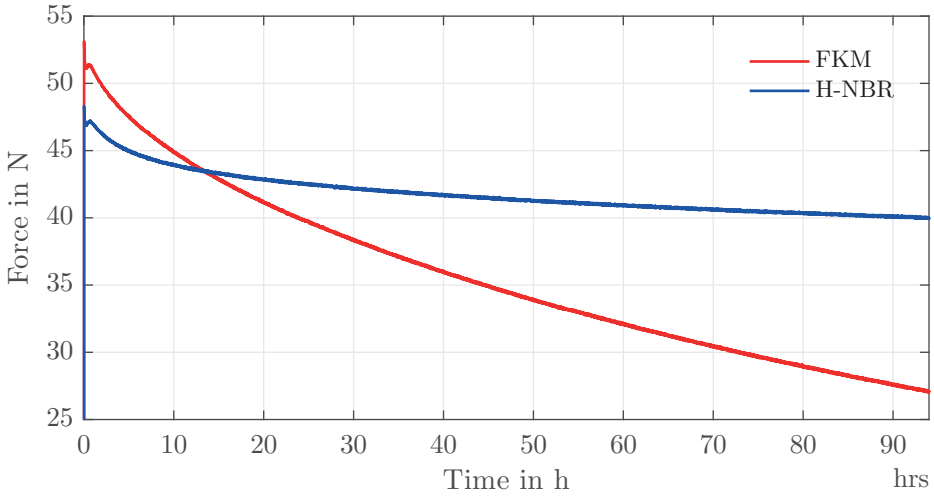

(c) Relaxation at 160 °C for 96 h

Figure 3.20: Relaxation of compression force at three different levels of temperature

The relaxation was evaluated in conformity of [1]. The stress relaxation in % at a defined time t is given by

$$R_t = \frac{F_0 - F_t}{F_0} \times 100, \tag{3.3}$$

where F_0 is the force after 30 min and F_t the force at a specific time t (in h).
In Tab. 3.10 the results for both materials at the three different temperatures are shown. Both materials showed a significant relaxation already at 26 °C and after 16 h. At 80 °C the relaxation rate R_{16} was lower for both materials. This is caused by the temperature-mechanical behaviour of rubbers. The higher entropy blocks the molecular movement of the macromolecules, thus leading to an increase in stiffness (see [15]). Also the initial force F_0 at the beginning of the measurement was higher. The relaxation rate R_{96} of the H-NBR rubber showed only a small increase, indicating a near plateau of its relaxation process. The relaxation rate R_{96} of the FKM rubber did not indicate a plateau of its relaxation process. At 160 °C the relaxation rates R_{16} were higher, especially for the FKM rubber. The H-NBR rubber was at its limit of the operational temperature (see [14]) and chemical processes began to alter the material properties, thus leading to an increased relaxation rate. The FKM rubber showed a failure-like behaviour. After 96 h the relaxation rates R_{96} were doubled for the H-NBR, indicating a further relaxation beyond this timespan. The FKM rubber lost 57.3 % of its initial stiffness.

Table 3.10: Results of the compression stress relaxation measurement

		F_0 in N	F_{16} in N	$\boldsymbol{R_{16}}$ **in %**	F_{96} in N	$\boldsymbol{R_{96}}$ **in %**
26 °C	**H-NBR**	38.15	36.43	**4.72**	-	-
	FKM	33.58	31.58	**6.33**	-	-
80 °C	**H-NBR**	34.31	32.94	**4.16**	32.35	**5.95**
	FKM	39.78	38.12	**4.35**	36.57	**8.42**
160 °C	**H-NBR**	47.10	43.23	**8.95**	40.04	**16.33**
	FKM	51.33	42.49	**20.80**	27.03	**57.19**

Results of the long-time relaxation measurement

The relaxation processes were effectively changing the stiffness of the material. As the material stiffness was used to develop an elastomer spring, this property was critical to the function of the ElastoSpring concept. By measuring and quantifying the impact of the relaxation on the material behaviour a proper design was still possible. Therefore the relaxation rate had to be considered in the initial design of the ElastoSpring concept. The measurement duration of 16 h at 26 °C or 96 h at 80 °C and 160 °C was too short to qualify the material for a lifetime of up to three years. Further investigation with a longer measurement duration is necessary, to find plateaus where the relaxation effectively stops. The very fast relaxation of the FKM rubber at 160 °C was indicating a material problem. This could by caused by a low cross-linking density of the produced test specimen. A heat treatment of injection moulded rubber parts can post cross-link the material and thereby influence the relaxation mechanism.

3.7 Material modelling

The material characterisation regarding the application of the material showed effects, which have to be included in the design of the ElastoSpring concept. This means the preliminary design (see Sec. 3.3) had to be extended. The used Young's modulus in tension (given in [13] and [14]) could be

combined with the information of the compression stress measurement (see Sec. 3.6.1) and the long-time relaxation of compression stress measurement (see Sec. 3.6.2). The goal of this task was to verify how a material model gathered by measurements of test specimens could predict the behaviour of an ElastoSpring prototype. As calculation tool an FEM (Finite Element Method) software (Abaqus/CAE 2016) was used. The task was to

1. derive a material model for the FKM rubber,
2. make a FEM model calculation for one prototype and
3. compare measurement and calculation.

With this task it was desired to evaluate the possibilities of simulating the mechanical behaviour of rubber parts.

3.7.1 Material model for the FKM rubber

The FKM rubber can be described as a visco-elastic body. It is elastically deformable with a time dependent relaxation of the deformation force. These are two different effects and are considered separately.

Modelling of the elastic behaviour

From the compression stress measurement (see Fig. 3.18) a nominal stress-strain curve was derived. As the curve is very linear up to 15 %, four points are enough to approximate the behaviour. The nominal stress σ is calculated by

$$\sigma = \frac{F}{A} \tag{3.4}$$

where F is the measured compression force and A is the initial cross-sectional area of the test specimen. The strain ε is calculated with

$$\varepsilon = \frac{h_0 - x}{h_0} \tag{3.5}$$

where h_0 is the initial height of the test specimen and x is the displacement. In Tab. 3.11 the four stress-strain values of the compression measurement and the known stress-strain value for tension are shown. The value at a strain of $\varepsilon = 1$ is the given modulus from the data sheet (see [13]). In Fig. 3.21 the measured and the given stress-strain value pairs are shown. One can see, that the stress strain curve is non-linear. The Young's modulus of compression is stiffer than the given modulus of tension.

Table 3.11: Nominal stress-strain values for compression and tension of the FKM rubber

Stress σ in N/mm^2	**Strain ε in absolute**
-0.7	-0.15
-0.545	-0.12
-0.3	-0.08
-0.183	-0.04
0	0
2.1	1

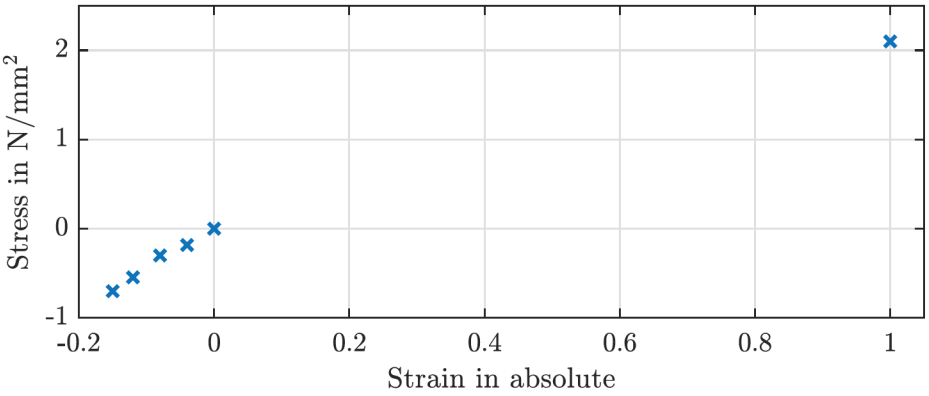

Figure 3.21: Stress-strain value pairs of the FKM rubber

According to [16] there are various effects, which are to describe. A material model for non-linear elastic and incompressible behaviour is called hyper-elastic and describes the short-time behaviour. This material model derives the stress-strain relationship from the strain energy density W. In the approach of Rivlin (see [16]), a polynomial describes the deformation in dependence of the invariants of the Cauchy-Green tensor.

$$W = \sum_{i+j=1}^{N} C_{ij}(I_1 - 3)^i (I_2 - 3)^j \tag{3.6}$$

with:
C_{ij} Material parameter
N Degree of order of the polynomial
I_1, I_2 First and second invariants of the Cauchy-Green tensor

The Cauchy-Green tensor describes the stretching conditions λ_1,λ_2 and λ_3 of the material in the principal axis. The first invariant I_1 is describing the change in length of an observed cube, the second invariant I_2 describes the change of the surface. The relationship between stretching λ_i and strain ε_i is

$$\lambda_i = 1 + \varepsilon_i \tag{3.7}$$

with $i = 1, 2, 3$ as principal axis of stress.

The simplest material model of this approach is the Mooney-Rivlin model with a polynomial degree of $N = 1$, it is formulated as

$$W = C_{10}(I_1 - 3)C_{01}(I_2 - 3). \tag{3.8}$$

It is suitable for strains ε of up to 100 %. The Marlow model (see [17]) assumes, that the strain energy density is independent of the second invariant I_2. This enables a smoother reproduction of the measurement data. The stress-strain relationship is calculated by a formal derivative of the strain energy density W with respect to the stretching conditions λ.

$$\sigma_{nominal} = \frac{\partial W}{\partial \lambda} \tag{3.9}$$

To enhance the material about the visco-elasticity, the material parameters C_{ij} are formulated as time dependent like

$$W = \sum_{i+j=1}^{N} C_{ij}(t)(I_1 - 3)^i (I_2 - 3)^j. \tag{3.10}$$

In Abaqus it is possible to enter the stress-strain value pairs and generate approximations with the mentioned models and specific variations thereof. To enhance the stability of the computation, the stress-strain value at $\varepsilon = 1$ was neglected, because there was no tension stress expected. In Fig. 3.22 various approximations for the values in Tab. 3.11 are shown. The most stable material model was the Marlow-model. For further calculations this one is used.

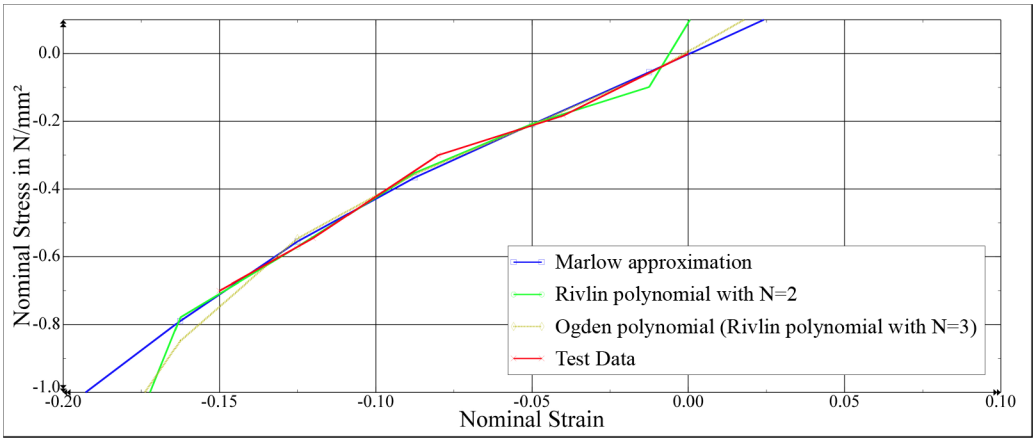

Figure 3.22: Approximation of material behaviour with various material models

Modelling of the relaxation behaviour

The time dependency of the material parameters C_{ij} can be described with a Prony-series:

$$C_{ij}(t) = C_{ij}^0 \left\{ 1 - \sum_{i=1}^{N} g_i \left[1 - e^{\left(-\frac{t}{\lambda_i}\right)} \right] \right\} \tag{3.11}$$

with:
C_{ij}^0 Material parameter at time $t = 0$
g_i, λ_i Material parameters of the Prony-series

Further material effects, like the compressibility, were neglected. The compressibility is important to consider if the observed part has no volumetric degree of freedom like an O-Ring or other sealing components. Therefore the Poisson ratio was as $\nu = 0.5$. From the relaxation measurement shown in Fig. 3.20a the necessary data was derived. With

$$\sigma = \frac{F}{A} \tag{3.12}$$

$$E = \frac{\sigma}{\varepsilon} \tag{3.13}$$

the Youngs' modulus E at various times was calculated from the measured force F and the cross-sectional area A of the test specimen. The approximation of the relaxation behaviour is calculated in

Abaqus with the shear modulus G. The following correlation to the Young's modulus E (see [16]) is valid for isotropic materials.

$$G = \frac{E}{2(1+\nu)} \tag{3.14}$$

with:
ν Poisson ratio

Additionally, it was necessary to normalise the shear modulus to its initial value. In Tab. 3.12 the relaxation data for the approximation is shown.

Table 3.12: Relaxation data of the FKM rubber at 26 °C for 16 h

Time in h	**Force in N**	**Stress in N/mm²**	**Young's modulus in N/mm²**	**Shear modulus in N/mm²**	**Normalised shear modulus**
0	38.20	0.486	4.864	1.621	1.000
0.9	34	0.433	4.329	1.443	0.890
2	33.5	0.427	4.265	1.422	0.877
4	33.1	0.421	4.214	1.405	0.866
6	32.9	0.419	4.189	1.396	0.861
8	32.8	0.418	4.176	1.392	0.859
10	32.7	0.416	4.163	1.388	0.856
12	32.6	0.415	4.151	1.384	0.853
14	32.5	0.414	4.138	1.379	0.851
16	32.45	0.413	4.132	1.377	0.849

The approximation of the relaxation behaviour is shown in Fig. 3.23.

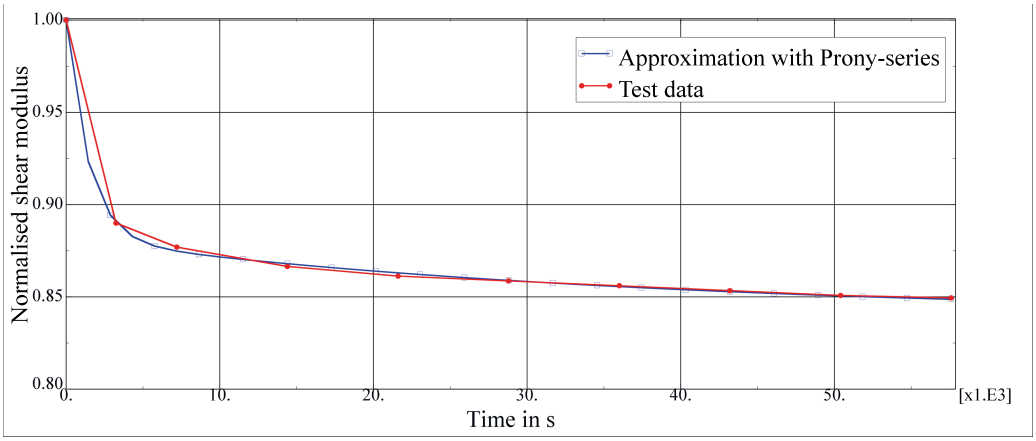

Figure 3.23: Approximation of relaxation behaviour with a Prony-series

3.7.2 FEM simulation of test specimen and ElastoSpring

An FEM simulation enables to compute stress and strain distributions in complex geometries, which are not analytically calculable. Furthermore, material models as shown in Sec. 3.7.1 are includable. To compare the material model with the measured data the test specimen and the more complex geometry of an ElastoSpring prototype were simulated.

FEM simulation of the test specimen

The test specimen was a cylinder with diameter $d = 10\,\text{mm}$ and height $h = 10\,\text{mm}$. This geometry is symmetrical around the centre axis of rotation. Therefore an axisymmetric and planar shell model was sufficient to build the geometry. In Fig. 3.24a the model with its constraints is shown. At the bottom line the fixed constraints (blue and orange triangles) fixed the location of the geometry. On the upper side the direction of the displacement is indicated (long orange arrow). Both surfaces suppressed radial movements of single nodes. This boundary condition is conform with a very high friction coefficient between the surfaces. The observation of the compression stress measurement confirmed this assumption, as a clear bulging of the cylindrical test specimen was visible. In Fig. 3.24b the Van-Mises stress distribution and the deformation after a displacement of 1 mm are shown. The summation of all nodal forces on the upper side of the model yielded the reaction force, which was necessary to compare the results with the measurement.

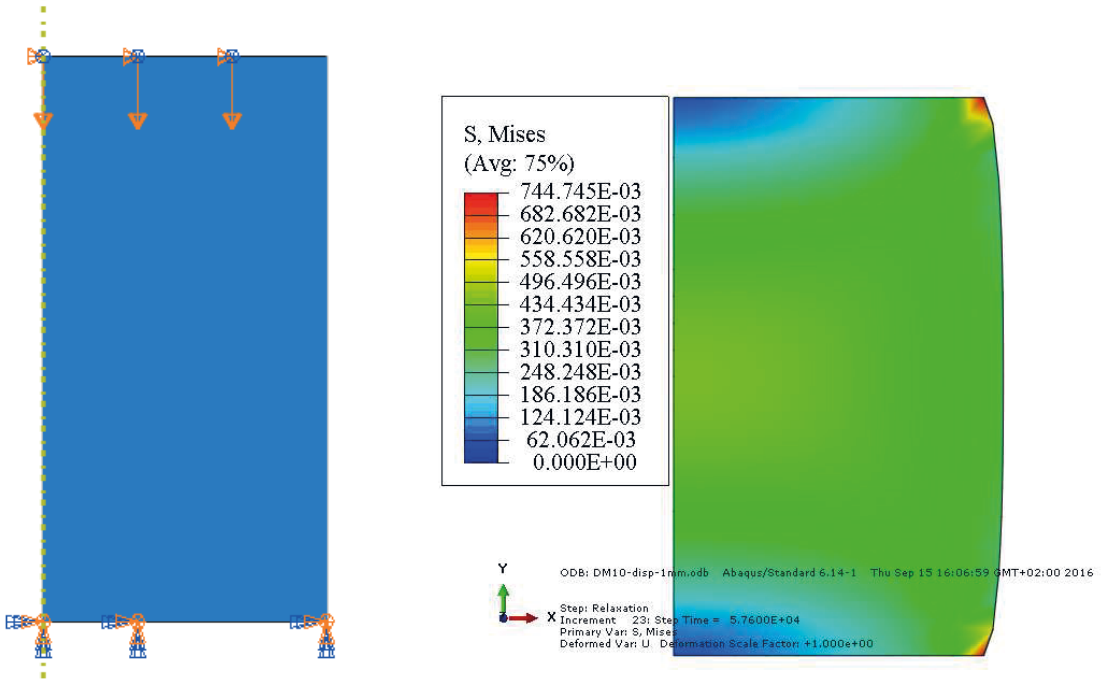

(a) Model of FEM simulation in Abaqus with boundary conditions

(b) Compression stress (in MPa) distribution at 1 mm displacement and time $t = 0$

Figure 3.24: FEM simulation in Abaqus of cylindrical test specimen

FEM simulation of an ElastoSpring design

The advantage of the FEM software is to calculate complex geometries. In Sec. 3.3 the design of the ElastoSpring was approximated as cylinders. This neglected the stress distribution in the combining ring. Therefore it was decided to calculate one design with the FEM software and the material model for the FKM rubber. The ElastoSpring design with eight cylinders and a height of 4.5 mm was chosen. The design had to be modelled with a 3D mesh, because there is no rotational symmetry. To spare computation time, the model was divided in a quarter sectional model with according symmetry boundary conditions. The model with its boundary conditions is shown in Fig. 3.25a. The result of the simulation with a displacement of 0.5 mm is shown in Fig. 3.25b. The resulting force was gathered by summation of the nodal forces on the upper side of the cylinders.

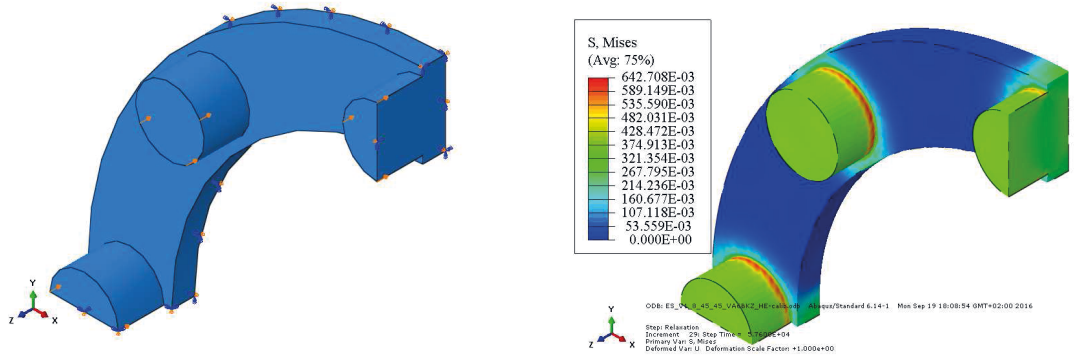

(a) Model of the ElastoSpring concept FEM simulation in Abaqus with boundary conditions

(b) Compression stress distribution of the ElastoSpring concept at 0.5 mm displacement and time $t = 0$ (initial force)

Figure 3.25: FEM simulation in Abaqus of the ElastoSpring concept

3.7.3 Comparison of FEM simulation and measurement

The FEM simulation is a discrete approximation of the continuous reality. Thus differences were expected. As the implemented models additionally based on assumptions like neglecting the compressibility an evaluation of the simulation results was necessary.

Comparison of the test specimen

In Fig. 3.26 the simulated resulting compression force at a displacement of 0.5 mm is shown. To compare it with the measurement, the results from the long-time relaxation measurement are added. The maximum force at the beginning of the measurement is matching very close. The maximum force calculated is 39.68 N and the maximum force measured is 40.09 N, which is a difference of 1 %. The calculated relaxation behaviour deviated stronger from the measured relaxation behaviour. The relaxation at the FEM simulation was slower at the beginning and showed overall less reduction of the compression force. The difference after 16 h was 1.38 N, which was a difference of 4 %. The difference may have been caused by a generally stiffer behaviour of the computation (discrete number of freedom) compared to the measured test specimen. A difference of 4 % was still valid for a helpful preliminary design process.

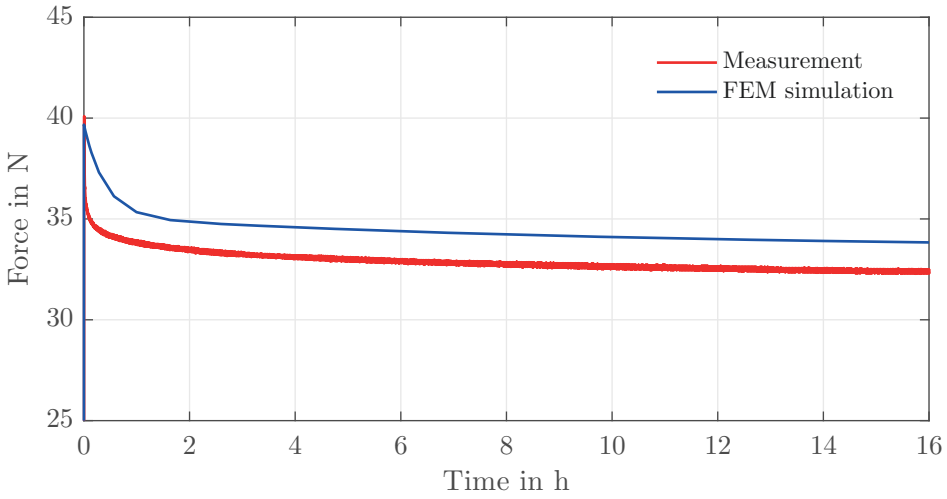

Figure 3.26: Comparison of simulated and measured compression force of the test specimen over time

Comparison of the ElastoSpring design

In Fig. 3.27 the results of the simulated compression force at a displacement of 0.5 mm and the corresponding measurement are compared. The measurement of the compression force was done on the Zwick tensile testing machine (see 3.6.1), because the part was too large for the relaxation measurement set-up. Therefore the measurement was limited to room temperature. The maximum compression forces differed by 2.5 N, which is less than 4 %. The calculated relaxation showed again the characteristic of a slower relaxation rate at the beginning of the compression and less reduction of the compression force. The difference after 16 h was 7.5 N, which was a difference of 13 %.

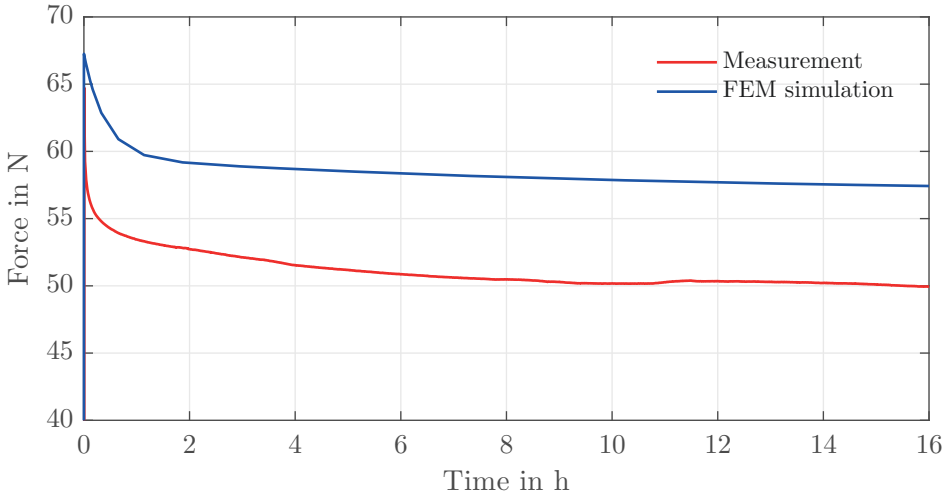

Figure 3.27: Comparison of simulated and measured compression force of the ElastoSpring concept with eight cylinders and height $h = 4.5$ mm

The shape of both curves in Fig. 3.27 is very similar, thus the difference can be considered as constant.

3.8 Conclusion

In this chapter it was described how the concept of replacing a metallic spring by a polymer spring can be implemented and evaluated. At first the specific requirements regarding the function and the material have been discussed. As a solution a simple concept was presented. A focused material selection and a preliminary design, together with a manufacturing concept led to a series of prototypes. The used material was further investigated with regard to unknown material properties. The reverse engineering shown in the material modelling section enabled a more precise design of new prototypes.

To enhance the concept of the polymer ElastoSpring various information gathered during this process can be used. First of all, the working principle can be verified. The polymer spring provides an axial pressure under axial displacement. The problems during the sampling can be solved by small changes of the design. It is recommended to add a draft angle to the cylinders (5° or more), to improve the demoulding of the parts. Additionally, the runner of the test mould should be reworked. The hole of the runner and the nozzle side should be reamed to smooth the surface. Furthermore, the usage of an appropriate size of the injection moulding machine reduces the sampling effort.

The material characterisation showed, that the material performance is heavily time and temperature depending. The relaxation measurement should be extended by longer measurement times, to gather a better prediction with regard to the lifetime of the product. Additionally, the impact of oil swell on the material properties has to be investigated.

The procedure shown in Sec. 3.7 should be extended by the H-NBR rubber and longer measurement periods of the relaxation behaviour. Also the temperature dependency should be implemented, because the product environment demands it. The preliminary design of new prototypes (e.g. with a draft angle) should be calculated with the material models and an FEM simulation.

4 New ring designs

There are two reasons why new ring designs are required. The first reason is to minimise the production costs. As the wiper material is maintained and therefore offers no opportunity to cut costs, the best way to do so is minimising the production effort. The effort is mainly generated by machining time and assembling of the single parts. To effectively reduce the machining time, it is essential to reduce the number of single parts forming the oil wiper ring. Fewer single parts also simplify the assembling. The second reason is to improve the oil wiping performance. As mentioned in [10] the current product has performance problems in compressors used in the PET blow moulding industry. Therefore new ring designs with changed geometry of wear compensation, wiping edge or number of wiping edges are presented. Concepts addressing these aims are shown in Sec. 4.1.

The reason of fabricating the oil wiper ring of multiple parts is the wear compensation. Multiple parts enable to compensate the wear geometrically. A concept of compensating the wear by deformation of the ring itself is shown in Sec. 4.2.

4.1 Cut wipers

The wear compensation mechanism of the OFD wiper is very elaborative to manufacture. Thus the reduction of the production costs is best achieved with reducing the number of parts to manufacture. The concepts shown in Sec. 4.1.1 to 4.1.3 were designed with regard to this consideration. The concept shown in Sec. 4.1.4 is a replacement of an existing ring design with a metallic wiper ring by a polymer ring design with the same geometry. This inhibits the advantage of a known manufacturing process.

4.1.1 Concept with tangential cut

This concept is called tangential wiper and consists of a two part ring (see Fig. 4.1). The two parts have the same shape and overlap each other. The overlapping is necessary to form a tight geometry, preventing any leakage paths for the oil. The tangential cut (shown in Fig. 4.2) enables a tangential movement of the two parts towards each other. This wear compensation movement is powered by the garter spring around the circumference of the ring, which is constantly pressing the two parts towards each other and thereby also ensuring the contact to the piston rod. An axial lug spring presses the ring against the cup surface, to seal any flow paths through the wiper cup. As axial lug spring the existing metallic lug spring or the ElastoSpring concept are possible. On the backside of the ring segments (see Fig. 4.2b) a step centres the axial spring. A wiper packing consists of two rings consecutively arranged in one wiper cup. The production drawing is shown in Appendix, Sec. 7.7.

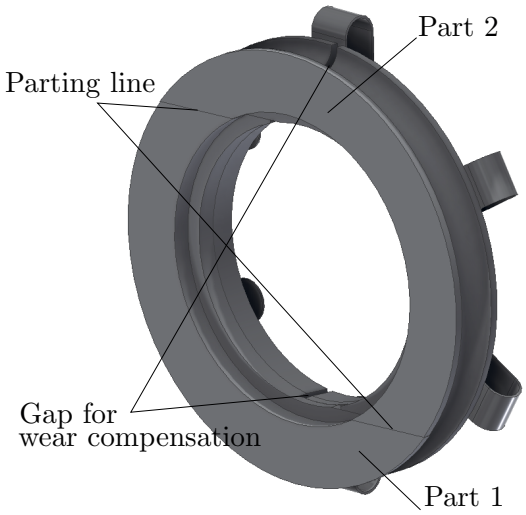

Figure 4.1: Concept with tangential cut for wear compensation

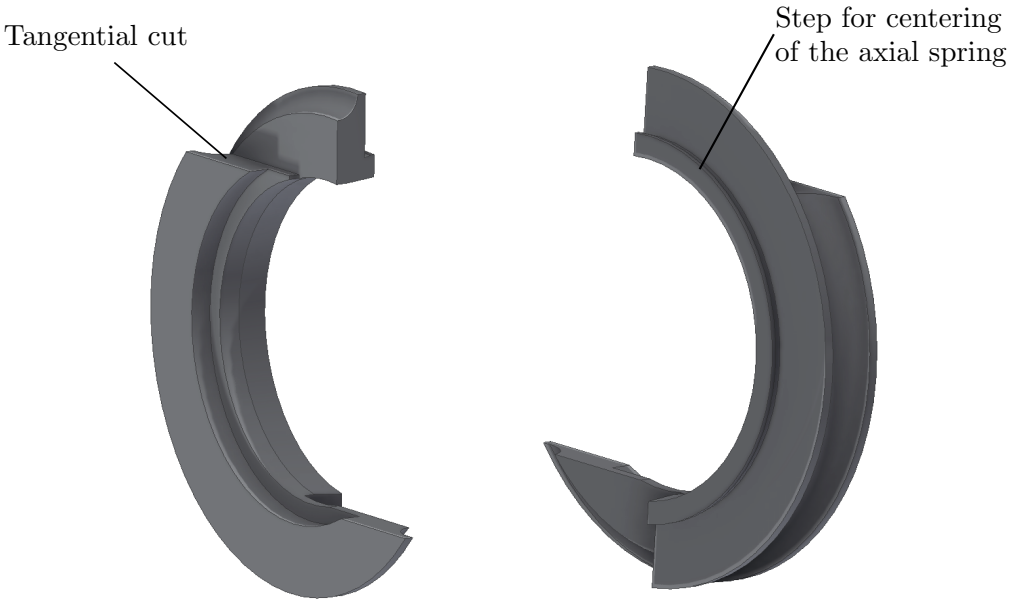

(a) Front side view of a single part of the tangential cut wiper concept

(b) Back side view of a single part of the tangential cut wiper concept

Figure 4.2: Front and back side view of a single part of the tangential cut wiper concept

4.1.2 Concept with gas tight cut

This concept is similar to the concept described in Sec. 4.1.1. The difference is in the geometry of the wear compensation (see Fig. 4.3). The two-part ring is overlapping in two radial pockets, covering any flow paths (see Fig. 4.4). This design is also found in piston rings because it is gas tight. This means a one sided applied pressure presses the single parts together and forms a gas tight barrier. Therefore the concept is called gas tight cut wiper. The wear compensation movement is powered by a garter spring around the circumference of the ring. Both, the metallic lug spring or the ElastoSpring are usable as axial springs for the sealing function. Again a wiper packing consists of two rings consecutively arranged in one wiper cup. The production drawing is shown in Appendix, Sec. 7.7.

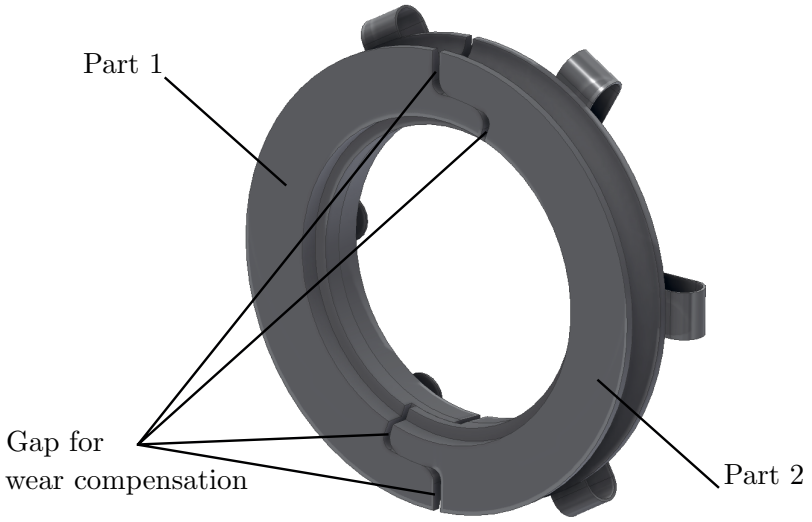

Figure 4.3: Concept with gas tight cut for wear compensation

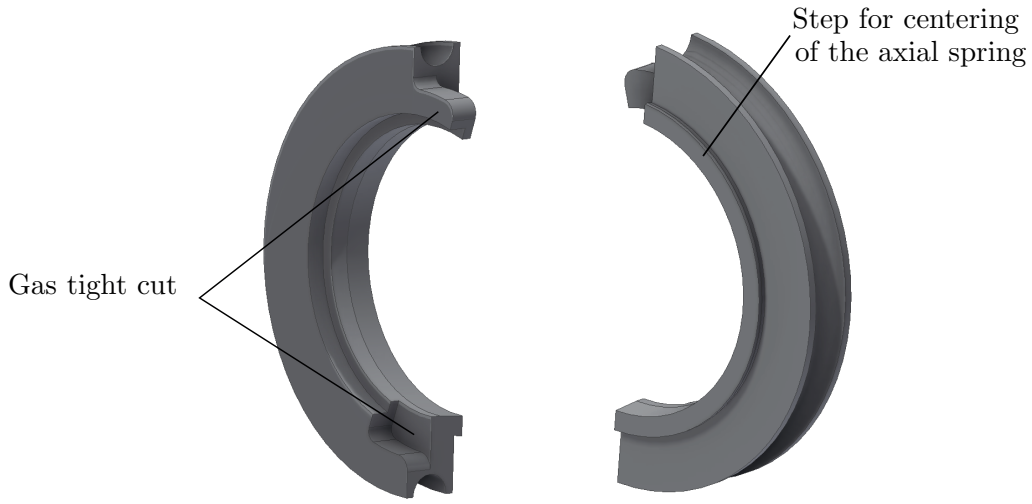

(a) Front side view of a single part of the gas tight cut wiper concept

(b) Back side view of a single part of the gas tight cut wiper concept

Figure 4.4: Front and back side view of a single part of the gas tight cut wiper concept

4.1.3 Concept with radial cut and additional wiping edge

This concept was developed to evaluate the influence of the geometry and the number of wiping edges on the oil wiping performance and is called double wiper concept (see Fig. 4.5). Each ring consists of two ring segments, overlapping each other with a radial cut (see Fig. 4.6). The oil gathered at the second wiping edge is vented through the ring via radial holes. Additionally, the oil wiping edges are pulled forward at each end (towards the wear compensation gap). The production drawing is shown in Appendix, Sec. 7.7.

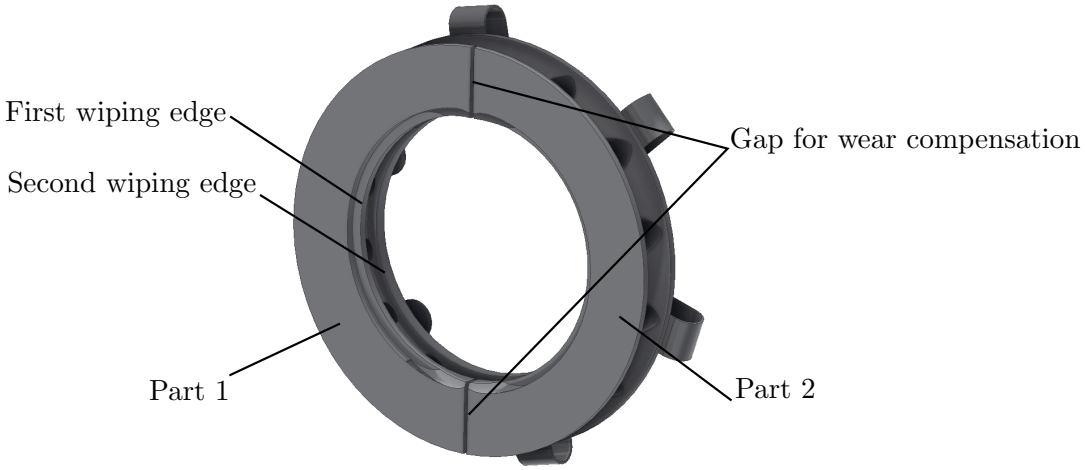

Figure 4.5: Concept with radial cut for wear compensation and additional wiping edge

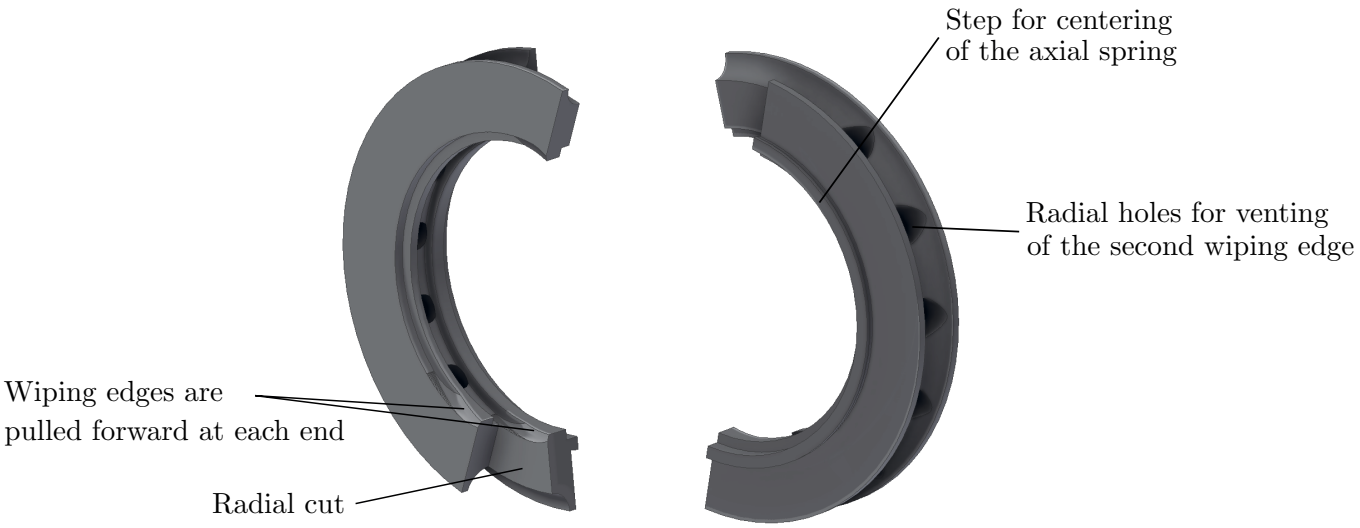

(a) Front side view of a single part of the double wiper concept

(b) Back side view of a single part of the double wiper concept

Figure 4.6: Front and back side view of a single part of the double wiper concept

4.1.4 Concept with radial cut and multiple wiping edges

This concept is based on an existing metallic wiper design and is called radial scraper. Contrary to the wiper designs shown in Sec. 4.1.1 to 4.1.3 it is floating within the crankcase. This means no axial

spring presses the wiper against the cup surface. A wiper ring consists of three segments, separated by straight radial cuts. A garter spring around the circumference of the wiper rings presses the wiper ring against the rod and enables wear compensation. Three rings together form a wiper packing where the gaps of each ring are angularly offset (see Fig 4.7). This covers all gaps in axial direction and no direct flow path for the oil film along the piston rod is given.

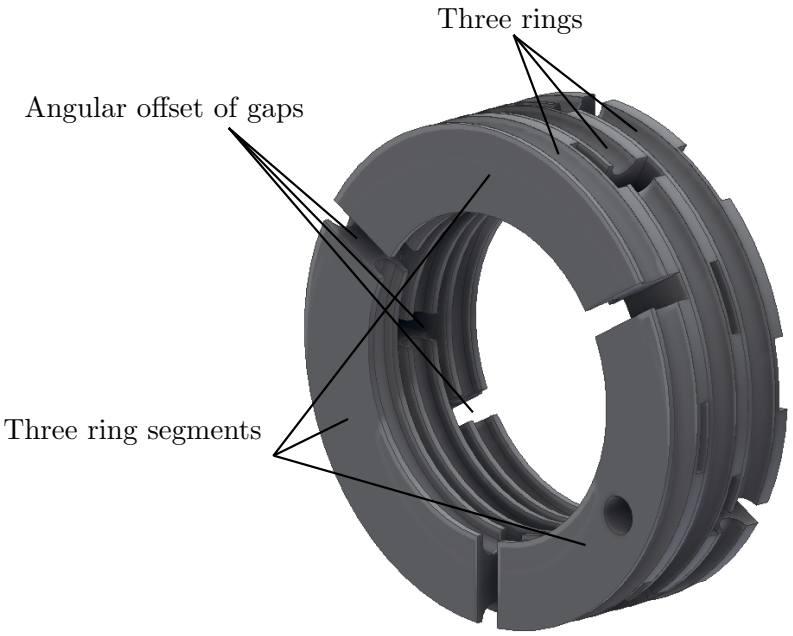

Figure 4.7: Concept with radial cuts for wear compensation and multiple wiping edges

The oil wiped off by any wiping edge can flow through the rings in radial direction into the cup via two milled pockets in each segment (see Fig 4.8). One segment additionally contains two holes, to pin the three separate rings together.

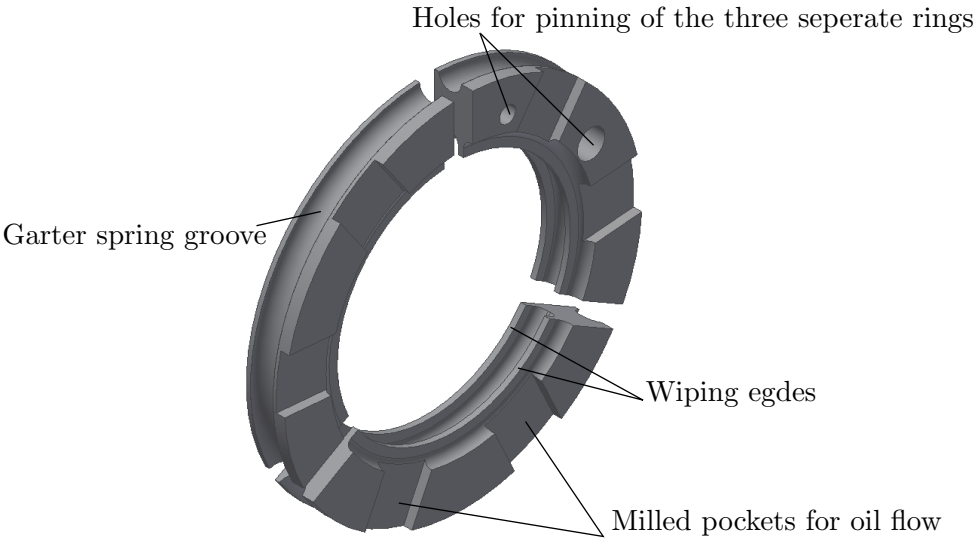

Figure 4.8: Single ring of concept with radial cuts for wear compensation and multiple wiping edges (view from the backside)

To manufacture this design, a multi-axis CNC lathe is necessary. The exact production drawing is shown in Appendix, Sec. 7.7. As there are tolerances in the manufacturing process, the width of the three rings together must be smaller than the cup width, which is also bound to manufacturing tolerances. The result of this chain of tolerances is that the wiper packing is floating within the wiper cup. Thus an oil leakage through the cup is possible. The exact investigation of the oil wiping performance is shown next.

Oil loss measurement of the radial scraper

The oil loss measurement of this concept was particularly interesting, because the floating of the oil wiper packing within the cup provides a direct flow path for the oil. Furthermore it was expected, that the axial space would cause an axial movement (shuttling) of the packing. This was measured with the shuttling sensor. The experimental procedure was done according to Sec. 2.2.2. In Fig. 4.9 the oil loss measurement of the experiment at 700 rpm is shown. The result of this experiment is shown in two graphs, because the amount of oil gathered in the measurement container was widely varying. The oil loss in the wiper cup (see Fig.4.9a) was very high, this led to short measurement times, because the measurement container was filled up. Additionally an oil loss of more than 2 l was endangering the constant lubrication of the cross head in the crankcase. Thus the experiment was terminated after 2.7 h. The high oil loss in the wiper cup was assumed to be caused by the missing sealing effect at the first ring and the wide gaps of 2.5 mm between the ring segments for the wear compensation. Such a high oil loss in the wiper cup is no problem during normal operation of the compressor, because the oil is guided back into the crankcase by a vent pipe. The oil loss in the pressure section (see Fig.4.9b) was unstable during the 1.5 h and stable for the rest of the measurement period.

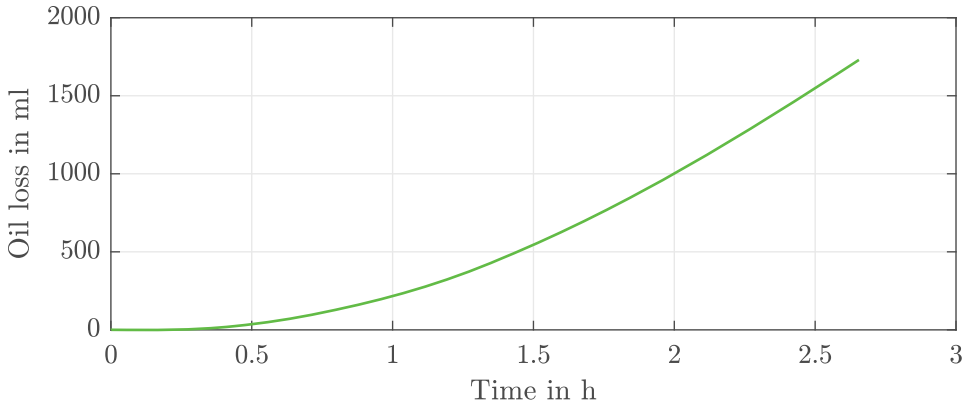

(a) Oil loss in the wiper cup

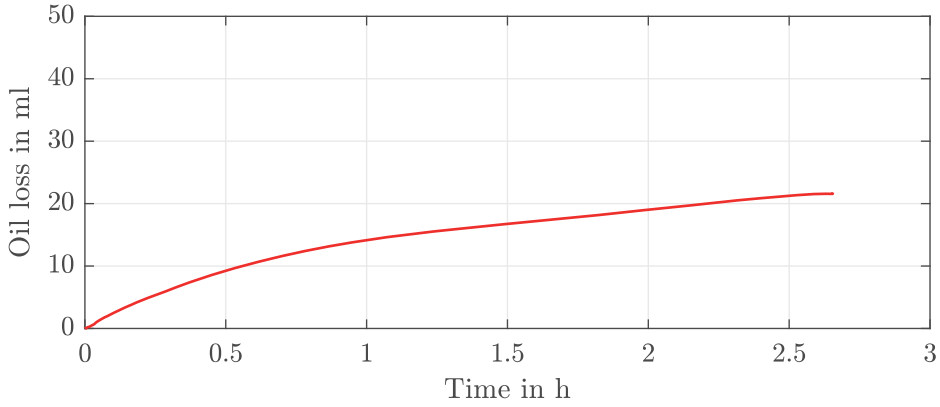

(b) Oil loss in the pressure section

Figure 4.9: Oil loss of experiment at 700 rpm for 2.7 h

According to Sec. 2.3, the continuously measured oil loss was split up in four equal intervals. Additionally due to the big difference of the results it was split up in a wiper cup and pressure section graph which are shown in Fig. 4.10. The oil loss rate in the wiper cup was increasing with measurement time. In contrast the oil loss rate in the pressure section was decreasing with time and was nearly constant after 1.5 h. Compared to the measurements shown in Sec. 2.3 the measurement duration of 2.7 h was very short. Thus it was decided to forgo the measurement of the oil loss in the wiper cup and use the oil loss in the pressure section for the evaluation of the wiper efficiency.

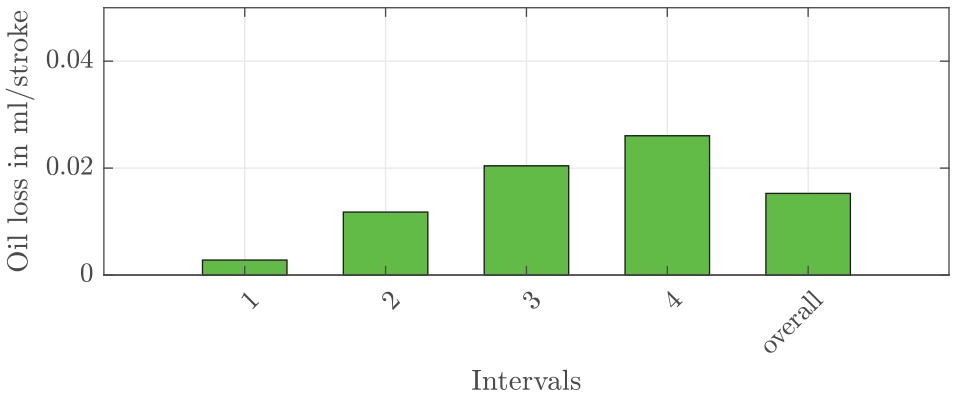

(a) Oil loss per stroke in the wiper cup

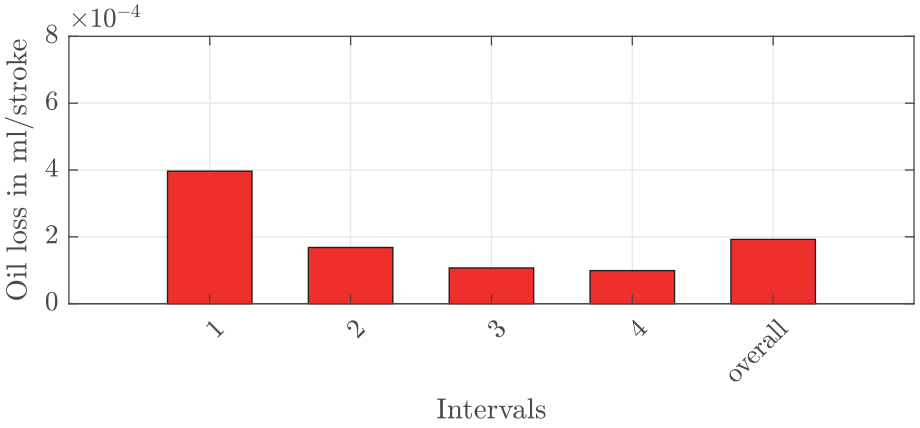

(b) Oil loss per stroke in the pressure section

Figure 4.10: Results of experiment at 700 rpm for 2.7 h

To measure the oil loss for 24 h it was necessary to modify the measurement set-up. The vent path for the measurement of oil loss in the wiper cup was closed and the oil guided back into the crank case. The measurement curve of the experiment at 700 rpm for 24 h is shown in the Appendix (see Fig. 7.14). The corresponding evaluation of the oil loss rates in four intervals showed that the oil loss is very low at the beginning (see Fig. 4.11b, interval 1), but increasing with time. It was stable after approximately 8 h. This oil loss rate is more representative and was used for evaluation of this wiper concept.

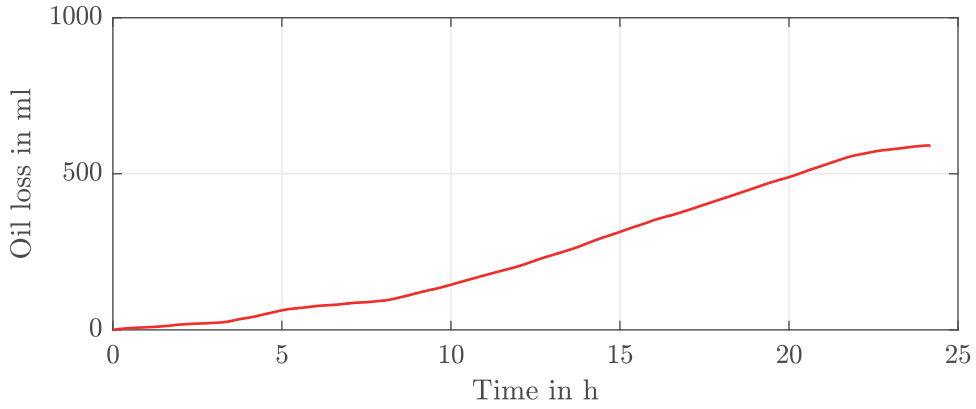

(a) Oil loss in the pressure section

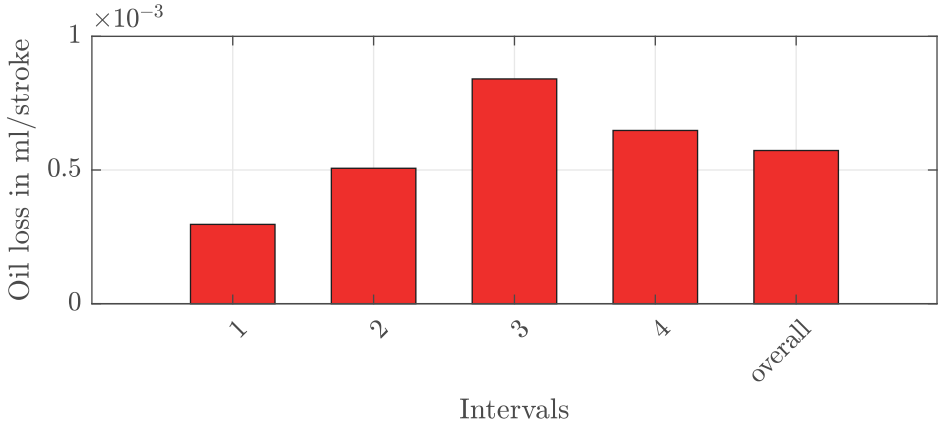

(b) Oil loss per stroke in the pressure section

Figure 4.11: Results of experiment at 700 rpm for 24 h

As mentioned before, an axial movement of the radial scraper wiper packing was suspected. This was confirmed by the measurement exemplarily shown in Fig. 4.12 (experiment at 700 rpm). The axial displacement given on the left axis is the axial movement within a measurement interval of 0.3 s each minute. The baseline offset is the minimum measured distance during this interval, indicating the initial position of the wiper packing. At the power-up this position was varying strongly, indicating that the wiper packing was floating backwards and forwards again. After this, a stable position was found. At approximately 2.5 h the wiper packing began to move stronger, the baseline offset was reaching a minimum. This means the wiper packing was moving towards the cup surface and fully contacting it. Simultaneously the magnitude of displacement was increasing. After approximately 8 h the baseline was stable at 0.072 mm. Thus the wiper packing was not in full contact with the cup surface. At the same time the axial displacement was reduced below 0.01 mm, indicating that the wiper packing was floating stably in this position in the wiper cup. The axial movement of the wiper packing shown in this measurement was sporadically occurring during the other measurements of the radial scraper. There was no interaction detectable between the measured oil loss and the shuttling of the radial scraper packing. During phases of strong axial movements no kinks occured on the oil loss graphs.

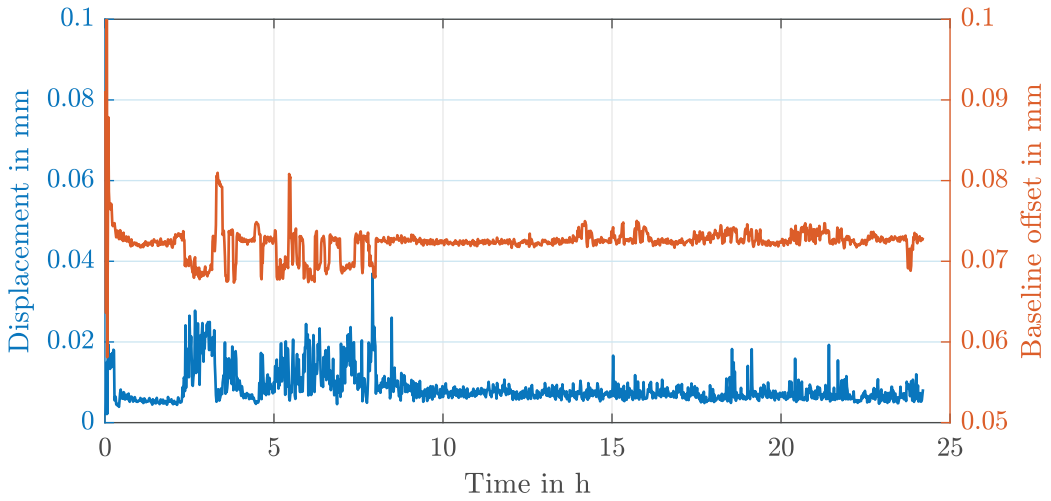

Figure 4.12: Axial displacement of the radial scraper oil wiper packing at 700 rpm for 24 h

According to the experimental procedure (see Sec. 2.2.2) the measurement was extended to all three levels of drive speed and repeated twice. The results of these experiments are summarised and shown in Fig. 4.13. In Fig. 4.13a the oil loss per hour is given. The highest oil loss occurred at the experiments at 700 rpm drive speed. In contrast to the results it was expected that at a higher drive speed more reciprocating movements deliver oil from the crankcase towards the cylinder. Therefore the normalised oil loss at 700 rpm was also the highest oil loss. As a result the performance of the radial scraper concept wiper with multiple wiping edges has the worst performance at the speed level of 700 rpm. At higher drive speeds of 1100 rpm and 1500 rpm the oil loss was not varying significantly, therefore a statement about the oil wiping performance at higher speeds compared to the lowest level of speed is not possible.

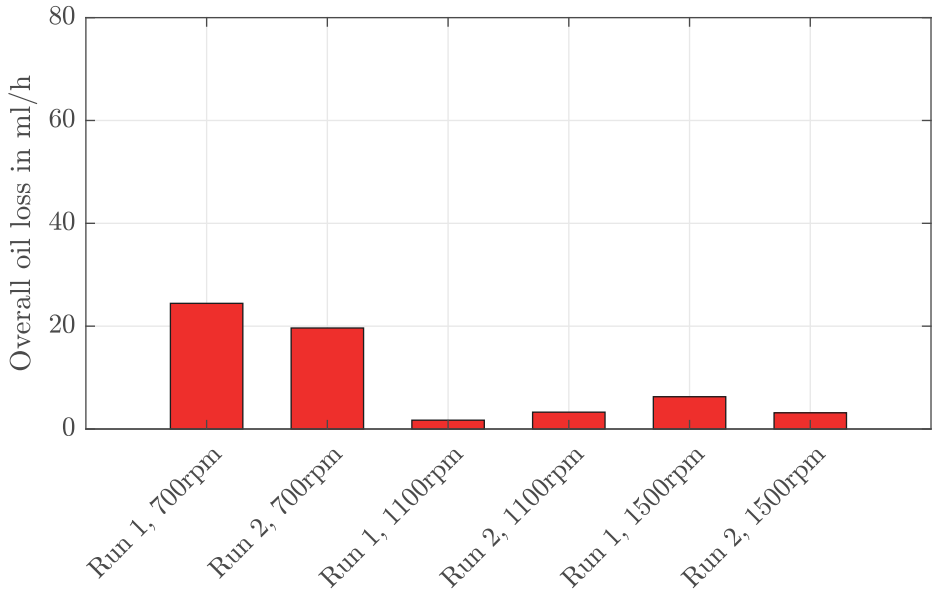

(a) Overall oil loss of the radial scraper oil wiper

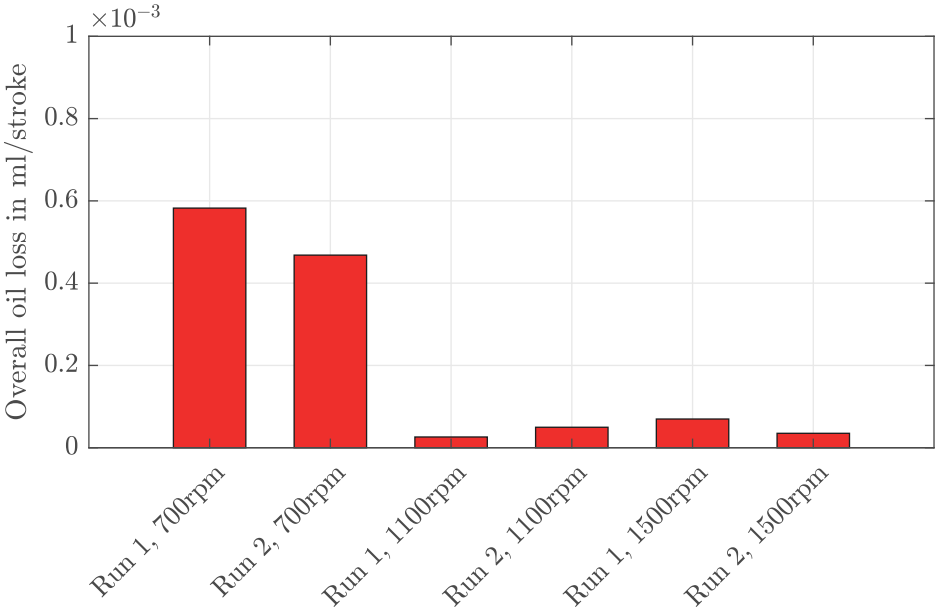

(b) Normalised oil loss of the radial scraper oil wiper

Figure 4.13: Results of the radial scraper oil wiper packing

Conclusion of the radial scraper concept

As the concept is based on classic metallic designs, the manufacturing process had just to be adapted to the new material. The manufacturing process itself is rather complex, because a packing consists of nine single ring segments and three garter springs. Pins for the fixation of the three rings as a packing are additional pieces. The wiping mechanism differs from the other designs, because there is no sealing of the wiper cup. This results in a huge amount of oil loss in the wiper cup, which is guided back into the crankcase.

4.2 Uncut wiper

The idea of this concept was to use the flexibility of the polymeric ring material to generate a wear compensation mechanism. Doing so it is necessary to deform the ring in radial direction. In Fig. 4.14 an overview of the concept is shown. The present axial spring can be used to achieve a radial force by splitting the force into a radial and an axial component using a wedge ring. The radial force puts a constant pressure on the outside of the ring. In the case of wear on the inner surface of the oil wiper ring, the ring can deform under this pressure and compensate the wear. The wedge ring does not transform the complete axial force into radial pressure, a significant amount is used to press the rings against the cup surface. This fully seals the cup and prevents an oil flow through the cup. The length of the uncut wiper packing is longer then the cup length. During the mounting the cup is tightened and with it the axial spring is compressed generating the axial force.

This concept consists of two single-part rings made of PTFE. The two wedge rings are made of a soft metal (e.g. brass) to prevent scratches on the surface of the piston rod. In general any axial spring (ElastoSpring or a disc spring) can be used. The presented work was done with the polymeric ElastoSpring.

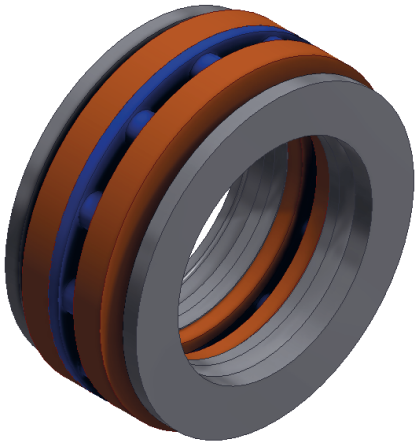

Figure 4.14: Uncut wiper packing with: oil wiper rings (grey), metallic wedge rings (brown) and elastomer spring (blue)

The cross-sectional profile is defined by two design features (shown in Fig. 4.15). The first is a solid ring sealing against the surface of the cup. The sealing pressure is provided by the axial force transmitted over the wedge surface. This seals the first ring towards the crankcase and the second ring towards the cylinder side. So no oil should be able to flow into the cup and no gathered oil at the

second wiper ring should be able to flow through the cup. The second feature is the deformable ring (see dashed red arrow in Fig. 4.15). It is very thin to allow a deformation at a low pressure. The wedge surface of the first ring is kinked. This allows to focus the pressure on the wiping edge. At the second ring the wedge surface is also kinked to focus the pressure on its wiping edge. The fronts of the wiping edges are aligned vertically to the surface of the piston rod to form a sharp oil wiping edge. The back edges form a low angle between wiper ring and rod surface, allowing the ring to pump oil back into the crankcase (feature of the OFD wiper). The inner diameters of both rings are exactly matching the piston rod diameter. This results in the claim that during installation of the wiper packing no rod insertion tools with a diameter larger than the rod diameter are allowed to be used.

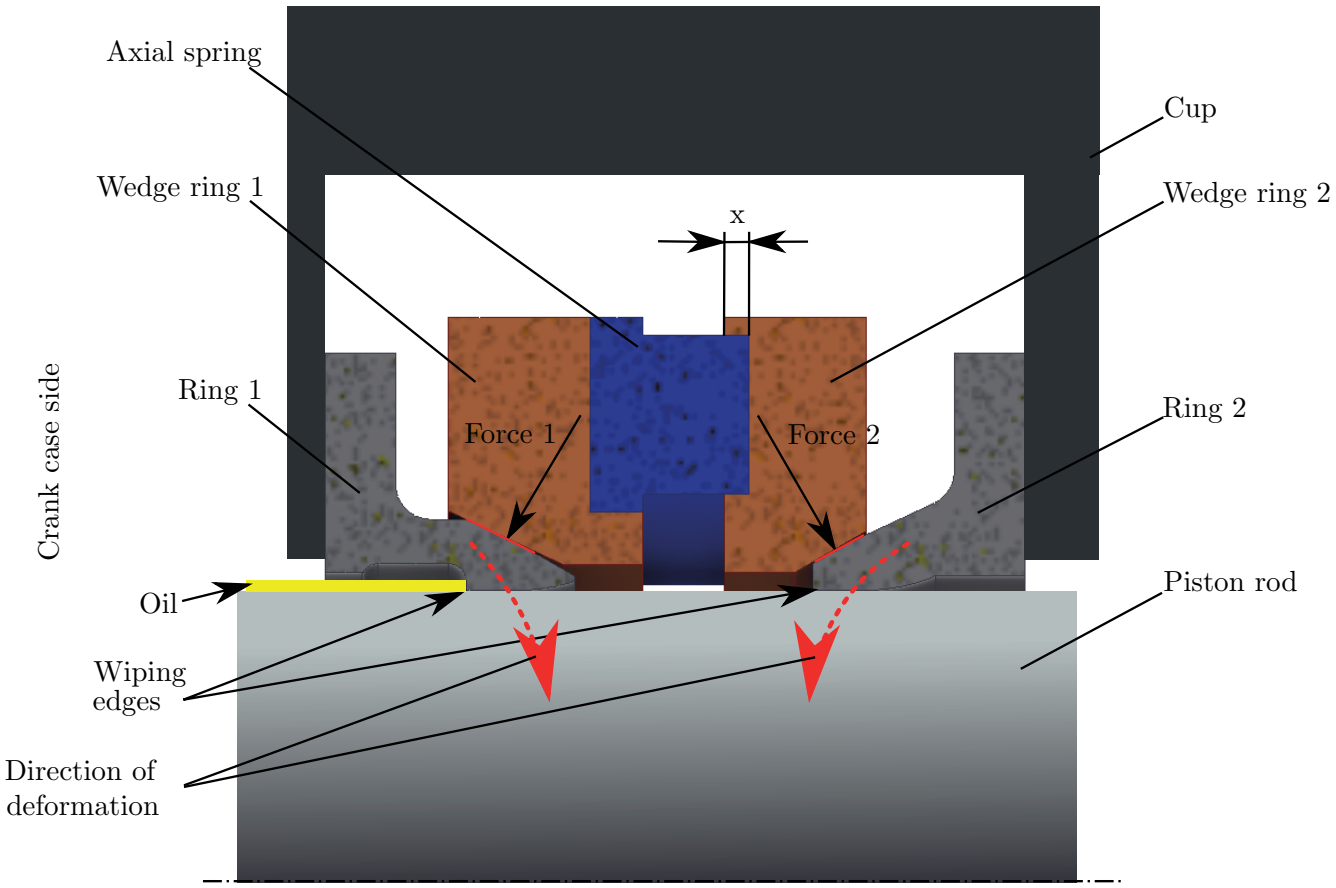

Figure 4.15: Concept of an uncut wiper packing with two solid rings. As example for the axial spring the polymeric ElastoSpring is shown. The distance x is the displacement to compress the spring. The wedge surface is marked red. The dashed red arrows indicate the direction of deformation of the two rings.

4.2.1 Design of the uncut wiper

The exact design of the wiper was done with regard to the pressure between the wiper rings and the moving piston rod. To develop a feasible design the concept was evaluated with an FEM simulation in Abaqus. As the geometry is axisymmetric a 2D model with shell elements, representing the axisymmetric geometry, was chosen. The model is shown in Fig. 4.16. The first step was to calculate the maximum displacement of the wiper lip in radial direction. The simulation was done with short-term values for the stiffness of the ElastoSpring as well as for the PTFE wiper rings. The ElastoSpring was modelled with a hydrostatic pressure on the inward surfaces of the wedge rings. The axial force of 170 N (axial force of ElastoSpring with 12 cylinders and 4.5 mm height at 0.7 mm compression, see

Appendix, Fig. 7.1) was split upon the according surfaces (dimensions see Appendix, Sec. 7.7). For the load step of calculating the displacement (first load step), the surface contact of the wiper rings and the rod was neglected. The surface condition between the wedge rings and the wiper rings was assumed to be frictionless, as the friction between PTFE and metal and the relative displacement are very small.

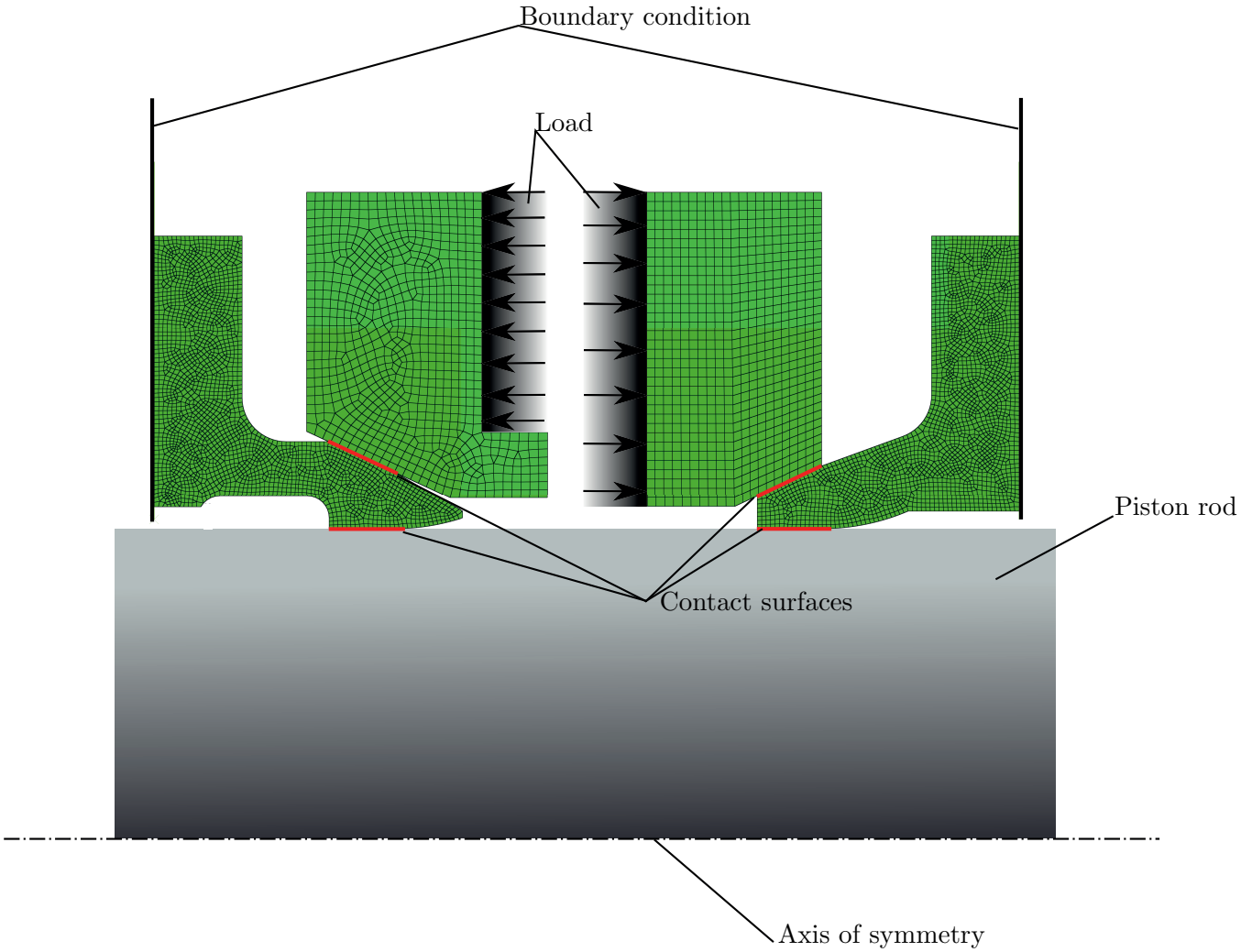

Figure 4.16: Axisymmetric FEM model of the uncut wiper design. The vertical black lines mark the boundary condition representing the cup surface, the red lines mark interaction surfaces between bodies.

The results of the analysis are shown in Fig. 4.17. The maximum displacement of the wiping edge of wiper ring 1 was 0.085 mm in radial direction. This means that ring 1 could compensate a wear of 0.17 mm in diameter. The radial displacement of wiper ring 2 was 0.17 mm, thus the ring could compensate a wear of 0.34 mm. The wear compensation of wiper ring 1 was very low compared to the current product. The OFD wiper can compensate a wear of 0.8 mm in diameter. In the analysis of the uncut wiper two factors were neglected which would lead to stronger deformations than calculated. At first the creeping behaviour of the PTFE material is very strong (see [4]). Thus the statical load caused by the axial spring would enhance the calculated displacement of the statical analysis. At second the calculation was done with the Young's modulus of PTFE at room temperature. As the ambient temperature in the wiper cup is above room temperature, the stiffness of PTFE would be lowered. Therefore also the displacement would be enhanced.

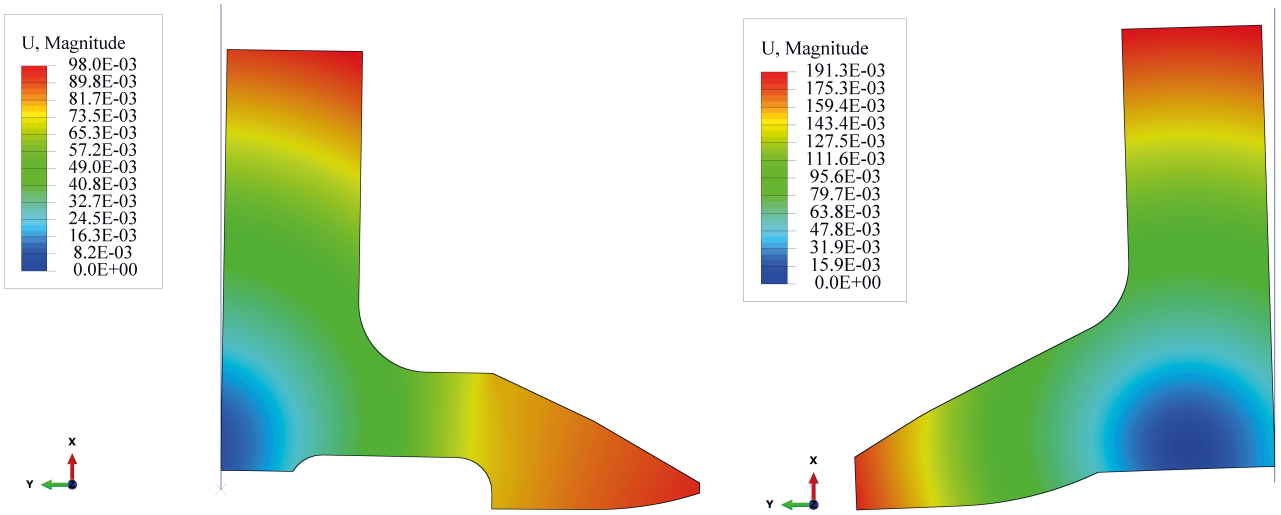

(a) Displacement of wiper ring 1. The maximum deflection of the wiping edge is 0.085 mm.

(b) Displacement of wiper ring 2. The maximum deflection of the wiping edge is 0.17 mm.

Figure 4.17: Results of the displacement analysis. The given magnitude of the displacement is in millimeters.

The second load step was calculating the pressure distribution on the surfaces of the rings. This is important to prevent pressure peaks, which would cause locations with a high wear rate. In Fig. 4.18 the results of the contact pressure distribution analysis are shown. The contact pressure was calculated by splitting the nodal force of the surface nodes according to the size of the related surface patch. The contact pressure was calculated for the surface contact between the wedge rings and the wiper rings, the wiper ring and the piston rod, as well as the wiper ring and the cup surface. The highest contact pressure at wiper ring 1 occurred at the wiping edge with 13.5 MPa. This should lead to a high oil wiping efficiency, because the oil cannot get between the two surfaces. The contact pressure between wiper ring and wedge ring was concentrated at the kink in the surface. The surface pressure distribution between wiper ring and cup surface showed that the pressure profile did not begin at the inner edge of the wiper ring but in the middle of the surface. A better sealing effect could be achieved by an evenly distributed contact pressure beginning at the inner edge of the wiper ring. The contact pressure profile of the wiping surface of wiper ring 2 was contrary to the profile of wiper ring 1. The highest contact pressure of 20.4 MPa did not occur at the wiping edge but at the end of the wiping surface (towards the cylinder end). The contact pressure between wiper ring and wedge ring was concentrated at the front lip. The contact pressure on the cup surface was neither beginning at the inner edge. The calculated values of contact pressure were feasible for the used highly filled PTFE materials.

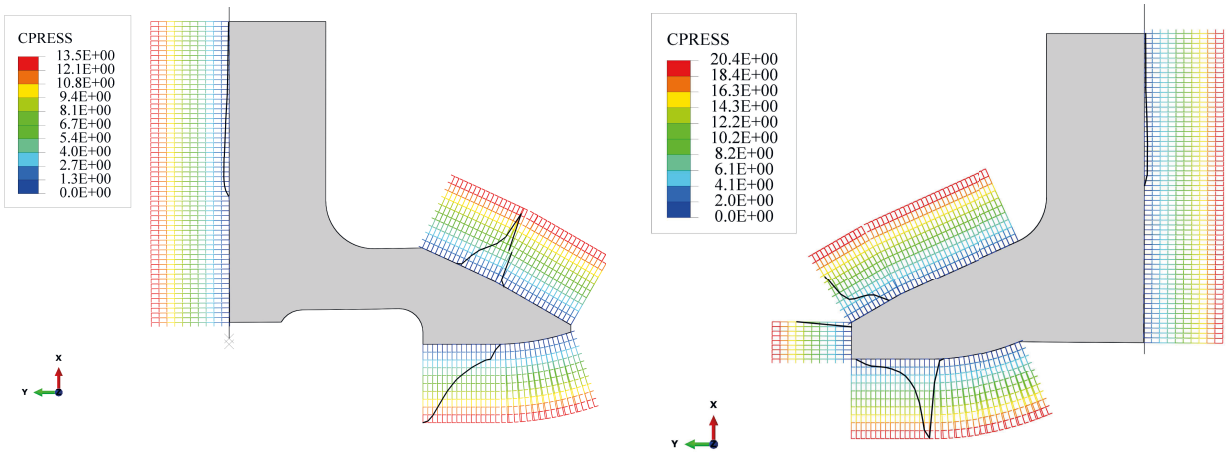

(a) Contact pressure of wiper ring 1

(b) Contact pressure of wiper ring 2

Figure 4.18: Results of the contact pressure analysis for each surface node with contact to another surface. The magnitude is given in separate coloured graphs, normal to the surface nodes in MPa.

4.2.2 Friction force measurement

It was expected that the contact pressure shown in Sec. 4.2.1 leads to more friction force between wiper ring and piston rod compared with the measured friction force of the OFD wiper (see Sec. 3.1.2). To determine the exact friction force the measurement procedure shown in Sec. 3.1.2 was used. The results of the measurements are shown in Fig. 4.19. The measurement in Fig. 4.19a shows that the static friction on a dry rod is 50 N, which is more than three times higher compared with the OFD wiper (see Tab. 3.1). The dynamic friction force during the reciprocating movement was also on the same level. The static friction force of the measurement with an oil film stays unchanged with 50 N, but the dynamic friction force with approximately 45 N differed. With a heavily wet rod the static friction force stayed again unchanged, but the dynamic friction force was decreasing to approximately 45 N at 100 mm/min displacement speed and approximately 40 N at 500 mm/min and 1000 mm/min displacement speed. This speed dependency was only visible in the heavily wet measurement. The results are summarised in Tab. 4.1.

Table 4.1: Results of friction force F_F measurement of the uncut wiper

Measurement	Static friction in N	Dynamic friction in N
Dry rod	50	50
Lightly wet rod	50	45
Heavily wet rod	50	40-45

4.2.3 Conclusion of the uncut wiper concept

Although the friction force of the uncut wiper was significantly higher than at the OFD wiper it should be suitable for a performance evaluation. Pressure rings (e.g. BCD rings), which are used to seal pressure between different sections along the piston rod, are exposed to higher contact pressures and therefore also cause more friction on the rod. But the achievable lifetime of the uncut wiper ring is a critical point in the evaluation of this concept. The practical evaluation of the uncut wiper concept

on the MPTC (oil loss measurement) was not available due to problems mentioned in Sec. 2.2.1.

The advantage of this concept is two-fold. The first advantage is the simple production process of the rings. They can be produced very fast on a standard 3-axis CNC lathe. Although the metallic wedge rings are additional parts, they have to be produced only once for each compressor packing because they are not subjected to any wear and therefore can be re-used. The most critical parameters to the feasibility of this concept are the mounting process and the long-term behaviour. As the inner diameter of the wiper ring is matching the rod diameter, a widening of the ring geometry by a rod insertion tool must be prohibited. This has to be further evaluated with focus on the mounting routines present at operators of reciprocating compressors. The applied pressure has to be balanced with the long-term creep behaviour of the material. On the one hand too high pressure would surely cause a desired deformation of the wiping edge but on the other hand results in a high wear rate.

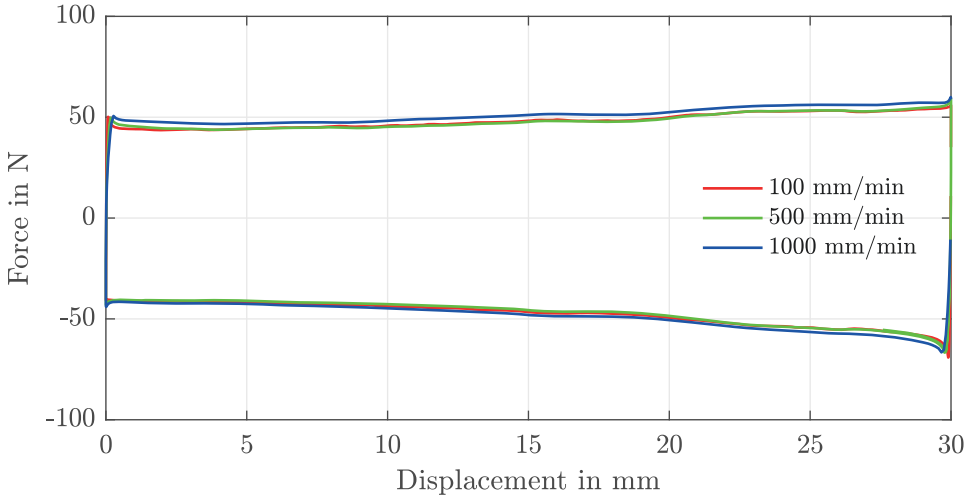

(a) Friction force on dry rod at different displacement speeds

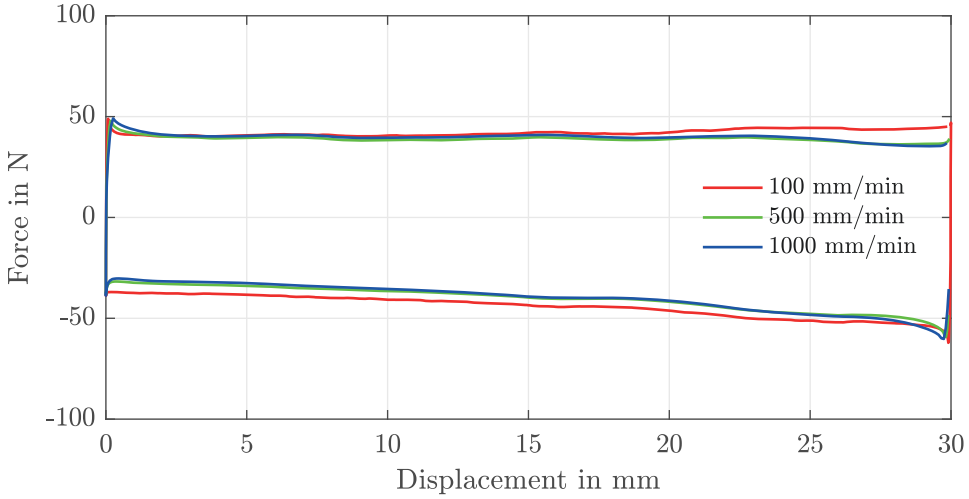

(b) Friction force on lightly wet rod at different displacement speeds

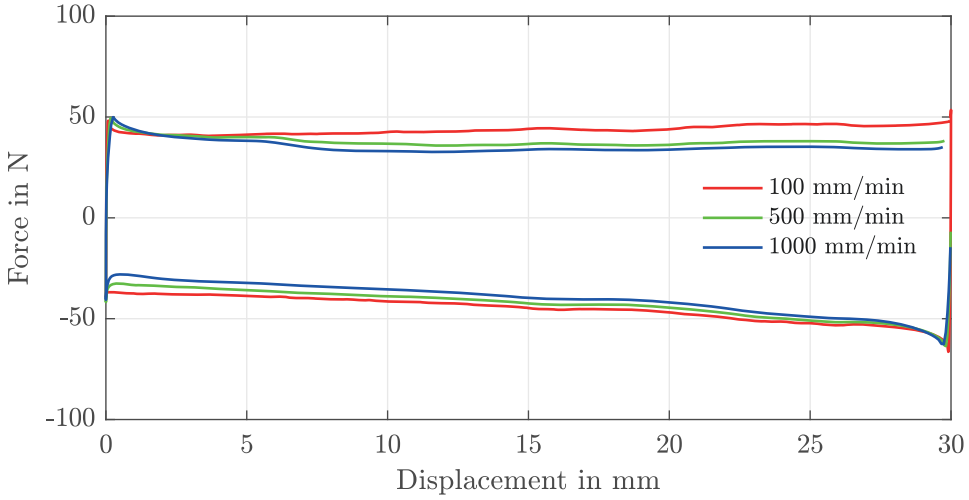

(c) Friction force on heavily wet rod at different displacement speeds

Figure 4.19: Measurement of the friction force at different friction conditions

4.3 Conclusion of the new ring designs

In this chapter several new concepts for ring designs were shown. They inhibit the potential of reducing the production costs and improving the operational performance. The next step is to determine the production costs to evaluate the potential of the cost reduction.

The evaluation of the oil wiping performance was incomplete due to the fact that the measurement procedure is very time consuming. The available results of the radial scraper concept are shown in Tab. 4.2 and compared with the results of the OFD wiper. The results of the oil loss in the pressure section of each two runs are averaged (minding the present variation). The oil wiping performance at 700 rpm was about on the same level. At 1100 rpm and 1500 rpm the oil wiping performance of the radial scraper concept was significantly better than the performance of the OFD wiper, because there was less oil loss in the pressure section.

Table 4.2: Comparison of the normalised oil wiping performance of the OFD wiper and the radial scraper concept in 10^{-3} ml/stroke

	Level of speed in rpm		
Concept	**700**	**1100**	**1500**
OFD wiper	0.475	0.28	0.134
Radial scraper	0.524	0.037	0.052

The further evaluation of the oil wiping performance of the other concepts will lead to the next steps of designing a final concept for the product re-design. In particular it is possible to combine different approaches e.g. the higher number of wiping edges of the radial scraper concept and the wear compensation and sealing function of the concepts with radial or tangential cut.

5 Conclusion and outlook

In this thesis an approach to evaluate the potential of a product re-design was shown. The basis of the feasibility project was a detailed product requirements document. This includes all necessary information concerning the functional requirements of the product. Additionally, the surrounding circumstances regarding the economic motivation for a re-design project as well as the functional difficulties of the current product were thoroughly investigated. The evaluation of the current product is a central task in any product re-design, because it shows the highest potential for a focused improvement. In case of the OFD wiper the two main approaches in the re-design process were reducing the production costs and enhancing the oil wiping performance. For comparability of the oil wiping performances of the current product and new concepts a measurement set-up has been developed. This set-up allowed to measure the oil loss occurring directly during the operation of the oil wiper in a reciprocating compressor. This yielded application-oriented but complex results at the same time. The significance of the gathered data was limited due to high variability of the results. To improve the reproducibility the complexity of the measurement set-up could be reduced. The direct attachment of the measurement system to the crankcase of a reciprocating compressor did not allow to measure or influence the amount of oil reaching the oil wiper in the wiper cup. Furthermore, the oil and the crankcase temperatures were not adjustable but only responding to the set drive speed. This limited the measurement significance to compressors with a similar or similar type of crankcase reaching the same oil temperature. A future set-up should be focused on a defined level of oil flow towards the oil wiper on the reciprocating piston rod. Additionally, a temperature control of the oil allows to reproduce various situations and compressors (with cooling or without cooling). The interaction between the wiper packing and a directly attached pressure packing (combined packing) should be investigated when the oil wiping mechanism is repeatedly measurable.

The motivation for replacing the metallic lug spring was given by the potential harm to the surface of the piston rod in case of a failure as well as by reducing the production cost. Both issues were addressed by replacing the lug spring with a polymer spring. The presented concept was evaluated by production of various prototypes. These prototypes have been evaluated with regard to the long term application at higher temperatures. The results showed that a concept of a polymer axial spring is feasible. The next steps on the way to a worked up product are further measurements of the long term relaxation behaviour. Additionally, the influence of ambient substances on the mechanical behaviour, especially mineral oil from the crankcase, has to be evaluated. With this information a detailed design can be worked out. To do so the presented methods of material modelling can be extended by longer measurement periods, different levels of temperature and the influence of ambient oil. A final evaluation in operation is still necessary.

The oil wiping function of the current product could also be designed with various different approaches. The presented new concepts addressed performance improvements and cost reductions. Due to the time consuming measurement procedure for the oil loss not all concepts were compared and evaluated in this thesis. Therefore the next steps are the complete oil loss measurements of all wiper ring concepts. If there is a concept with clearly the best oil wiping performance, this concept should be pursued in the product development process. It is also possible to combine several design features to form a new concept. In the situation of an unclear optimal solution the measurement set-up has to

be refined. What can be determined is the potential of reducing the production cost. Therefore the next step is to discuss the detailed manufacturing of each.

The present thesis ends without a clear result, but can be used as a valuable basis for further development of the described tasks, indicating the path to a final re-designed oil wiper concept.

6 Bibliography

[1] ISO 3384-1. Rubber, vulcanized or thermoplastic — determination of stress relaxation in compression, December 2011.

[2] Silvia Brunbauer. *Design and development of a testing machine for compressive creep tests on polymers at elevated temperatures.* Master thesis, Montanuniversitaet Leoben, 2016.

[3] Andreas Dittmann. *Microscopic characterisation of tribological systems.* Dissertation, TU Graz, 2015.

[4] Hans Domininghaus, Peter Elsner, Peter Eyerer, and Thomas Hirth. *Kunststoffe, Eigenschaften und Anwendungen.* Springer Verlag, Heidelberg, 2012.

[5] Sina Ebnesajjad and Richard Morgan. *Fluoropolymer Additives.* Elsevier Inc., Oxford, UK, 2011.

[6] Gottfried Ehrenstein and Sonja Pongratz. *Resistance and Stability of Polymers.* Carl Hanser Verlag GmbH Co KG, Munich, 2013.

[7] MAPLAN GmbH. Produktübersicht - maplan edition und editions vertikalmaschinenbaureihe. `http://www.maplan.at/de/intern:33/gummi/articlearchivshow-maplan-edition-und-editions-vertikalmaschinenbaureihe`, 2017. [Online; Accessed: January 13, 2017].

[8] Karl-Heinrich Grote and Jörg Feldhusen. *Dubbel - Tachenbuch für den Maschinenbau.* Springer Verlag, Heidelberg, 2007.

[9] Marketing Hoerbiger. Valve and compressor images. Hoerbiger internal report, Hoerbiger Ventilwerke GmbH, 2016.

[10] R & D Hoerbiger. Oil wiper product requirements document. Hoerbiger internal report, Hoerbiger Ventilwerke GmbH, 2016.

[11] Gummiwerk KRAIBURG GmbH & Co. KG. *ACCEPTANCE TEST CERTIFICATE for VA6BKZ.* Teplitzer Str. 20, 84478 Waldkraiburg / Germany, February 2016. FKM.

[12] Gummiwerk KRAIBURG GmbH & Co. KG. *ACCEPTANCE TEST CERTIFICATE for VT6AHZ.* Teplitzer Str. 20, 84478 Waldkraiburg / Germany, February 2016. HNBR.

[13] Gummiwerk KRAIBURG GmbH & Co. KG. *TECHNICAL DATA SHEET for VA6BKZ.* Teplitzer Str. 20, 84478 Waldkraiburg / Germany, August 2016. FKM.

[14] Gummiwerk KRAIBURG GmbH & Co. KG. *TECHNICAL DATA SHEET for VT6AHZ.* Teplitzer Str. 20, 84478 Waldkraiburg / Germany, August 2016. HNBR.

[15] Fritz Röthemayer and Franz Sommer. *Kautschuktechnologie, Werkstoffe - Verarbeitung - Produkte.* Carl Hanser verlag, München, 2013.

[16] Markus Stommel, Marcus Stojek, and Wolfgang Korte. *FEM zur Berechnung von Kunststoff-*

und Elastomerbauteilen. Carl Hanser Verlag GmbH Co KG, Munich, 2011.

[17] Dassault Systèmes. Abaqus 6.14 online documentation. `http://50.16.225.63/v6.14/books/usb/default.htm?startat=pt05ch22s05abm07.html#usb-mat-chyperelastic`, April 2014. [Online; Accessed: January 20, 2017].

[18] Vanessa Trautmann. *Dichthalten von OFD-Ölabstreifringen unter verschiedenen Betriebsbedingungen*. Bachelor thesis, TU Wien, 2015.

7 Appendix

7.1 Detailed drawing of the OFD wiper

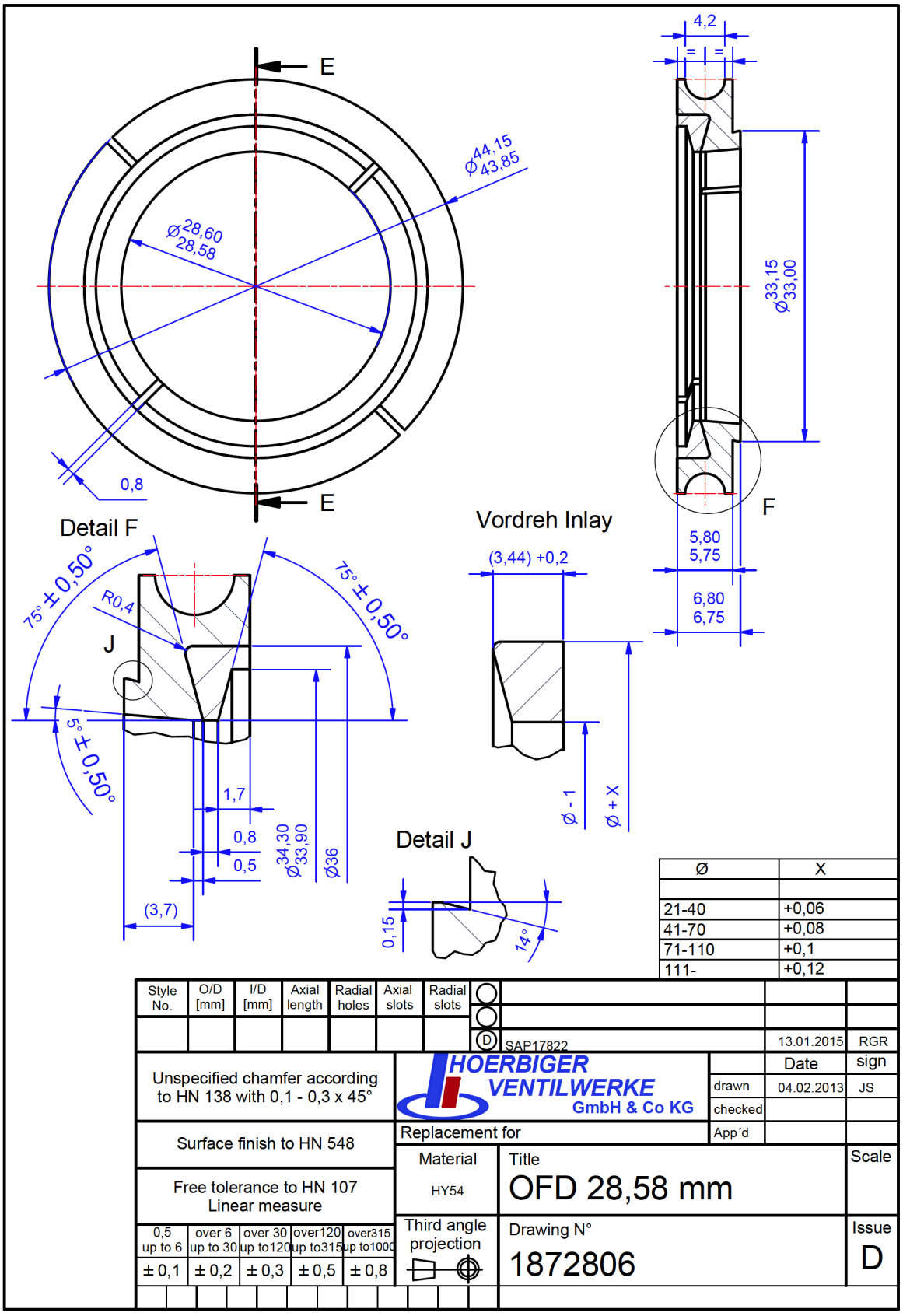

7.2 Product requirements document

HOERBIGER

Product requirements document
RAT 532.30 Best Value Oil Wiper

Summary:
The scope of this project is the analysis and focused improvement of the existing oil wiper solution especially for the CNG and PET-market. This is specifically important for the use of oil wiper rings in combined packings. The deployment of the oil wiping function is the object of a feasibility study. Within this study several concepts should be checked for fulfilling the functional and economical requirements and the customer benefit.

Functional requirements	**Economical requirements**
Oil-loss minimization	Production Costs
Mountability improvement	Investment Costs

Directory

1. General definitions of the product

Definition of the product	Polymer oil wiper ring
Definition of the project goals	Improvement of the function Reduction of production costs
Definition of the general product development strategy	• Development of concepts • Evaluation of new and existing concepts with scope on functional improvement • Analysis of expected production and investment costs

Definition of product development process (milestones)	• Creation of product requirements document
	• Design of concepts
	  ○ Part design
	  ○ Manufacturing
	• Test of concepts on the MPTC with oil loss measurement
	• Cost analysis, customer benefit analysis

Project team	• Marian Janko (R&D) • Bernhard Radler (R&D) • Martin Lagler (R&D) • Christian Hold (Product management) • Karl Markey (Head of Rings & Packings US) • Frank Schmidhofer (HVW)

2. Technical and economical investigation

2.1. Analysis of required functions

General and functional requirements	The function of the oil wiper ring is to remove oil from reciprocating piston rods of gas compressors. The oil comes from the crankcase of the compressor and forms an oil film on the surface of the piston rod. The function of the oil wiper ring is to prevent the oil flow further on in following compression areas and possible pollution of compression media.
Interfaces	• Piston rods with varying diameter (list see attachment) • Cup (mounting of rings) with varying diameter and cup width (list see attachment)
Geometry and design	see attachment
Mechanical and thermal requirements	see attachment
Chemical and electrical requirements	see attachment
Lifetime and long-term stability requirements	see attachment
Optical and surface quality requirements	see attachment
Legal and safety requirements	see attachment
Polymer type / class	see attachment
Economical requirements	see attachment
Logistical and regional requirements	see attachment

2.2. Technological analysis

Production technology available	• Chip-forming methods
	  ○ Milling
	  ○ Lathing
	• Injection Moulding

Production technology excluded	

2.3. Economic analysis

Cost analysis of reference product	see attachment
Overall annual quantities	Up to 75.000 Pcs. / year (based on ~37.500 installed bases in 2014 with 2 rings each and an annual growth rate of ~10%)
Lifetime	min 8.000 h

2.4. Evaluation matrices

Technical feasibility	Evaluation of prototypes with scope on: • production • strengths / weaknesses → customer benefit • Interaction between wiper and seal ring • Functional fulfilling
Economic feasibility	Evaluation of prototypes with scope on: • Production costs • Investment costs

3. Attachment

The attachment of the product requirements document contains information about the reference part and requirements according to chapter 2.

3.1. Reference part

Existing solutions are radial cut metallic wiper rings with traditional design or the RTV-wiper of Cook Compression.

3.1.1. Reference part cost analysis

As the batch size is unknown, the production costs are calculated for different batch sizes. All prices are taken from the Hörbiger SAP-database.

Costs for 28,58mm OFD-Wiper at HVW (1010):

	Batch Size	1	5	10	50	100
Wiper ring	Fix / pcs.	€ 20,07	€ 4,01	€ 2,01	€ 0,40	€ 0,20
	Var / pcs.	€ 25,74	€ 25,74	€ 25,74	€ 25,74	€ 25,74
		€ 45,81	**€ 29,76**	**€ 27,75**	**€ 26,14**	**€ 25,94**
Lug spring	Fix / pcs.	€ 138,78	€ 27,76	€ 13,88	€ 2,78	€ 1,39
	Var / pcs.	€ 9,37	€ 7,59	€ 6,10	€ 4,91	€ 4,76
		€ 148,15	**€ 35,34**	**€ 19,98**	**€ 7,68**	**€ 6,15**
Garter spring	Fix / pcs.	€ 3,48	€ 0,70	€ 0,35	€ 0,07	€ 0,03
	Var / pcs.	€ 0,52	€ 0,52	€ 0,52	€ 0,52	€ 0,52
		€ 4,00	**€ 1,22**	**€ 0,87**	**€ 0,59**	**€ 0,55**
complete wiper/pc.		**€ 197,96**	**€ 66,32**	**€ 48,59**	**€ 34,42**	**€ 32,64**

3.1.2. Reference part design

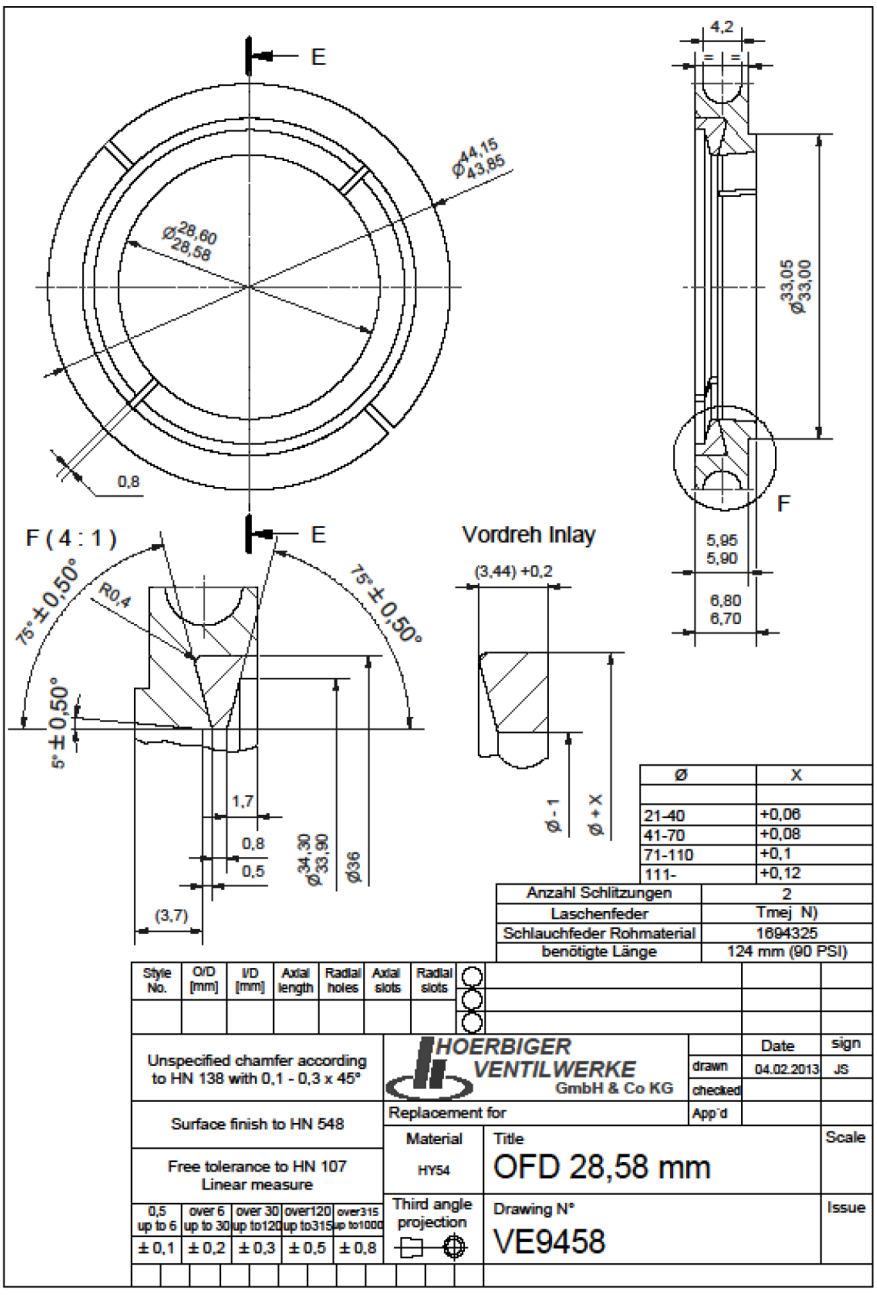

3.2. Requirements

All requirements must be valued. The following table contains an overview of the meaning of the values.

Value	Importance	Abbreviation	Status
1	absolute necessary	N	new
2	important	D	to be discussed
3	to be considered	F	fixed
4	not relevant	O	open

The sources of all requirements are listed in the following table. The source comprehensibly indicates the document, meeting or person giving the specific requirement.

Source of requirement	
Abbreviation	*Indication of source*
f1	general functional requirement
m1	Meeting with Christian Hold, Marian Janko, Bernhard Radler on 8th June, 2016
m2	Meeting with Christian Hold, Bernhard Radler on 20th July, 2016
m3	Meeting with Christian Hold, Marian Janko, Bernhard Radler on 6th September, 2016
d1	Document "Specification for OFD-Wiper" (DS-2-2-5-R1), Version 2014-02_en
d2	20160201_Market Intelligence_OEM CS_2014_CNG
e1	Email from Karl Markey on 25th August, 2016
n1	Norm/guideline xxx
s1	Sample xxx on Date
z1	Drawing xxx

Nr.	Requirement	Source	Value	Status
General and functional requirements				
1	Part name: Best value oil wiper			
2	Prevent oil loss from crank case	f1	1	F
3	Wipe oil from the piston rod	f1	2	F
4	Prevent oil flow through the cup (secondary flow path e.g. over rings)	m2	1	F
5	Compensate wear of the oil wiper	f1	3	F
6	Specification of mounting in the superior technical system: Mounting on piston rod: Due to the small form factor of the compressors in the target market it is not necessary to mount the ring over the rod. Nevertheless installation without pulling the rod should be evaluated for a possible transfer of the concepts to larger rod diameters.	m3	2	F
7	Specification of mounting in the superior technical system: Mounting in cups with different outer diameters and widths	m2	1	F
8	Installable in packing without additional tools. To mount the rod in the packing, installation tools with various geometries are placed on the tip of the rod. The diameter of the insertion tool can exceed the rod diameter by up to 1/16”.	e1	2	F

Nr.	Requirement	Source	Value	Status
Definition of interface to piston rod				
9	Interface 1: Inner diameter must be in contact with the piston rod	f1	1	F
10	No wear of the piston rod allowed	f1	1	F

Nr.	Requirement	Source	Value	Status
Definition of interface to cup				
11	Interface 1: Front side must be in contact with the cup	f1	1	F
12	Interface 2: Outer Diameter must not be in contact with the cup	f1	1	F
13	Maximum / minimum width			O

Nr.	Requirement	Source	Value	Status
Geometry and design requirements				
14	Permanent marking of material, production date, etc.	m2	3	F
15	Visible surfaces: none	f1	4	F

<table>
<tr><td>16</td><td>List of Piston rod diameter to be considered:
<table>
<tr><th colspan="2">Rod Diameter</th><th colspan="2">Cup Diameter</th></tr>
<tr><td>mm</td><td>inch</td><td>mm</td><td>inch</td></tr>
<tr><td>25,4</td><td>1</td><td></td><td></td></tr>
<tr><td>28</td><td></td><td></td><td></td></tr>
<tr><td>28,58</td><td>1 1/8</td><td></td><td></td></tr>
<tr><td>31,75</td><td>1 1/4</td><td></td><td></td></tr>
<tr><td>32</td><td></td><td></td><td></td></tr>
<tr><td>34,93</td><td>1 3/8</td><td></td><td></td></tr>
<tr><td>35</td><td></td><td></td><td></td></tr>
<tr><td>35,5</td><td></td><td></td><td></td></tr>
<tr><td>38</td><td></td><td></td><td></td></tr>
<tr><td>38,1</td><td>1 1/2</td><td></td><td></td></tr>
<tr><td>40</td><td></td><td></td><td></td></tr>
<tr><td>41</td><td></td><td></td><td></td></tr>
<tr><td>41,28</td><td>1 5/8</td><td></td><td></td></tr>
<tr><td>44,45</td><td>1 3/4</td><td></td><td></td></tr>
<tr><td>45</td><td></td><td></td><td></td></tr>
<tr><td>48</td><td></td><td></td><td></td></tr>
<tr><td>50</td><td></td><td></td><td></td></tr>
<tr><td>50,8</td><td>2</td><td></td><td></td></tr>
<tr><td>53,98</td><td>2 1/8</td><td></td><td></td></tr>
<tr><td>55</td><td></td><td></td><td></td></tr>
<tr><td>57</td><td></td><td></td><td></td></tr>
<tr><td>57,15</td><td>2 1/4</td><td></td><td></td></tr>
</table></td><td>m2</td><td>2</td><td>F</td></tr>
<tr><td>17</td><td>Threads</td><td>f1</td><td>4</td><td>F</td></tr>
<tr><td>18</td><td>Maximum / minimum wall thicknesses</td><td>f1</td><td>4</td><td>F</td></tr>
<tr><td>19</td><td>Maximum / minimum weight</td><td>f1</td><td>4</td><td>F</td></tr>
</table>

Nr.	Requirement	Source	Value	Status
Mechanical and thermal requirements				
20	Short-time or impact loads: occur during power up of the compressor	f1	2	F
21	Long-time load: Reciprocating movement of the piston rod Displacement per turn /Stroke: 2”-5”m Displacement speed: up to 1800 rpm	m2	1	F
22	Maximum mounting force: installation manually without additional tools	m2	2	F
23	Safety functions	f1	4	F
24	Safety functions in event of failure	f1	4	F
25	Temperature range short-time (up to 2 min) Rod temperature: 220-250°C Bulk case / ring temperature: below rod temperature	m3	2	F
26	Temperature range long-time: Rod temperature: 60-180°C (210°C) Bulk case / ring temperature: below rod temperature	m2	2	F

27	Thermal conductivity of material:	f1	4	F
28	No splintering fraction	m2	4	F
29	No leakage under special conditions	m2	4	F
30	Permitted misuse	m2	4	F
31	Permitted transport conditions: standard	m2	3	F
32	Permitted storage conditions: storage up to 2 years	m2	3	F

Nr.	Requirement	Source	Value	Status
Chemical and electrical requirements				
33	Resistance to H_2S sour gas	m2	1	F
34	Resistance to cleaning agents which are possibly given in industrial surroundings	m2	2	F
35	Resistance to mineral oil: ISO 100-250	m2	1	F
36	Resistance to test liquids	m2	4	F
37	Resistance to acids, alkalis, salts, gases	m2	4	F
38	Seawater resistance	m2	4	F
39	Resistance to adhesives	m2	4	F
40	Permeability (specify)	m2	4	F
41	Moisture absorption	m2	2	F
42	Antistatic properties	m2	4	F
43	Dielectrical properties	m2	4	F
44	Shielding against electromagnetic fields	m2	4	F
45	Electrical conductivity	m2	4	F
46	Requirements regarding explosion protection	m2	4	F
47	Fire protection classification	m2	4	F
48	Other restrictions (e.g. use in high voltage environments)	m2	4	F

Nr.	Requirement	Source	Value	Status
Lifetime and long-term stability requirements				
49	Product lifetime: CNG: 8.000h Lubricated Compressors: 16.000-24.000 h	m3	1	F
50	Tests after artificial aging	m2	4	F
51	All polymers lightfast	f1	4	F
52	All polymers UV-resistant	f1	4	F
53	All polymers UV-resistant for use in south Europe (e.g. Spain, Italy, Greece, …)	f1	4	F

54	All polymers UV-resistant for use in desert regions or tropics	f1	4	F
55	All polymers UV-resistant for inside/internal parts	f1	4	F

Nr.	Requirement	Source	Value	Status
Optical and surface quality requirements				
56	Coating, painting, galvanizing not allowed	f1	3	F
57	Colour	f1	4	F

Nr.	Requirement	Source	Value	Status
Legal and security requirements				
58	List all norms to be complied	m2	4	F
59	List all internal guidelines to be complied	m2	4	F
60	List all safety norms to be complied	m2	4	F
61	List all special norms regarding fire and explosion protection	m2	4	F
62	List all special norms regarding transportation (Train, subway, bus, ship, plane, ...)	m2	4	F
63	List all norms regarding public institutions (hospital, school, retirement home, ...)	m2	4	F
64	FDA admission	m2	4	F

Nr.	Requirement	Source	Value	STATUS
Polymer type / class				
65	Specify allowed polymer class (cross out forbidden class): • Thermoplastics • Elastomers • Preferred: Hörbger HY materials	m2	2	F
66	Only commercially available types allowed	m2	4	F
67	List other restrictions (e.g. silicon free, ...)	m2	4	F

Nr.	Requirement	Source	Value	Status
Economical requirements				
68	Patent protection required	m2	3	F
69	Estimated overall annual quantities			O
70	Lifetime >10 years	m2	3	F

<table>
<tr><td>71</td><td>Maximum production cost (with statement why, e.g. prices of competing products)</td><td></td><td></td><td>O</td></tr>
<tr><td>72</td><td>Estimated annual quantities per type:
<table>
<tr><th colspan="2">Rod Diameter</th><th>Annual Quantity</th></tr>
<tr><td>mm</td><td>inch</td><td></td></tr>
<tr><td>25,4</td><td>1</td><td></td></tr>
<tr><td colspan="2">28</td><td></td></tr>
<tr><td>28,58</td><td>1 1/8</td><td>main quantity</td></tr>
<tr><td>31,75</td><td>1 1/4</td><td></td></tr>
<tr><td colspan="2">32</td><td></td></tr>
<tr><td>34,93</td><td>1 3/8</td><td></td></tr>
<tr><td colspan="2">35</td><td></td></tr>
<tr><td colspan="2">35,5</td><td></td></tr>
<tr><td colspan="2">38</td><td></td></tr>
<tr><td>38,1</td><td>1 1/2</td><td></td></tr>
<tr><td colspan="2">40</td><td></td></tr>
<tr><td colspan="2">41</td><td></td></tr>
<tr><td>41,28</td><td>1 5/8</td><td></td></tr>
<tr><td>44,45</td><td>1 3/4</td><td></td></tr>
<tr><td colspan="2">45</td><td></td></tr>
<tr><td colspan="2">48</td><td></td></tr>
<tr><td colspan="2">50</td><td></td></tr>
<tr><td>50,8</td><td>2</td><td></td></tr>
<tr><td>53,98</td><td>2 1/8</td><td></td></tr>
<tr><td colspan="2">55</td><td></td></tr>
<tr><td colspan="2">57</td><td></td></tr>
<tr><td>57,15</td><td>2 1/4</td><td></td></tr>
</table></td><td>m2</td><td>3</td><td>F</td></tr>
<tr><td>73</td><td>Supply of spare parts</td><td></td><td></td><td>O</td></tr>
<tr><td>74</td><td>Production on existing equipment/technology</td><td>m2</td><td>2</td><td>F</td></tr>
<tr><td>75</td><td>List of existing equipment/technology available for production:
Engel E-Motion 2800
Mazak 5 axis CNC/ Fanuk Robodrill</td><td>m2</td><td>3</td><td>F</td></tr>
<tr><td>76</td><td>List of equipment/technology not available or forbidden:
E.g. 3D-printing</td><td>m2</td><td>4</td><td>F</td></tr>
</table>

Nr.	Requirement	Source	Value	Status
Logistical and regional requirements				
77	Batch size: typically 10-50 pcs.	m2	3	F
78	Stock size			O

The evaluation of all requirements referred above is confirmed by:

_____

(Date / responsible Manager)

7.3 MPTC data sheet

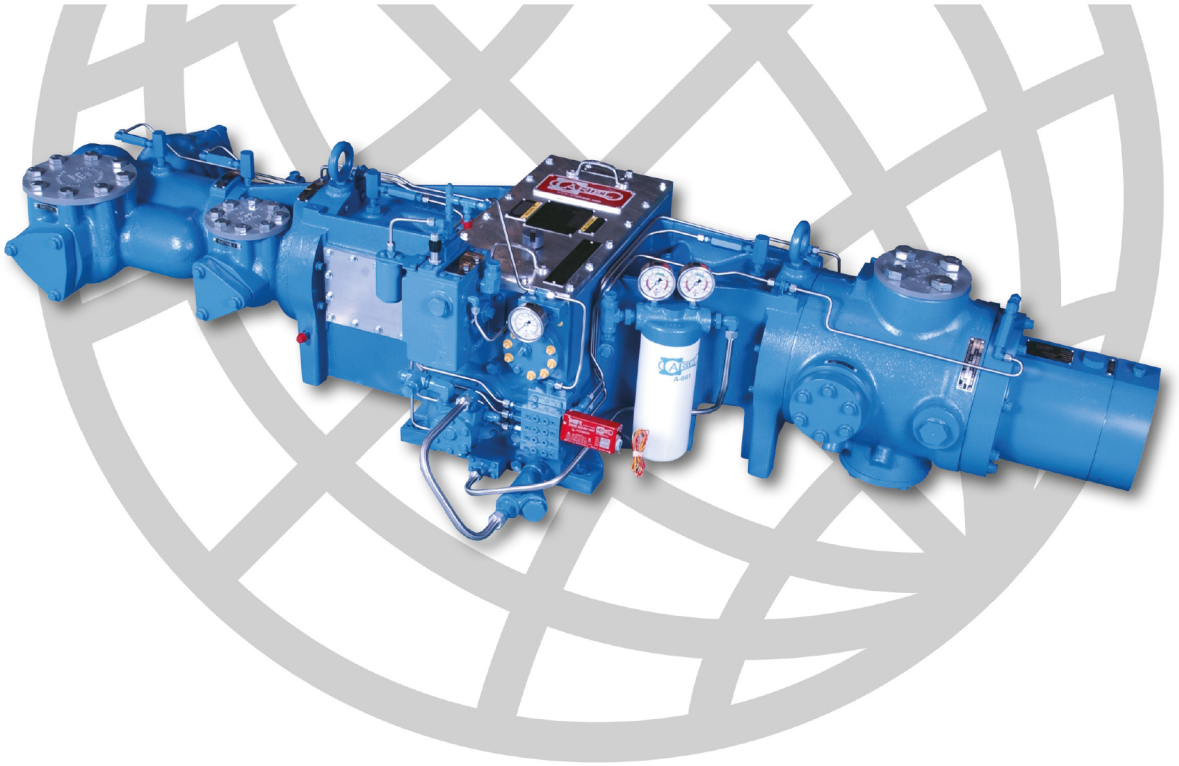

ARIEL JGM, JGP, JGN, JGQ COMPRESSORS

Frame	JGM/2	JGP/2	JGN/2	JGQ/2
Number of throws	2	2	2	2
Rated Power, BHP	167	170	252	280
Rated Power, kW	125	127	188	209
Stroke, inches	3.5	3	3.5	3
Stroke, mm	89	76	89	76
RPM, maximum	1500	1800	1500	1800
Piston speed, FPM	875	900	875	900
Piston speed, m/s	4.45	4.57	4.45	4.57
Total Rod Load, lbs	12000	12000	18000	20000
Total Rod Load, N	53379	53379	80068	88964
Tension, lbs	6000	6000	9000	10000
Tension, N	26689	26689	40034	44482
Compression, lbs	7000	7000	10000	11000
Compression, N	31138	31138	44482	48930
Average Weight with cylinders, lbs	2000	2000	2000	2000
Average Weight with cylinders, kg	905	905	905	905
Maximum Length, inches	35	35	35	35
Maximum Length, mm	889	889	889	889
Maximum Width, inches	83	83	83	83
Maximum Width, mm	2108	2108	2108	2108
Crankshaft ℄ (from bottom), inches	9.25	9.25	9.25	9.25
Crankshaft ℄ (from bottom), mm	235	235	235	235

7.4 ElastoSpring compression stress measurements

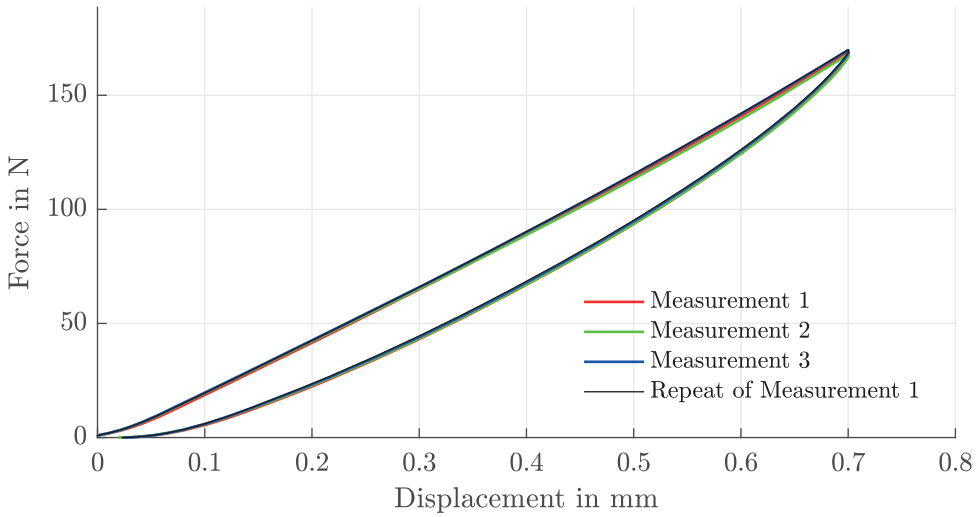

Figure 7.1: Compression test of the ElastoSpring concept with 12 cylinders and 4.5 mm height, FKM

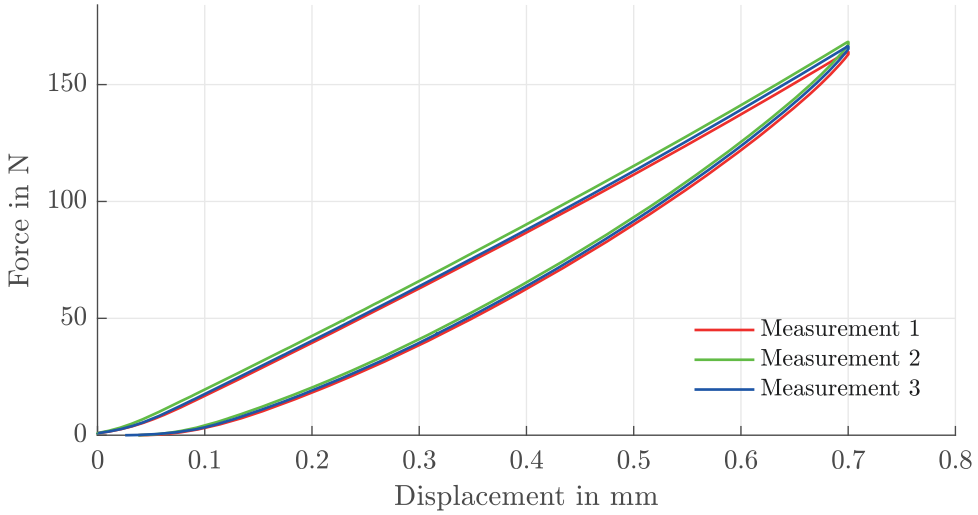

Figure 7.2: Compression test of the ElastoSpring concept with 12 cylinders and 4.5 mm height, H-NBR

7.5 Oil loss measurement results

Table 7.1: Overview of performed experiments

Experiment series	**Purpose**
V4	Evaluation of the MPTC set-up
V5	Evaluation of the repeatability of the MPTC set-up
V8	Evaluation of the OFD wiper
V9	Evaluation of the radial scraper

Test configuration: V4-3

Compressor speed: 1138 rpm, Maximum rod temperature: 223 ° C
Cup 1: OFD - OFD Cup 2: SL BCD Cup 3: BCD Cup 4: BCD

Oil Losses

Overall Cup1 (Wiper Cup): 55 ml/10 h – 5.3 ml/h – 7.7E-05 ml/round
Overall Cup2 (SL BCD Cup): 38 ml/10 h – 3.7 ml/h – 5.4E-05 ml/round
Overall Cup3 (Pressure Cup): 50 ml/10 h – 4.8 ml/h – 7.1E-05 ml/round
Total oil loss in all Cups: 143 ml/10 h

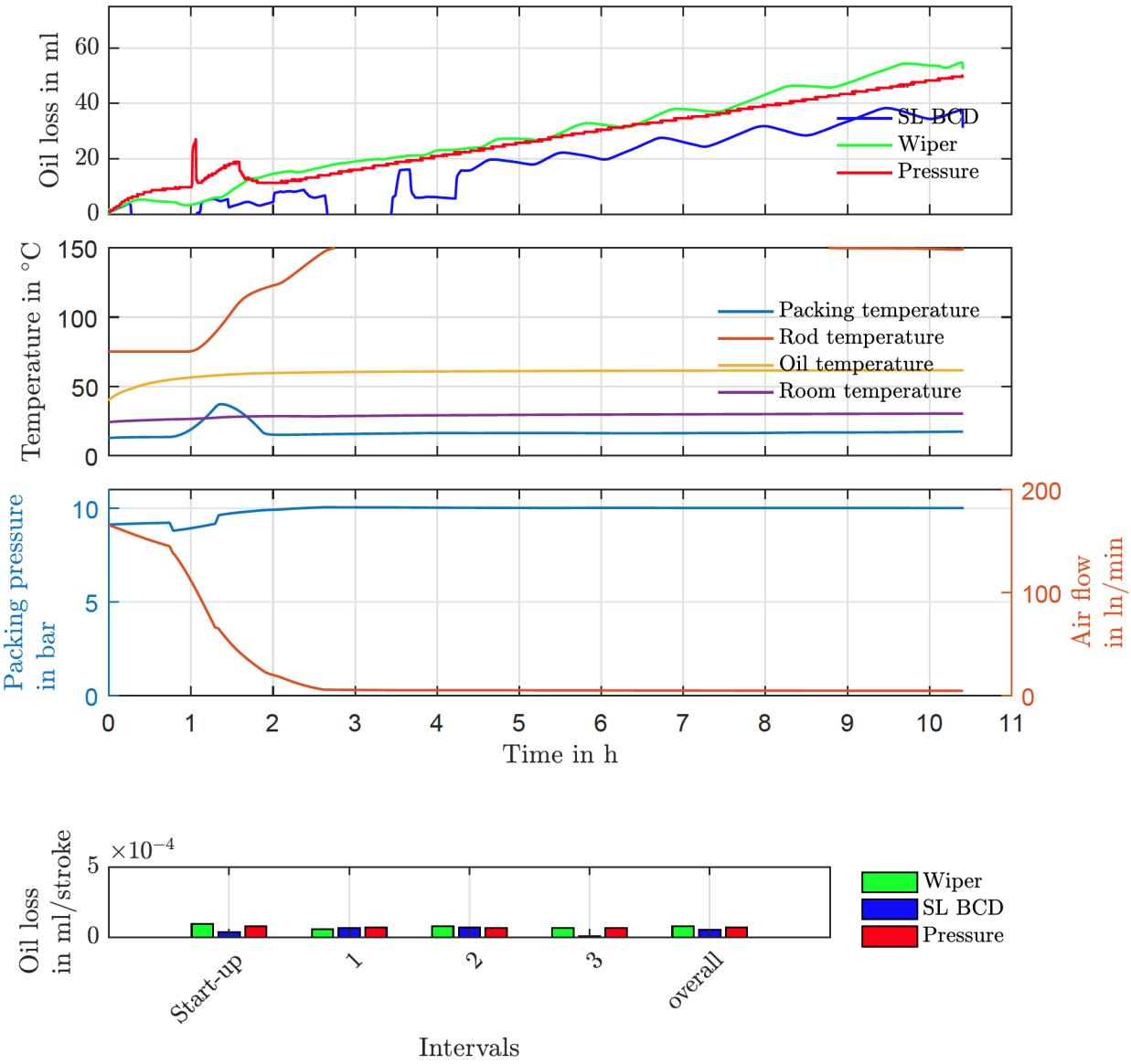

Figure 7.3: Measurement results of experiment V4-3

Test configuration: V5-1

Compressor speed: 1515 rpm, Maximum rod temperature: 169 ^{o} C
Cup 1: OFD - OFD Cup 2: SL BCD Cup 3: BCD Cup 4: BCD

Oil Losses

Overall Cup1 (Wiper Cup): 118 ml/6 h – 20.3 ml/h – 2.2E-04 ml/round
Overall Cup2 (SL BCD Cup): 118 ml/6 h – 20.2 ml/h – 2.2E-04 ml/round
Overall Cup3 (Pressure Cup): 115 ml/6 h – 19.8 ml/h – 2.2E-04 ml/round
Total oil loss in all Cups: 351 ml/6 h

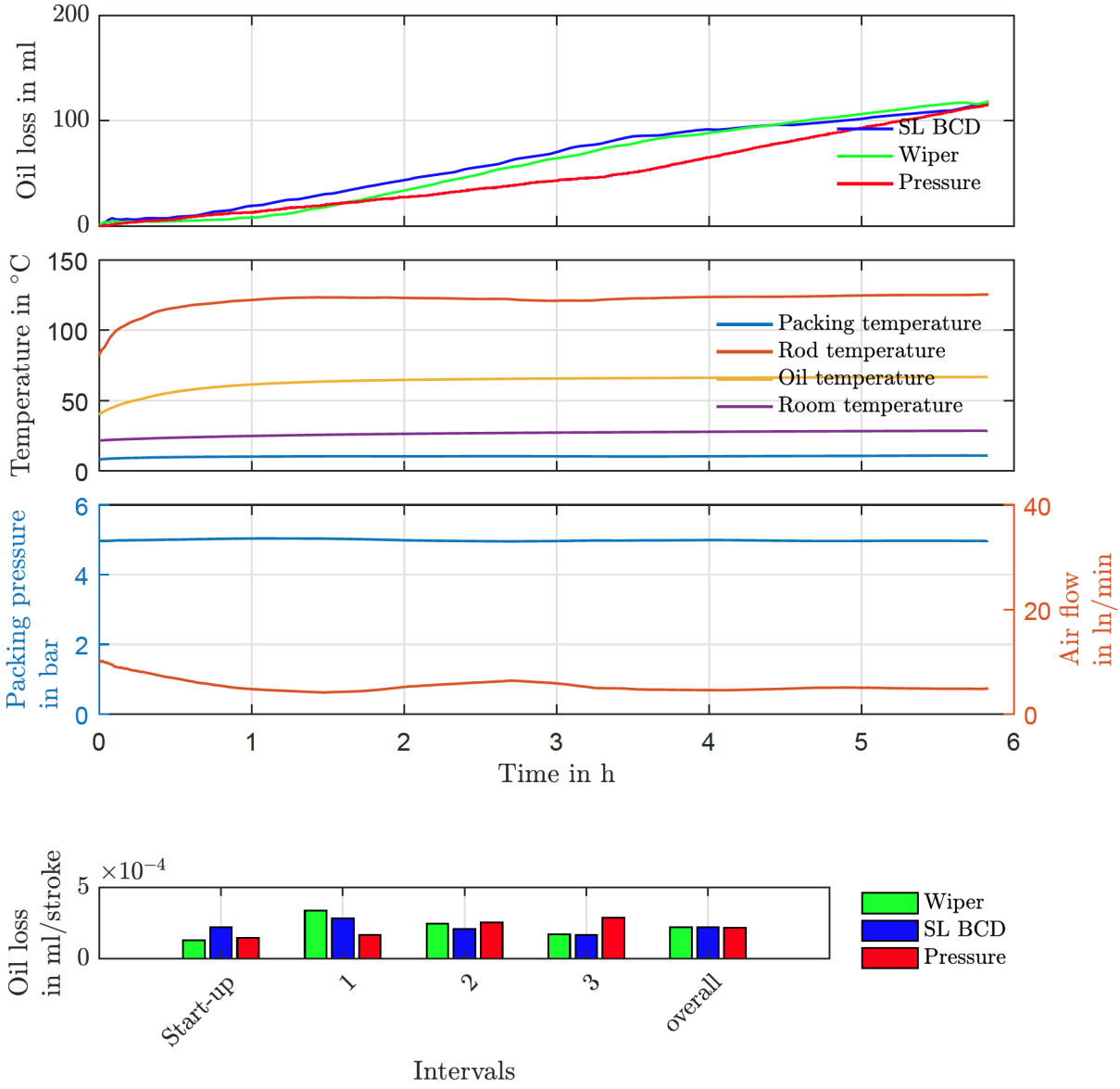

Figure 7.4: Measurement results of experiment V5-1

Test configuration: V5-2

Compressor speed: 1523 rpm, Maximum rod temperature: 201 ^{o} C
Cup 1: OFD - OFD Cup 2: SL BCD Cup 3: BCD Cup 4: BCD

Oil Losses

Overall Cup1 (Wiper Cup): 59 ml/6 h – 10.0 ml/h – 1.1E-04 ml/round
Overall Cup2 (SL BCD Cup): 18 ml/6 h – 3.1 ml/h – 3.4E-05 ml/round
Overall Cup3 (Pressure Cup): 135 ml/6 h – 22.9 ml/h – 2.5E-04 ml/round
Total oil loss in all Cups: 212 ml/6 h

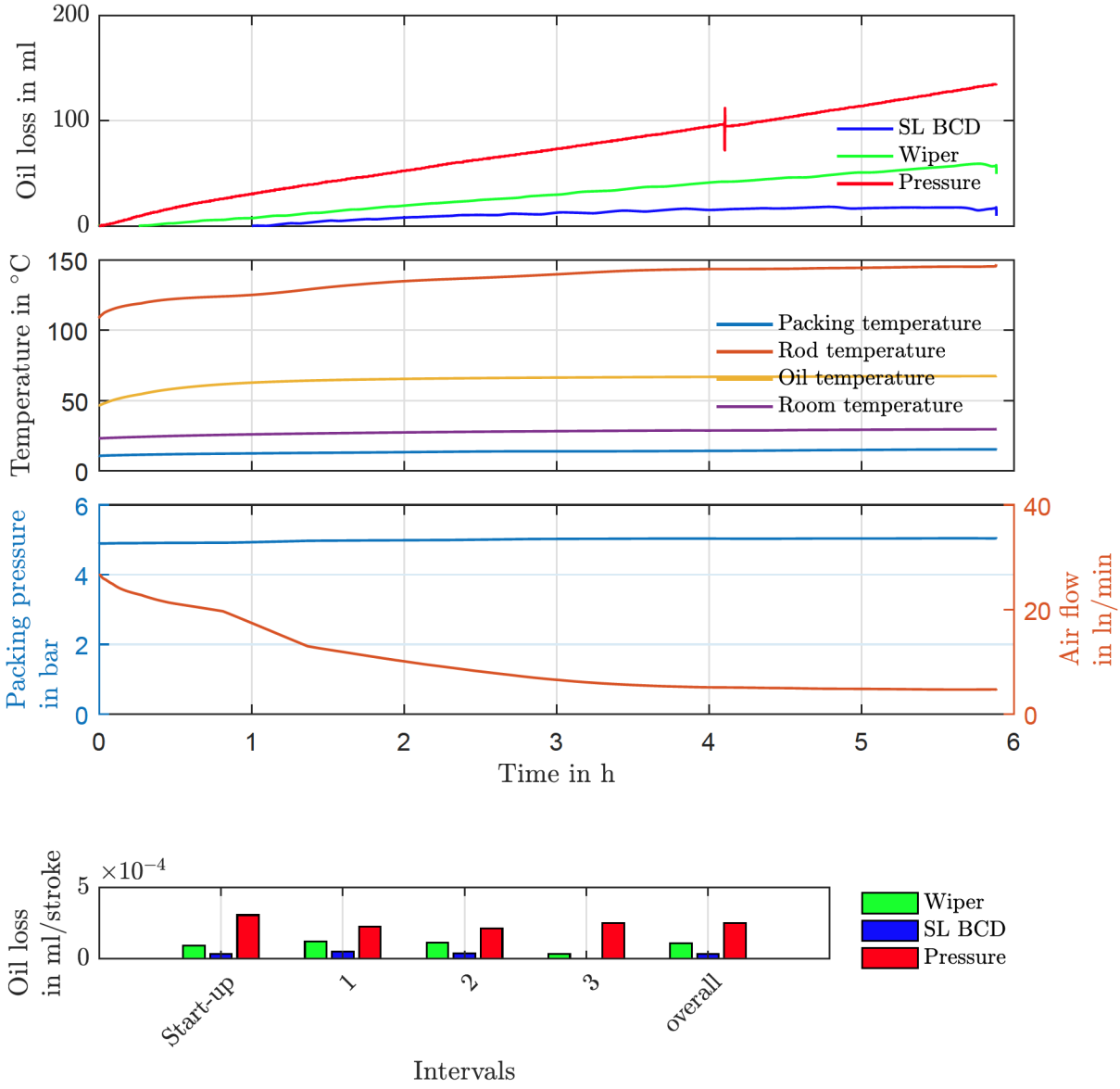

Figure 7.5: Measurement results of experiment V5-2

Test configuration: V5-3

Compressor speed: 1523 rpm, Maximum rod temperature: 169 ^{o} C
Cup 1: OFD - OFD Cup 2: SL BCD Cup 3: BCD Cup 4: BCD

Oil Losses

Overall Cup1 (Wiper Cup): 145 ml/7 h – 21.9 ml/h – 2.4E-04 ml/round
Overall Cup2 (SL BCD Cup): 60 ml/7 h – 9.0 ml/h – 9.8E-05 ml/round
Overall Cup3 (Pressure Cup): 161 ml/7 h – 24.3 ml/h – 2.7E-04 ml/round
Total oil loss in all Cups: 366 ml/7 h

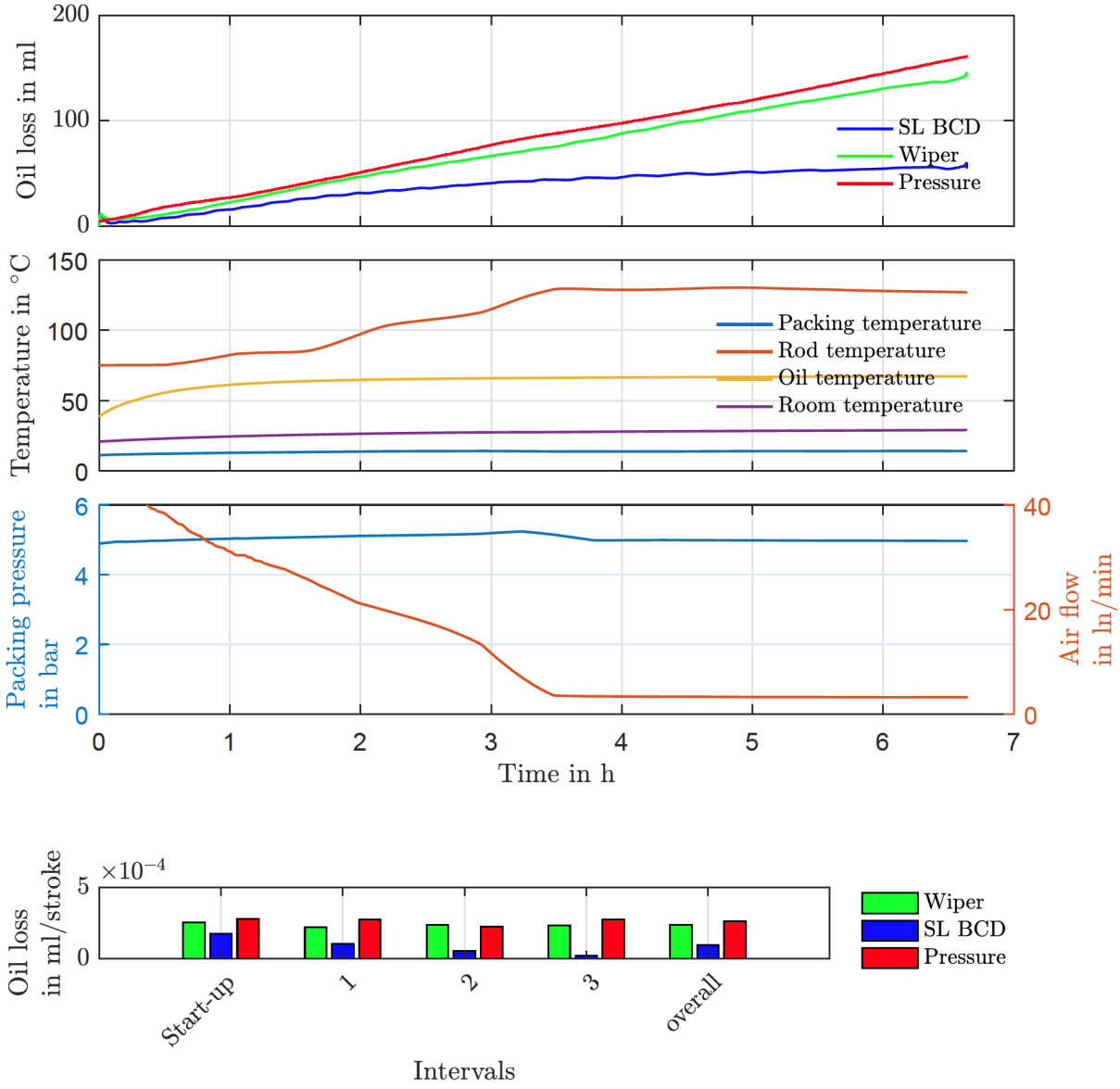

Figure 7.6: Measurement results of experiment V5-3

Test configuration: V5-4

Compressor speed: 1523 rpm, Maximum rod temperature: 179 ^{o} C
Cup 1: OFD - OFD Cup 2: SL BCD Cup 3: BCD Cup 4: BCD

Oil Losses

Overall Cup1 (Wiper Cup): 102 ml/7 h – 15.1 ml/h – 1.7E-04 ml/round
Overall Cup2 (SL BCD Cup): 7 ml/7 h – 1.1 ml/h – 1.2E-05 ml/round
Overall Cup3 (Pressure Cup): 128 ml/7 h – 19.0 ml/h – 2.1E-04 ml/round
Total oil loss in all Cups: 236 ml/7 h

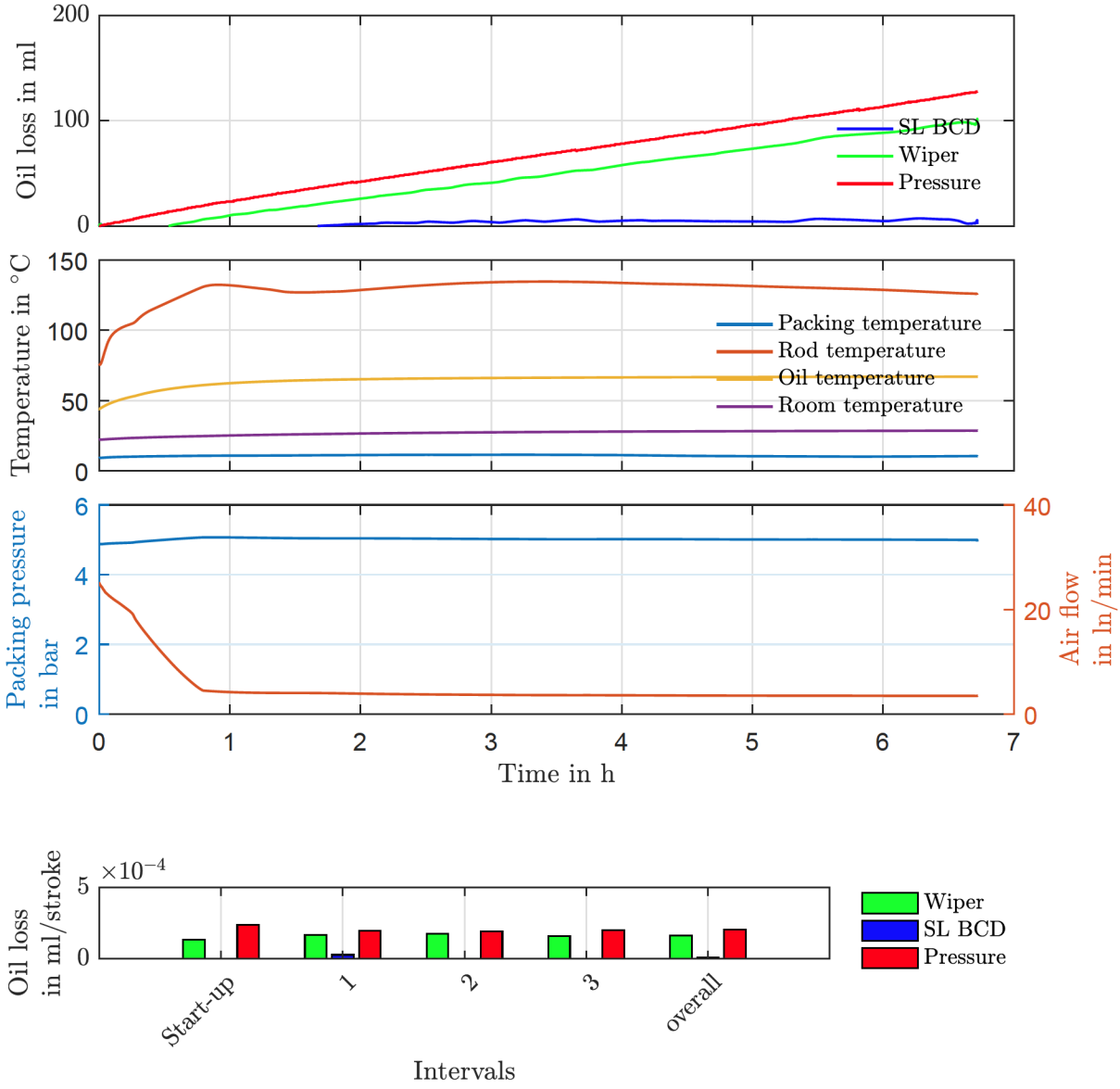

Figure 7.7: Measurement results of experiment V5-4

Oil loss measurement results of the OFD wiper

———— Test configuration: V8-1 ————

Compressor speed: 711 rpm, Maximum rod temperature: 92 ^{o} C
Cup 1: OFD - OFD Cup 2: no ring Cup 3: HCA Cup 4: SLP T2CC
———— Oil Losses ————
Overall Cup1 (Wiper Cup): 180 ml/24 h – 7.4 ml/h – 1.7E-04 ml/round
Overall Cup2 (SL BCD Cup): 0 ml/
Overall Cup3 (Pressure Cup): 309 ml/24 h – 12.7 ml/h – 3.0E-04 ml/round
Total oil loss in all Cups: 489 ml/24 h

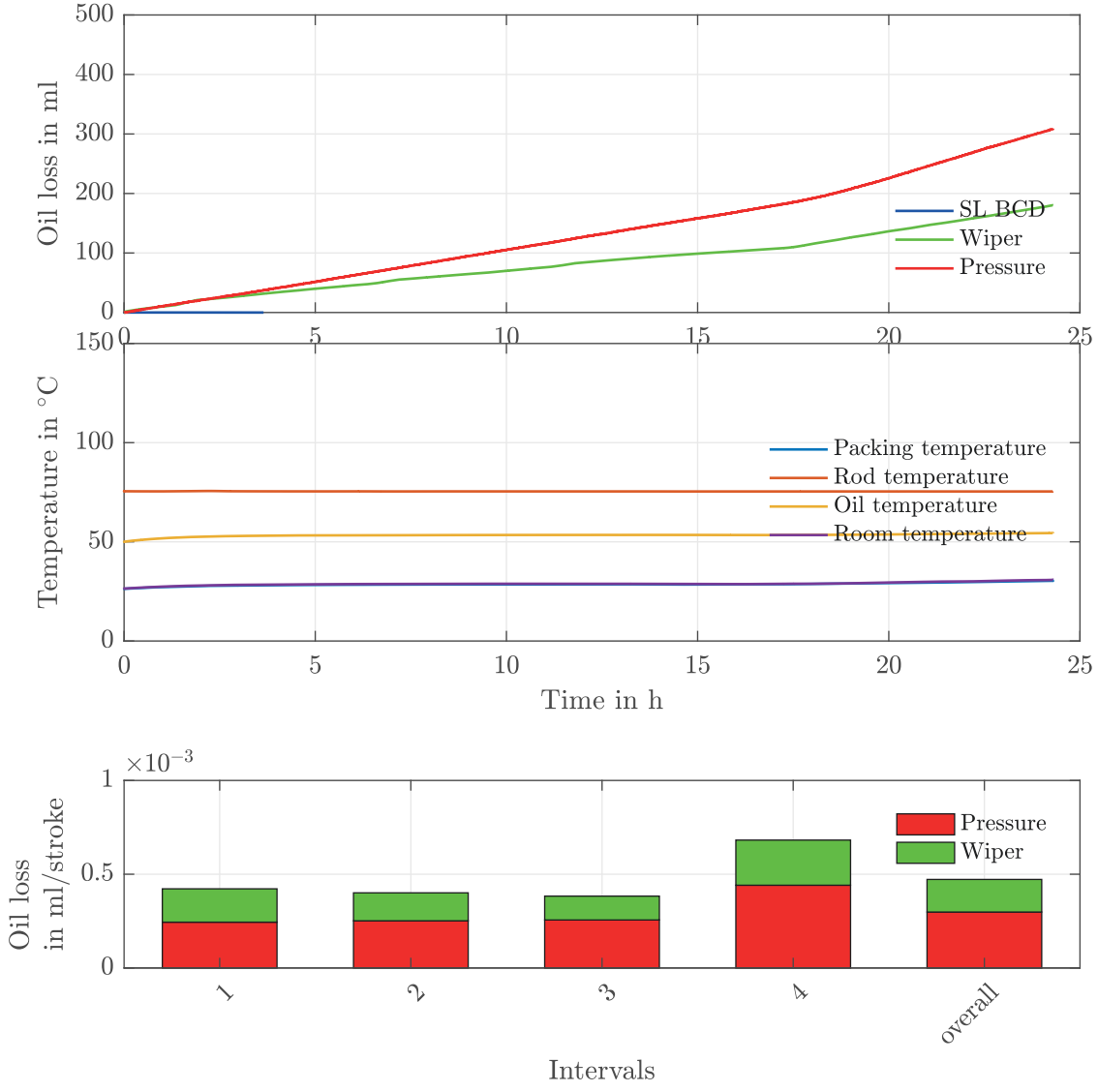

Figure 7.8: Measurement results of experiment V8-1

Test configuration: V8-2

Compressor speed: 1115 rpm, Maximum rod temperature: 101 ^{o} C
Cup 1: OFD - OFD Cup 2: no ring Cup 3: HCA Cup 4: SLP T2CC

Oil Losses

Overall Cup1 (Wiper Cup): 407 ml/20 h – 20.1 ml/h – 3.0E-04 ml/round
Overall Cup2 (SL BCD Cup): 0 ml/
Overall Cup3 (Pressure Cup): 418 ml/20 h – 20.6 ml/h – 3.1E-04 ml/round
Total oil loss in all Cups: 825 ml/20 h

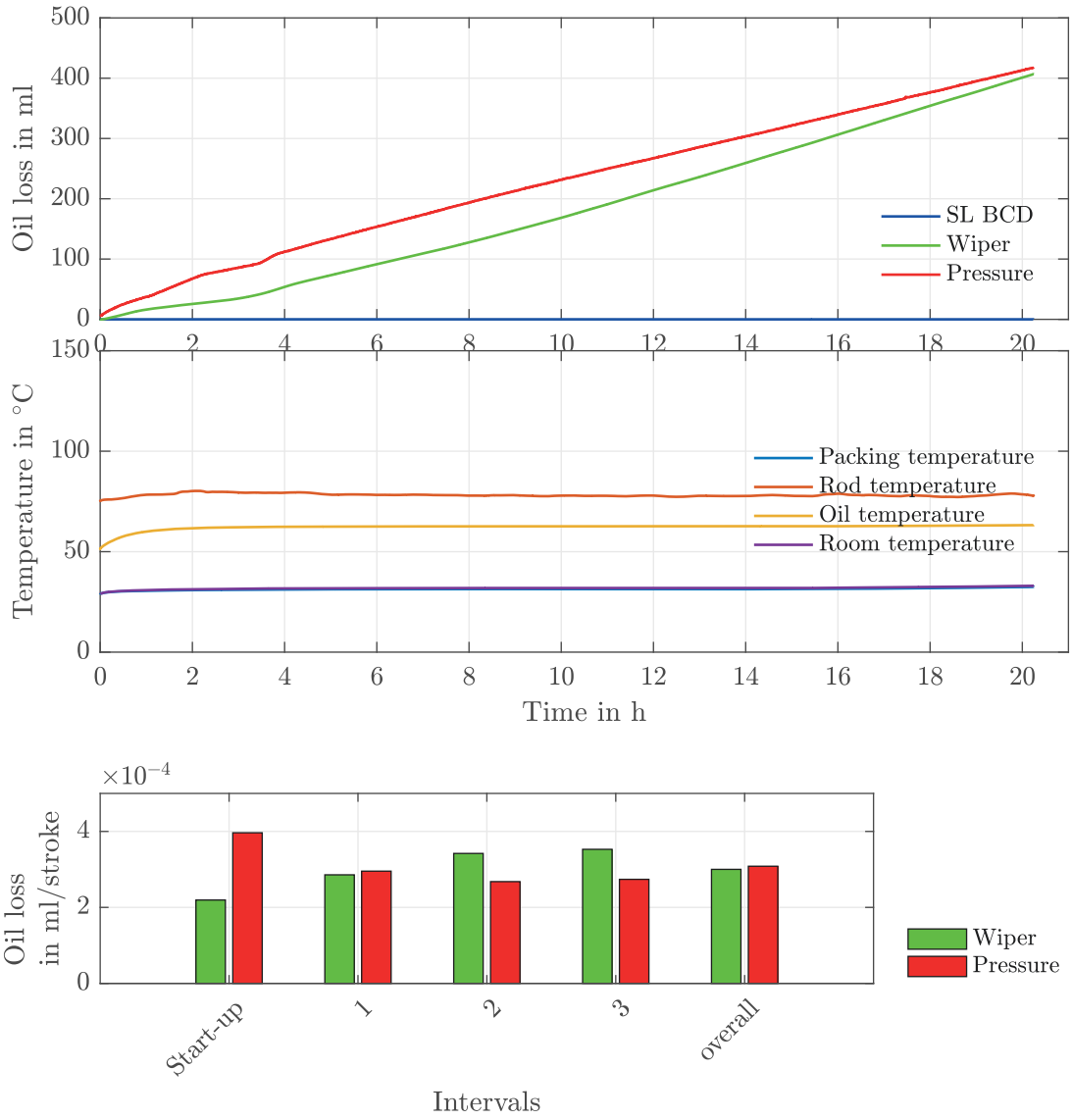

Figure 7.9: Measurement results of experiment V8-2

Test configuration: V8-3

Compressor speed: 1515 rpm, Maximum rod temperature: 112 ^{o} C
Cup 1: OFD - OFD Cup 2: no ring Cup 3: HCA Cup 4: SLP T2CC

Oil Losses

Overall Cup1 (Wiper Cup): 239 ml/24 h – 9.8 ml/h – 1.1E-04 ml/round
Overall Cup2 (SL BCD Cup): 1 ml/
Overall Cup3 (Pressure Cup): 298 ml/24 h – 12.2 ml/h – 1.3E-04 ml/round
Total oil loss in all Cups: 538 ml/24 h

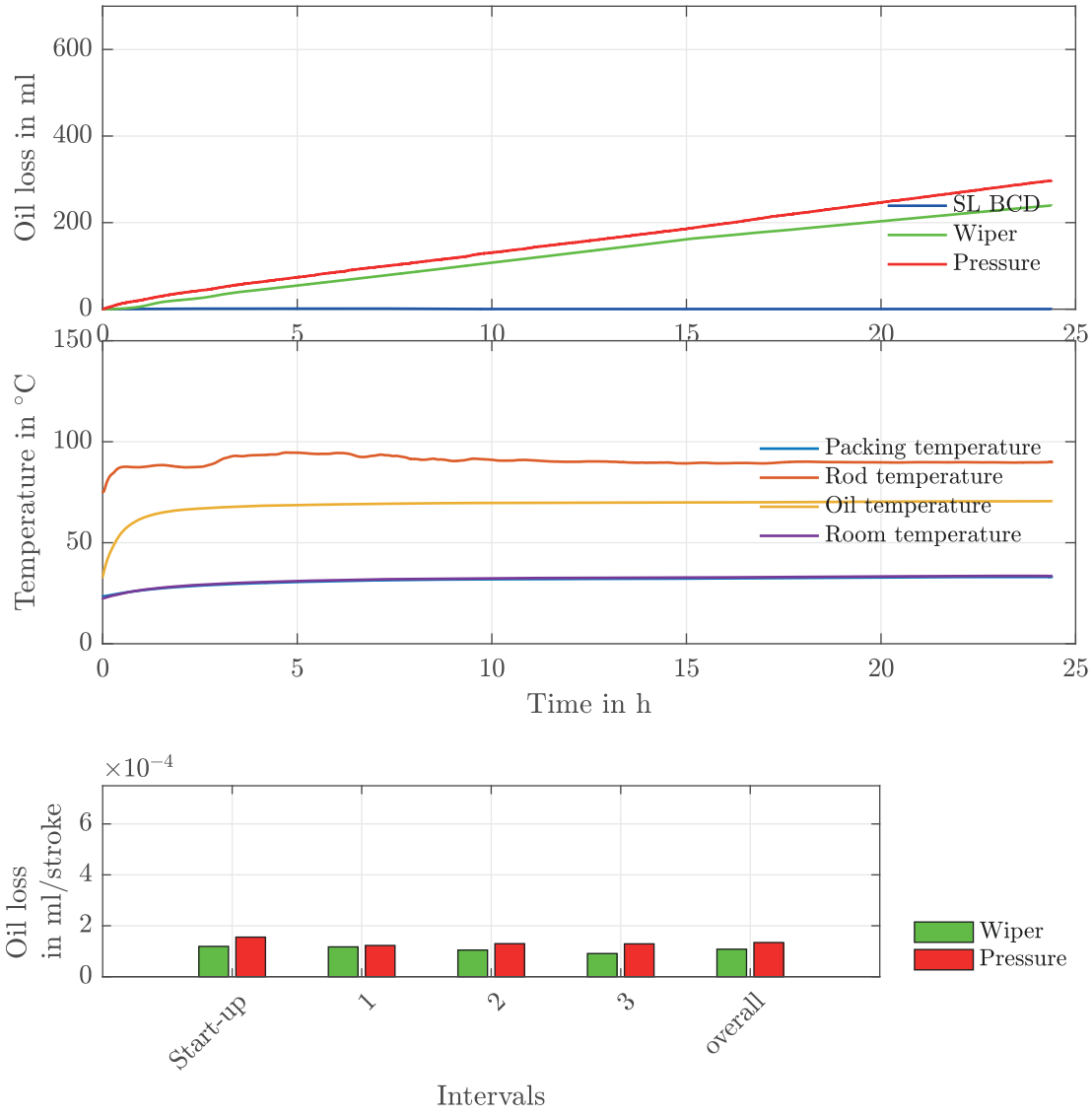

Figure 7.10: Measurement results of experiment V8-3

——————— Test configuration: V8-4 ———————

Compressor speed: 710 rpm, Maximum rod temperature: 92 ^{o} C
Cup 1: OFD - OFD Cup 2: no ring Cup 3: HCA Cup 4: SLP T2CC
——————— Oil Losses ———————
Overall Cup1 (Wiper Cup): 260 ml/25 h – 10.6 ml/h – 2.5E-04 ml/round
Overall Cup2 (SL BCD Cup): 2 ml/
Overall Cup3 (Pressure Cup): 664 ml/25 h – 27.0 ml/h – 6.3E-04 ml/round
Total oil loss in all Cups: 925 ml/25 h

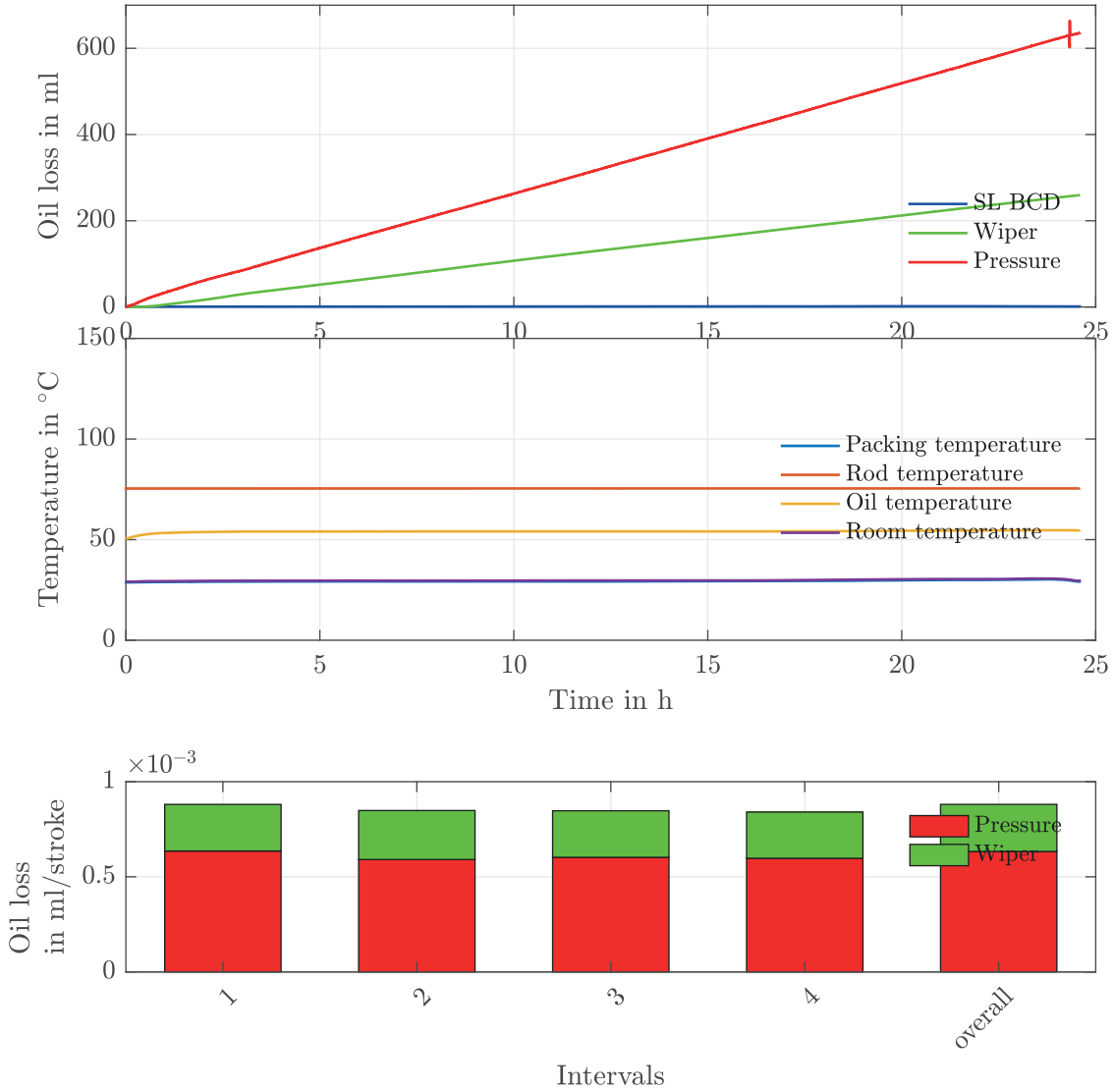

Figure 7.11: Measurement results of experiment V8-4

——————— Test configuration: V8-5 ———————

Compressor speed: 1115 rpm, Maximum rod temperature: 101 ^{o} C
Cup 1: OFD - OFD Cup 2: no ring Cup 3: HCA Cup 4: SLP T2CC
——————— Oil Losses ———————
Overall Cup1 (Wiper Cup): 1079 ml/24 h – 44.7 ml/h – 6.7E-04 ml/round
Overall Cup2 (SL BCD Cup): 0 ml/
Overall Cup3 (Pressure Cup): 388 ml/24 h – 16.1 ml/h – 2.4E-04 ml/round
Total oil loss in all Cups: 1467 ml/24 h

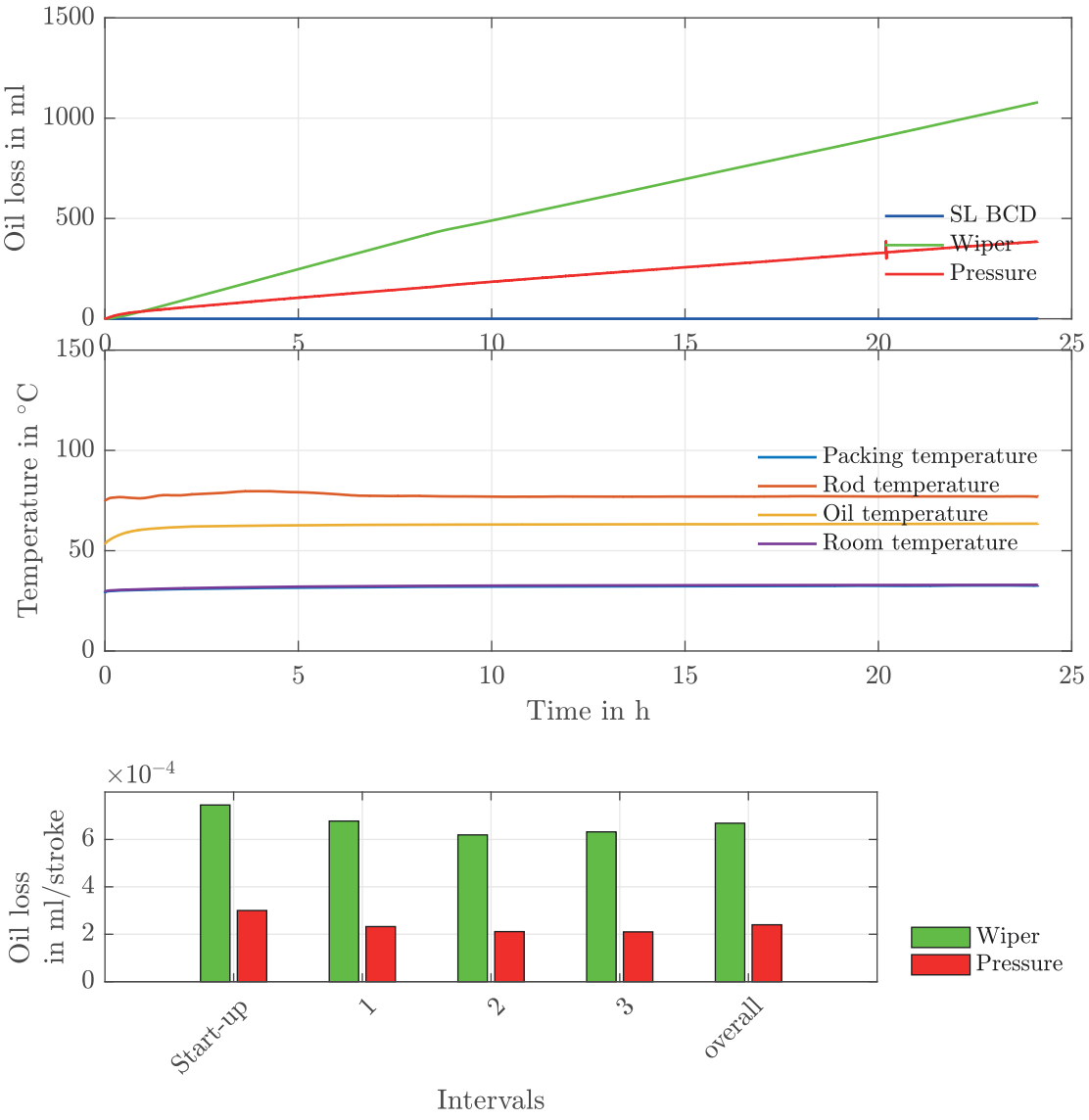

Figure 7.12: Measurement results of experiment V8-5

——————— Test configuration: V8-6 ———————

Compressor speed: 1515 rpm, Maximum rod temperature: 105 ^{o} C
Cup 1: OFD - OFD Cup 2: no ring Cup 3: HCA Cup 4: SLP T2CC
——————— Oil Losses ———————
Overall Cup1 (Wiper Cup): 914 ml/24 h – 38.1 ml/h – 4.2E-04 ml/round
Overall Cup2 (SL BCD Cup): 0 ml/
Overall Cup3 (Pressure Cup): 284 ml/24 h – 11.8 ml/h – 1.3E-04 ml/round
Total oil loss in all Cups: 1198 ml/24 h

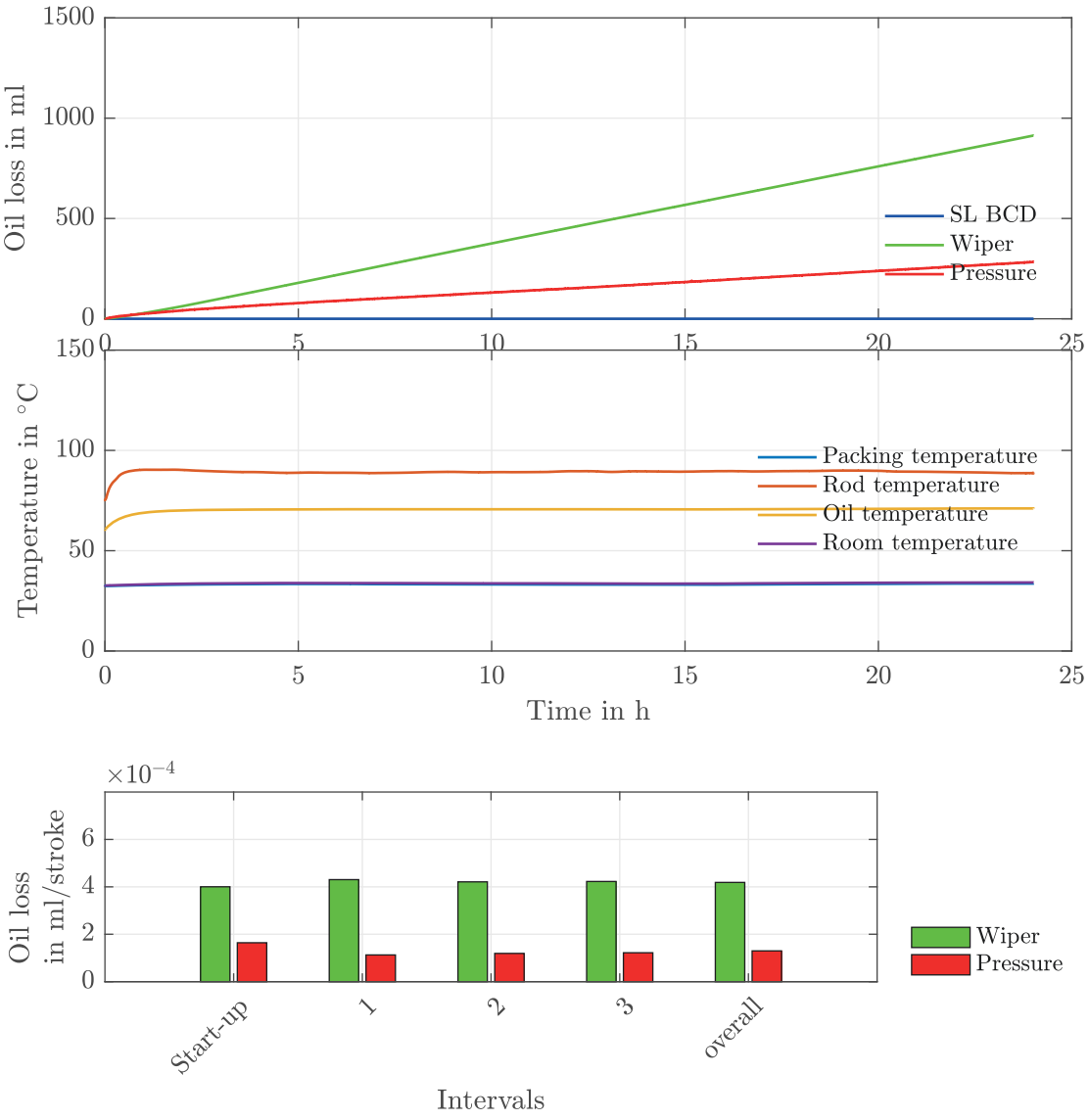

Figure 7.13: Measurement results of experiment V8-6

Oil loss measurement results of set-up without pressure section of the radial scraper

Test configuration: V9-7

Compressor speed: 711 rpm, Maximum rod temperature: 93 ° C
Cup 1: HCA Cup 2: no ring Cup 3: HCA Cup 4: SLP T2CC

Oil Losses

Overall Cup1 (Wiper Cup): 1 ml/24 h – 0.1 ml/h – 1.2E-06 ml/round
Overall Cup2 (SL BCD Cup): 0 ml/
Overall Cup3 (Pressure Cup): 591 ml/24 h – 24.4 ml/h – 5.7E-04 ml/round
Total oil loss in all Cups: 592 ml/24 h

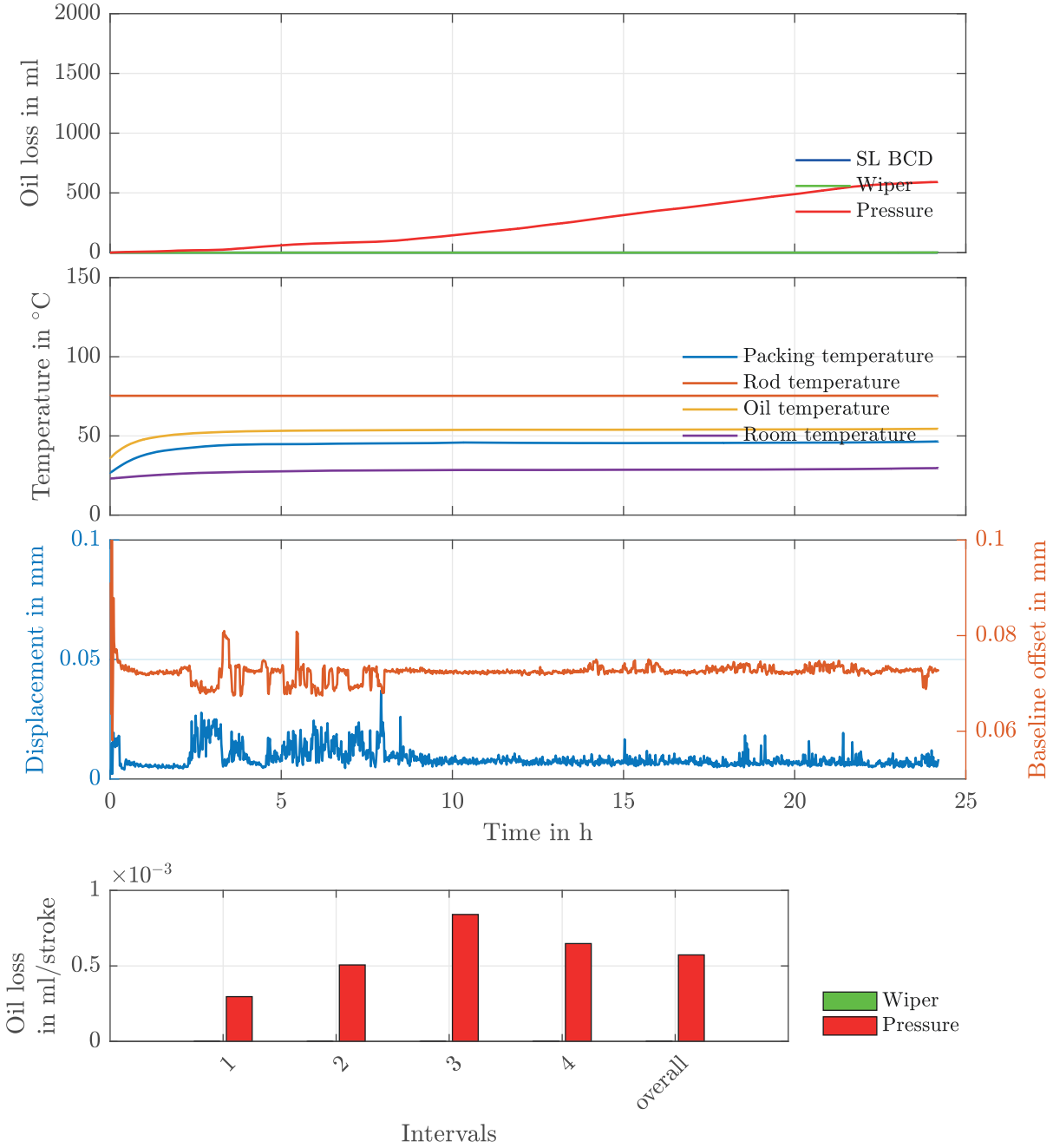

Figure 7.14: Measurement results of experiment V9-7

———— Test configuration: V9-8 ————

Compressor speed: 1115 rpm, Maximum rod temperature: 95 ^{o} C
Cup 1: HCA Cup 2: no ring Cup 3: HCA Cup 4: SLP T2CC

———— Oil Losses ————

Overall Cup1 (Wiper Cup): 1 ml/24 h – 0.1 ml/h – 7.5E-07 ml/round
Overall Cup2 (SL BCD Cup): 0 ml/
Overall Cup3 (Pressure Cup): 42 ml/24 h – 1.7 ml/h – 2.6E-05 ml/round
Total oil loss in all Cups: 43 ml/24 h

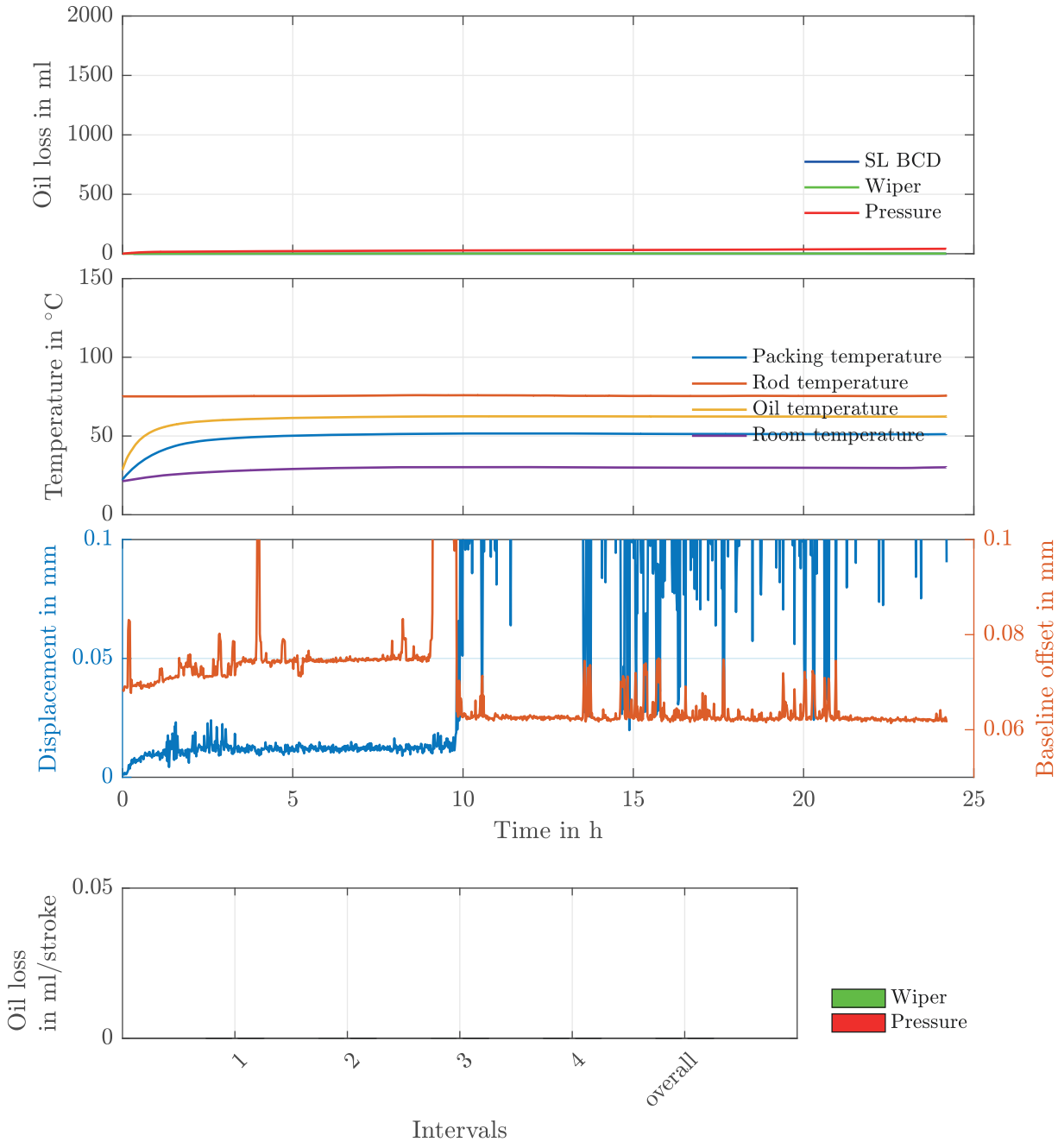

Figure 7.15: Measurement results of experiment V9-8

Test configuration: V9-9

Compressor speed: 1522 rpm, Maximum rod temperature: 107 ^{o} C
Cup 1: HCA Cup 2: no ring Cup 3: HCA Cup 4: SLP T2CC

Oil Losses

Overall Cup1 (Wiper Cup): 0 ml/24 h – 0.0 ml/h – 9.8E-08 ml/round
Overall Cup2 (SL BCD Cup): 4 ml/
Overall Cup3 (Pressure Cup): 153 ml/24 h – 6.3 ml/h – 6.9E-05 ml/round
Total oil loss in all Cups: 157 ml/24 h

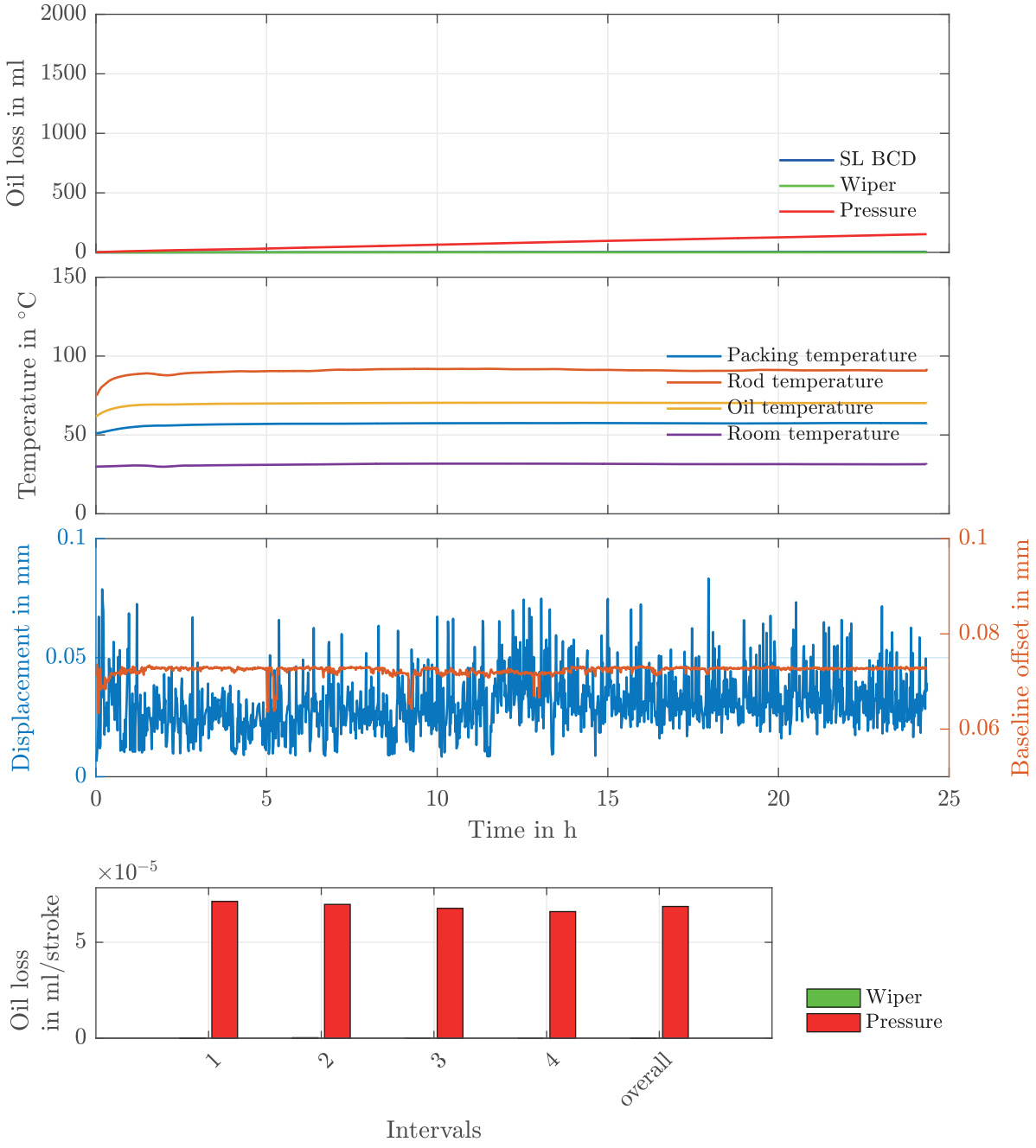

Figure 7.16: Measurement results of experiment V9-9

Test configuration: V9-10

Compressor speed: 711 rpm, Maximum rod temperature: 89 ^{o} C
Cup 1: HCA Cup 2: no ring Cup 3: HCA Cup 4: SLP T2CC

Oil Losses

Overall Cup1 (Wiper Cup): 0 ml/24 h – 0.0 ml/h – 8.3E-08 ml/round
Overall Cup2 (SL BCD Cup): 3 ml/
Overall Cup3 (Pressure Cup): 473 ml/24 h – 19.6 ml/h – 4.6E-04 ml/round
Total oil loss in all Cups: 475 ml/24 h

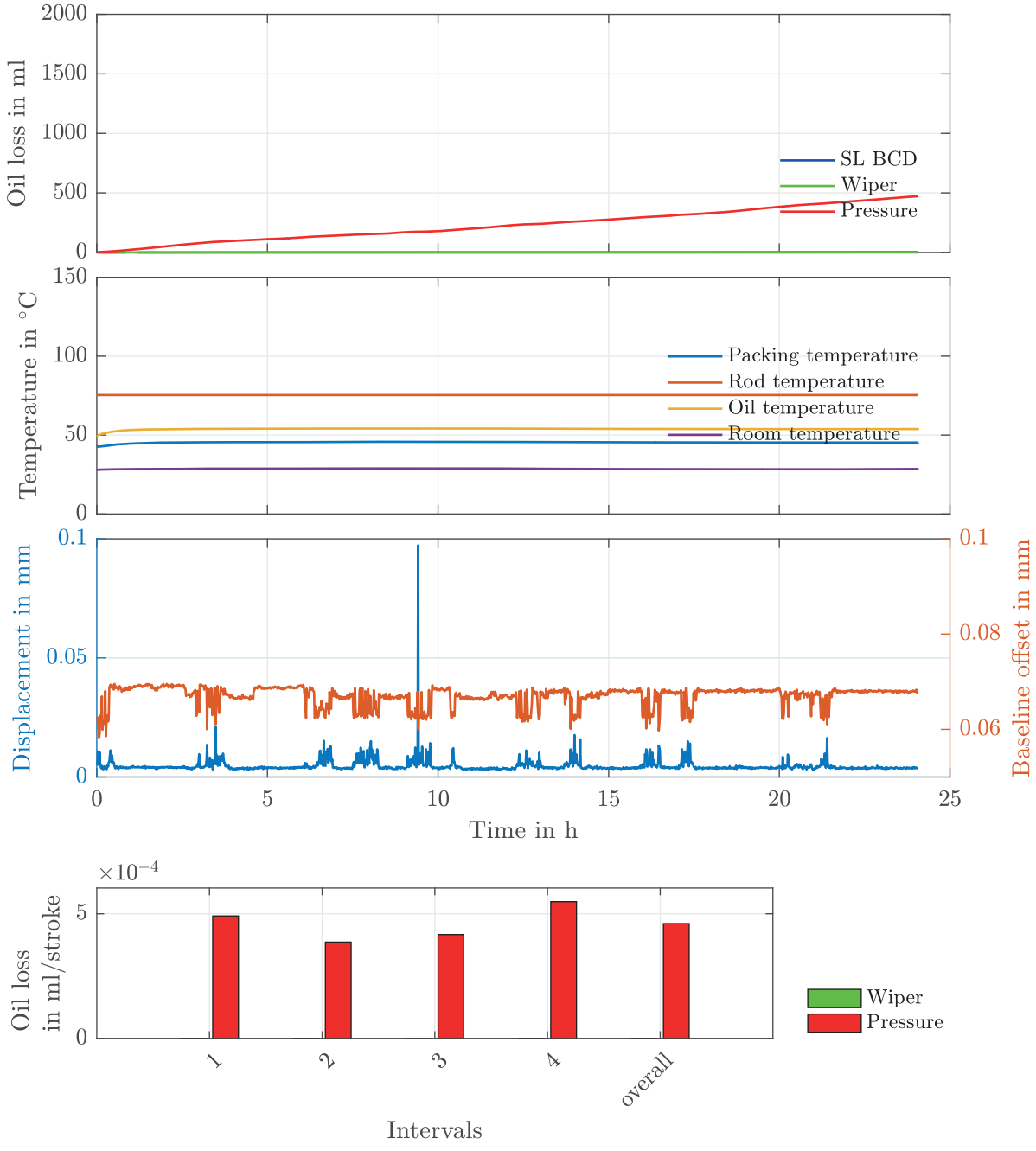

Figure 7.17: Measurement results of experiment V9-10

——————— Test configuration: V9-11 ———————

Compressor speed: 1115 rpm, Maximum rod temperature: 95 ^{o} C
Cup 1: HCA Cup 2: no ring Cup 3: HCA Cup 4: SLP T2CC

——————— Oil Losses ———————

Overall Cup1 (Wiper Cup): 1 ml/25 h – 0.0 ml/h – 6.5E-07 ml/round
Overall Cup2 (SL BCD Cup): 1 ml/
Overall Cup3 (Pressure Cup): 81 ml/25 h – 3.3 ml/h – 4.9E-05 ml/round
Total oil loss in all Cups: 83 ml/25 h

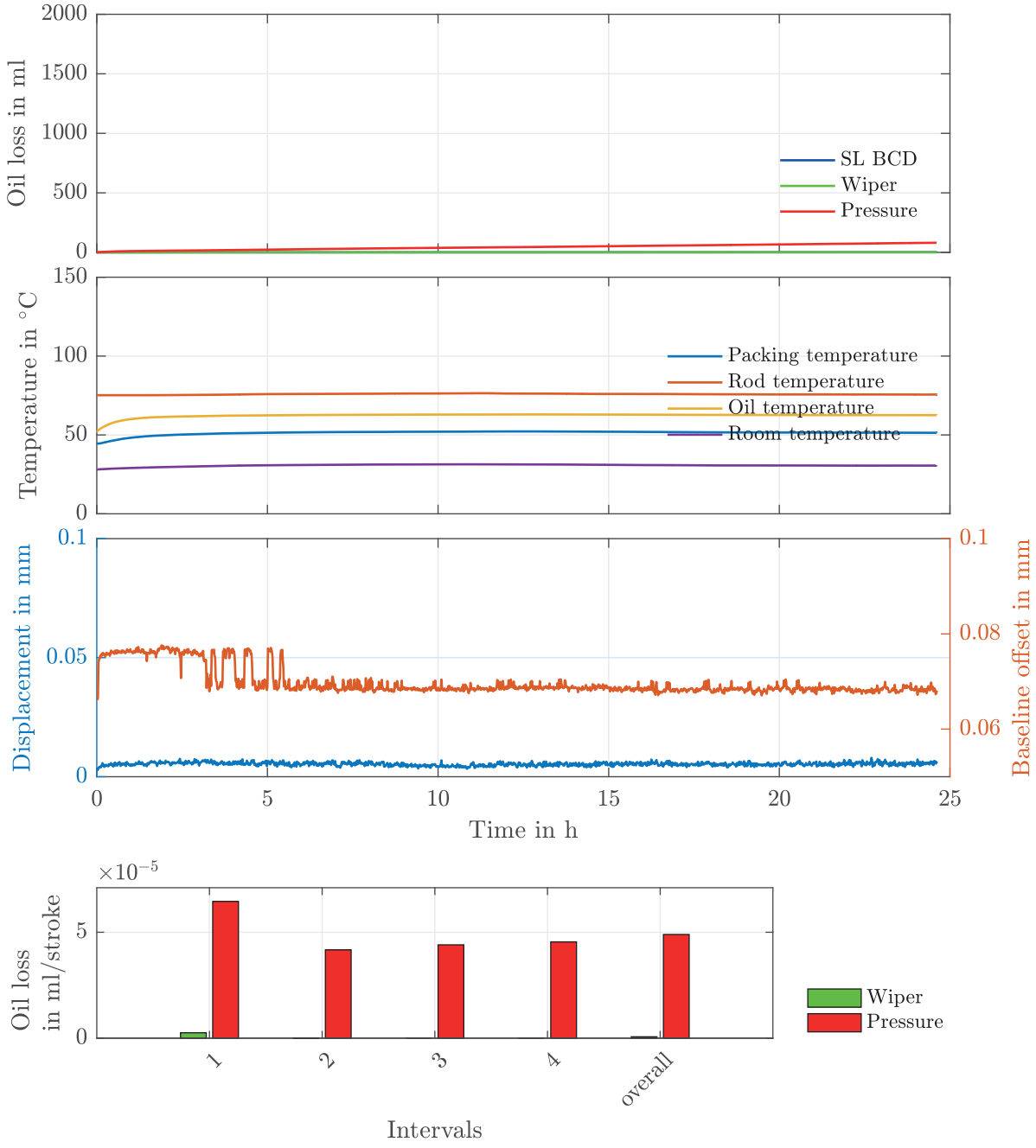

Figure 7.18: Measurement results of experiment V9-11

Test configuration: V9-12

Compressor speed: 1519 rpm, Maximum rod temperature: 104 ^{o} C
Cup 1: HCA Cup 2: no ring Cup 3: HCA Cup 4: SLP T2CC

Oil Losses

Overall Cup1 (Wiper Cup): 1 ml/24 h – 0.1 ml/h – 6.1E-07 ml/round
Overall Cup2 (SL BCD Cup): 1 ml/
Overall Cup3 (Pressure Cup): 77 ml/24 h – 3.1 ml/h – 3.5E-05 ml/round
Total oil loss in all Cups: 79 ml/24 h

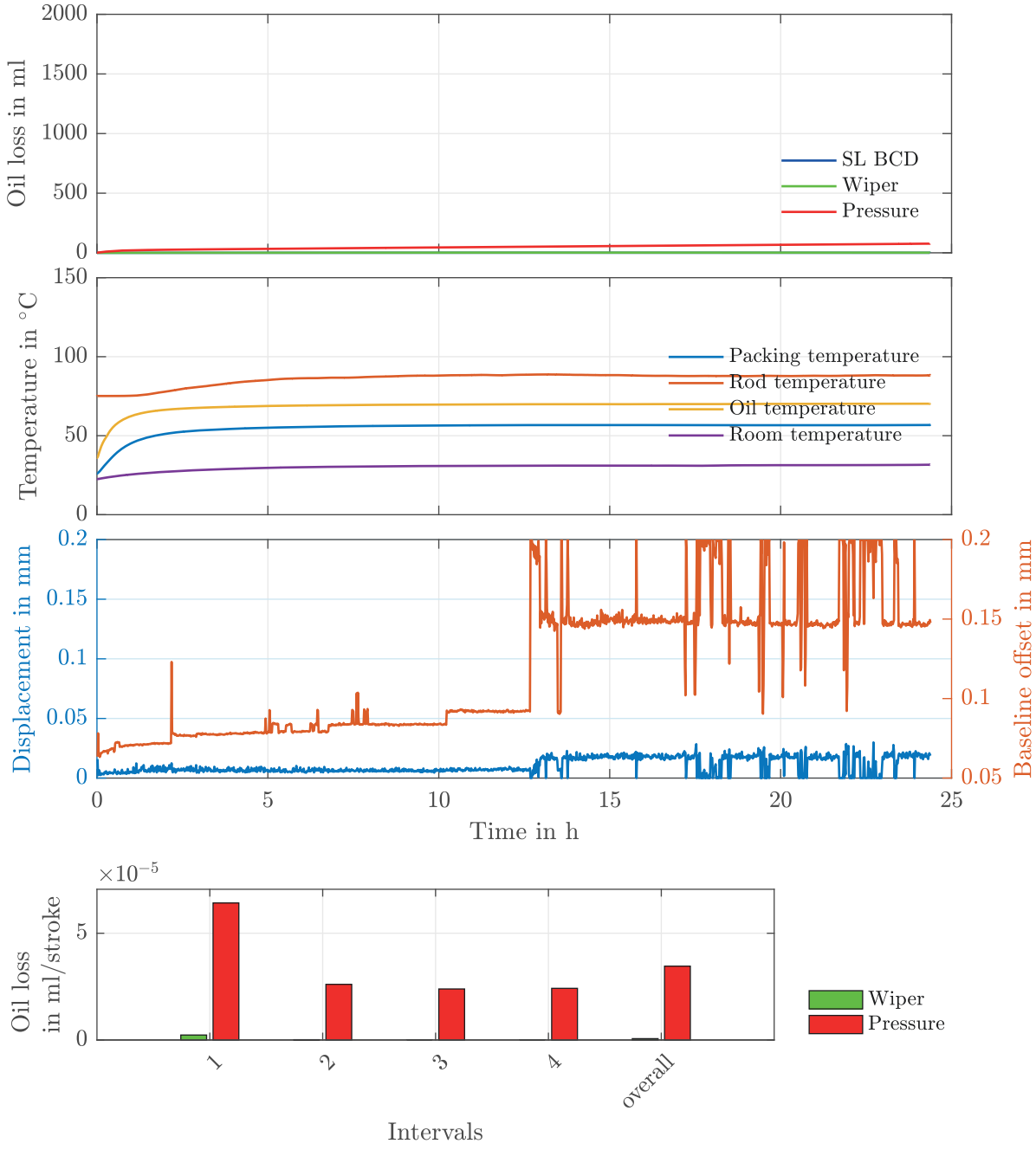

Figure 7.19: Measurement results of experiment V9-12

7.6 Test mould drawings

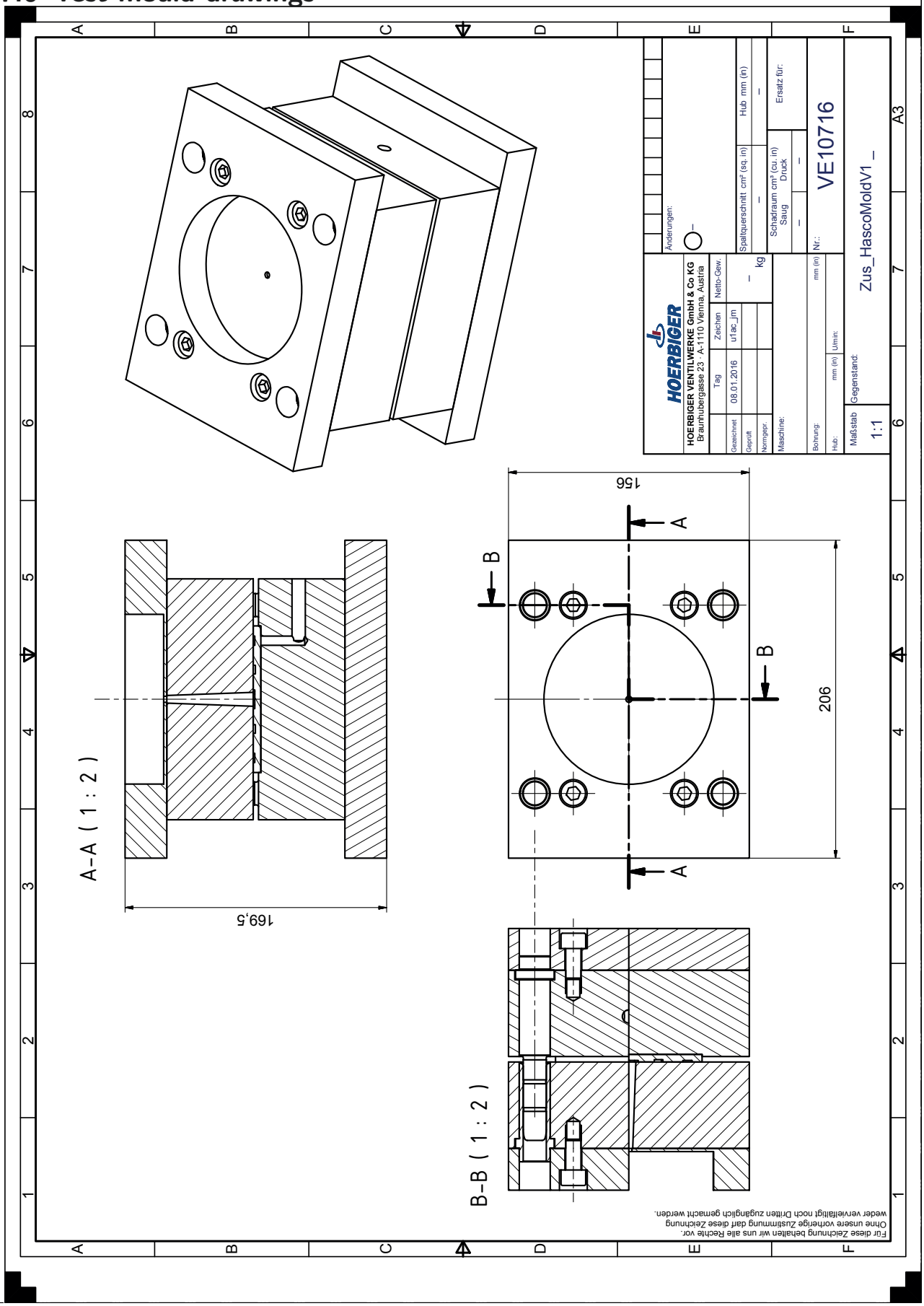

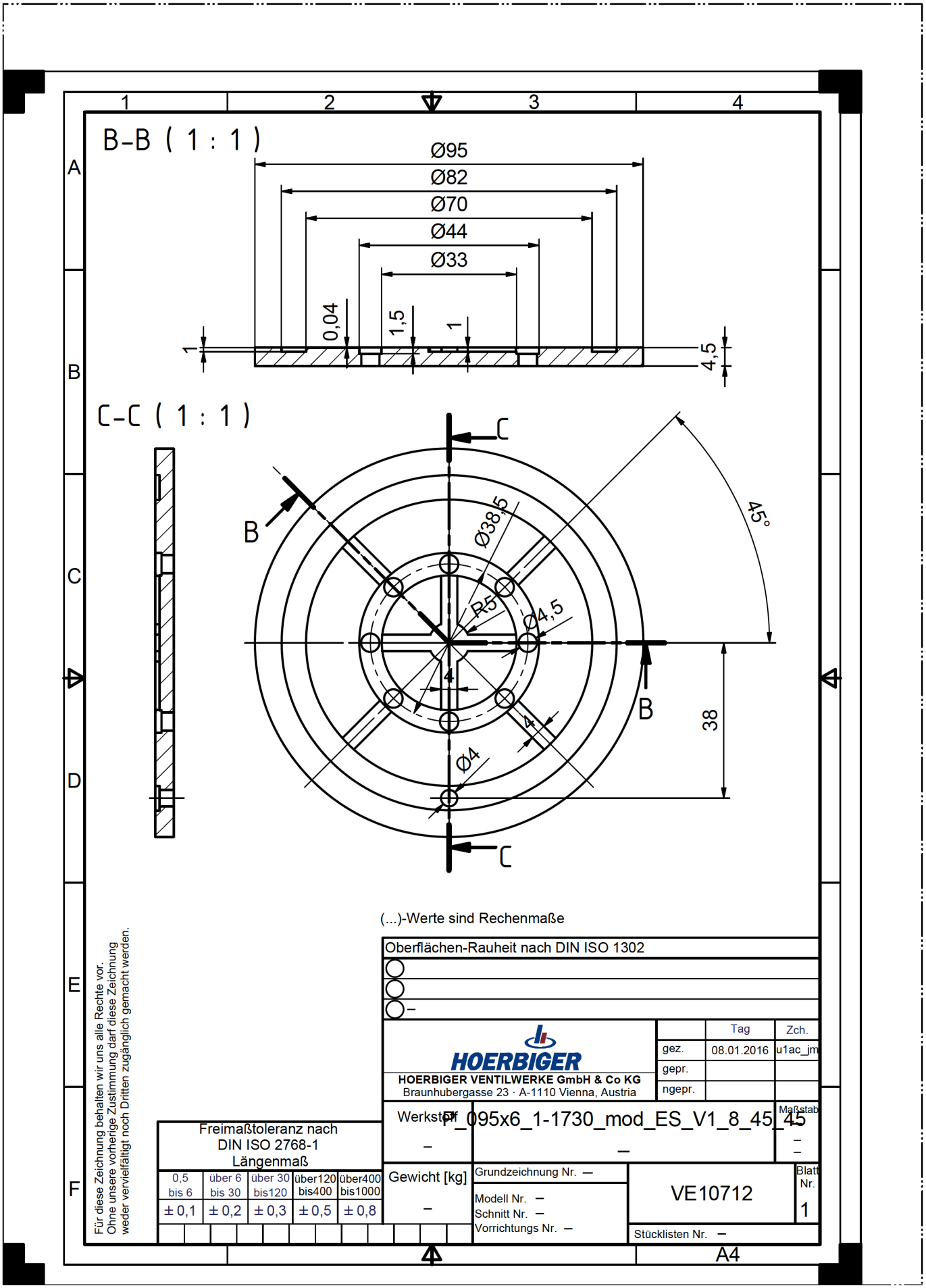
B-B (1 : 1)
Ø95
Ø82
Ø70
Ø44
Ø33
0,04
1,5
1
1
4,5
C-C (1 : 1)
C
B
Ø38,5
45°
R5
Ø4,5
4
B
38
4
Ø4
C
(...)-Werte sind Rechenmaße
Oberflächen-Rauheit nach DIN ISO 1302
HOERBIGER
HOERBIGER VENTILWERKE GmbH & Co KG
Braunhubergasse 23 · A-1110 Vienna, Austria
Tag
Zch.
gez.
08.01.2016
u1ac_jm
gepr.
ngepr.
Werkstoff
Pf_095x6_1-1730_mod_ES_V1_8_45_45
Maßstab
Freimaßtoleranz nach DIN ISO 2768-1 Längenmaß
0,5 bis 6
über 6 bis 30
über 30 bis120
über120 bis400
über400 bis1000
± 0,1
± 0,2
± 0,3
± 0,5
± 0,8
Gewicht [kg]
Grundzeichnung Nr.
Modell Nr.
Schnitt Nr.
Vorrichtungs Nr.
VE10712
Blatt Nr.
1
Stücklisten Nr.
A4
Für diese Zeichnung behalten wir uns alle Rechte vor.
Ohne unsere vorherige Zustimmung darf diese Zeichnung
weder vervielfältigt noch Dritten zugänglich gemacht werden.

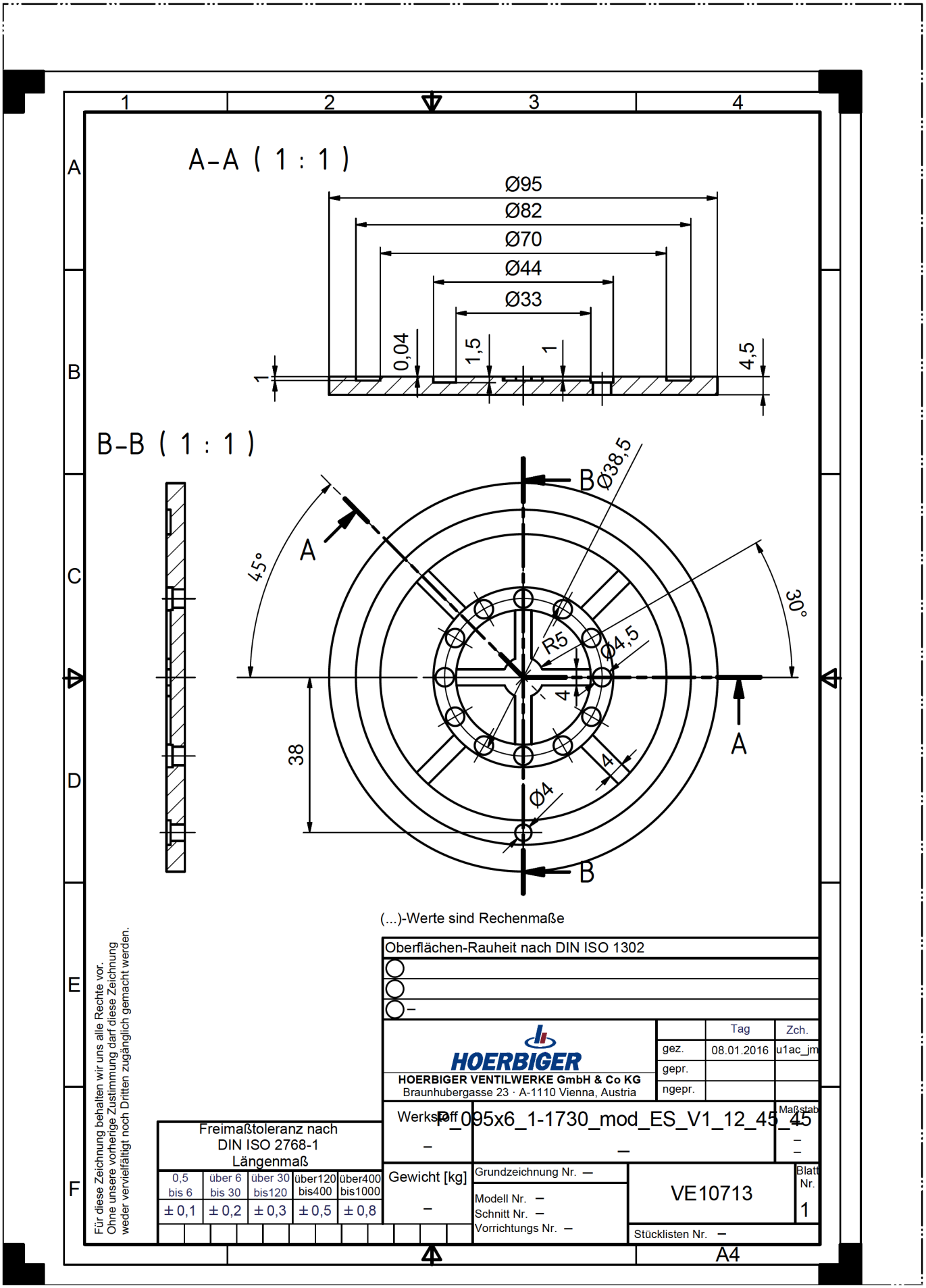
A-A (1 : 1)
Ø95
Ø82
Ø70
Ø44
Ø33
0,04
1,5
1
4,5
1
B-B (1 : 1)
Ø38,5
B
A
45°
30°
R5
Ø4,5
4
4
Ø4
38
A
B
(...)-Werte sind Rechenmaße
Oberflächen-Rauheit nach DIN ISO 1302
HOERBIGER
HOERBIGER VENTILWERKE GmbH & Co KG
Braunhubergasse 23 · A-1110 Vienna, Austria
Tag
Zch.
gez.
08.01.2016
u1ac_jm
gepr.
ngepr.
Werkstoff
P_095x6_1-1730_mod_ES_V1_12_45_45
Maßstab
Freimaßtoleranz nach DIN ISO 2768-1 Längenmaß
0,5 bis 6
über 6 bis 30
über 30 bis120
über120 bis400
über400 bis1000
± 0,1
± 0,2
± 0,3
± 0,5
± 0,8
Gewicht [kg]
Grundzeichnung Nr. –
Modell Nr. –
Schnitt Nr. –
Vorrichtungs Nr. –
VE10713
Blatt Nr.
1
Stücklisten Nr. –
A4
Für diese Zeichnung behalten wir uns alle Rechte vor.
Ohne unsere vorherige Zustimmung darf diese Zeichnung
weder vervielfältigt noch Dritten zugänglich gemacht werden.

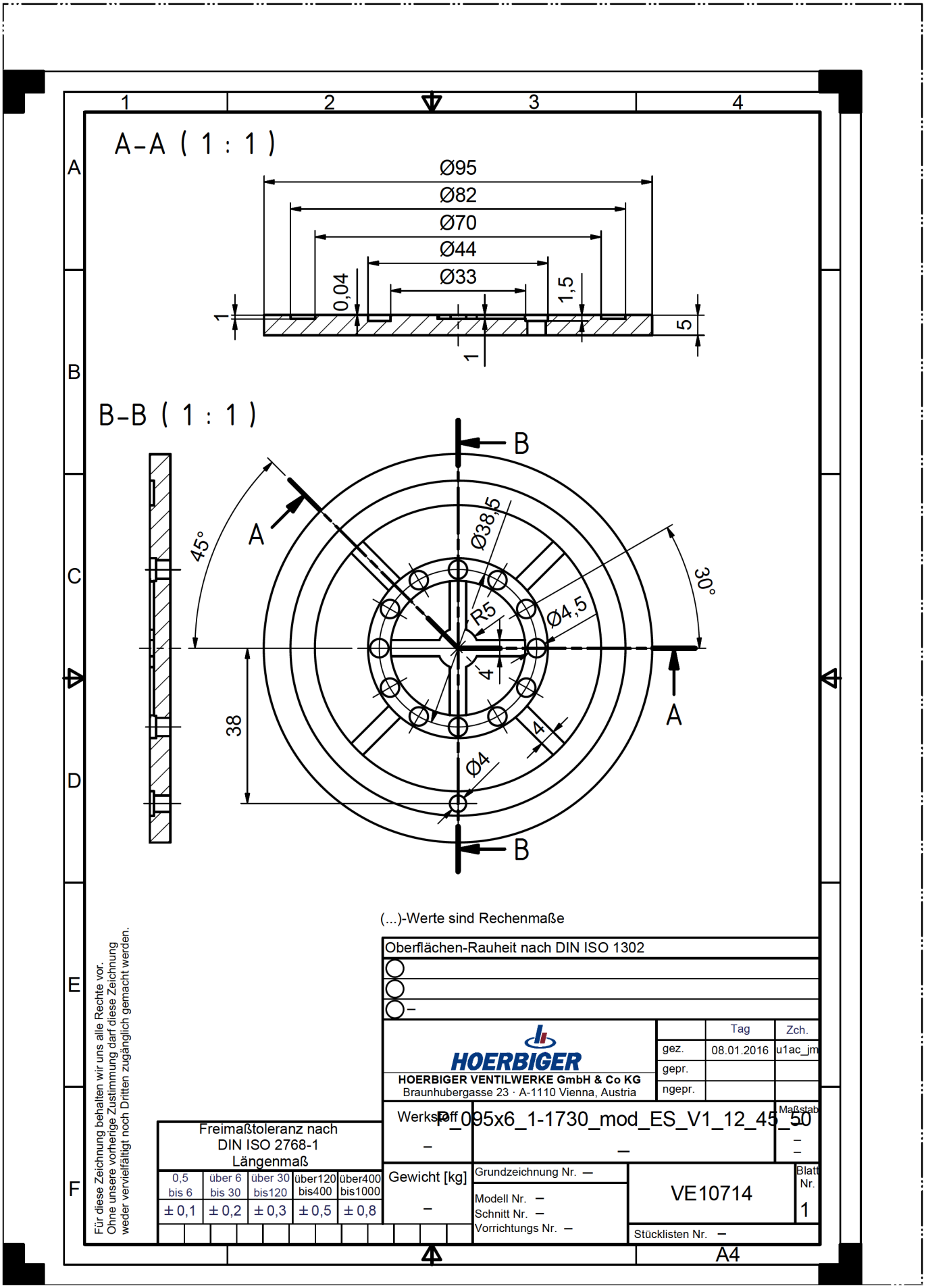
A–A (1 : 1)
Ø95
Ø82
Ø70
Ø44
Ø33
0,04
1,5
1
5
1
B–B (1 : 1)
B
A
45°
Ø38,5
30°
R5
Ø4,5
4
38
4
Ø4
A
B
(...)-Werte sind Rechenmaße
Oberflächen-Rauheit nach DIN ISO 1302
HOERBIGER
HOERBIGER VENTILWERKE GmbH & Co KG
Braunhubergasse 23 · A-1110 Vienna, Austria
Tag
Zch.
gez.
08.01.2016
u1ac_jm
gepr.
ngepr.
Werkstoff
P_095x6_1-1730_mod_ES_V1_12_45_50
Maßstab
Freimaßtoleranz nach DIN ISO 2768-1 Längenmaß
0,5 bis 6
über 6 bis 30
über 30 bis120
über120 bis400
über400 bis1000
± 0,1
± 0,2
± 0,3
± 0,5
± 0,8
Gewicht [kg]
Grundzeichnung Nr. –
Modell Nr. –
Schnitt Nr. –
Vorrichtungs Nr. –
VE10714
Blatt Nr.
1
Stücklisten Nr. –
A4
Für diese Zeichnung behalten wir uns alle Rechte vor.
Ohne unsere vorherige Zustimmung darf diese Zeichnung
weder vervielfältigt noch Dritten zugänglich gemacht werden.

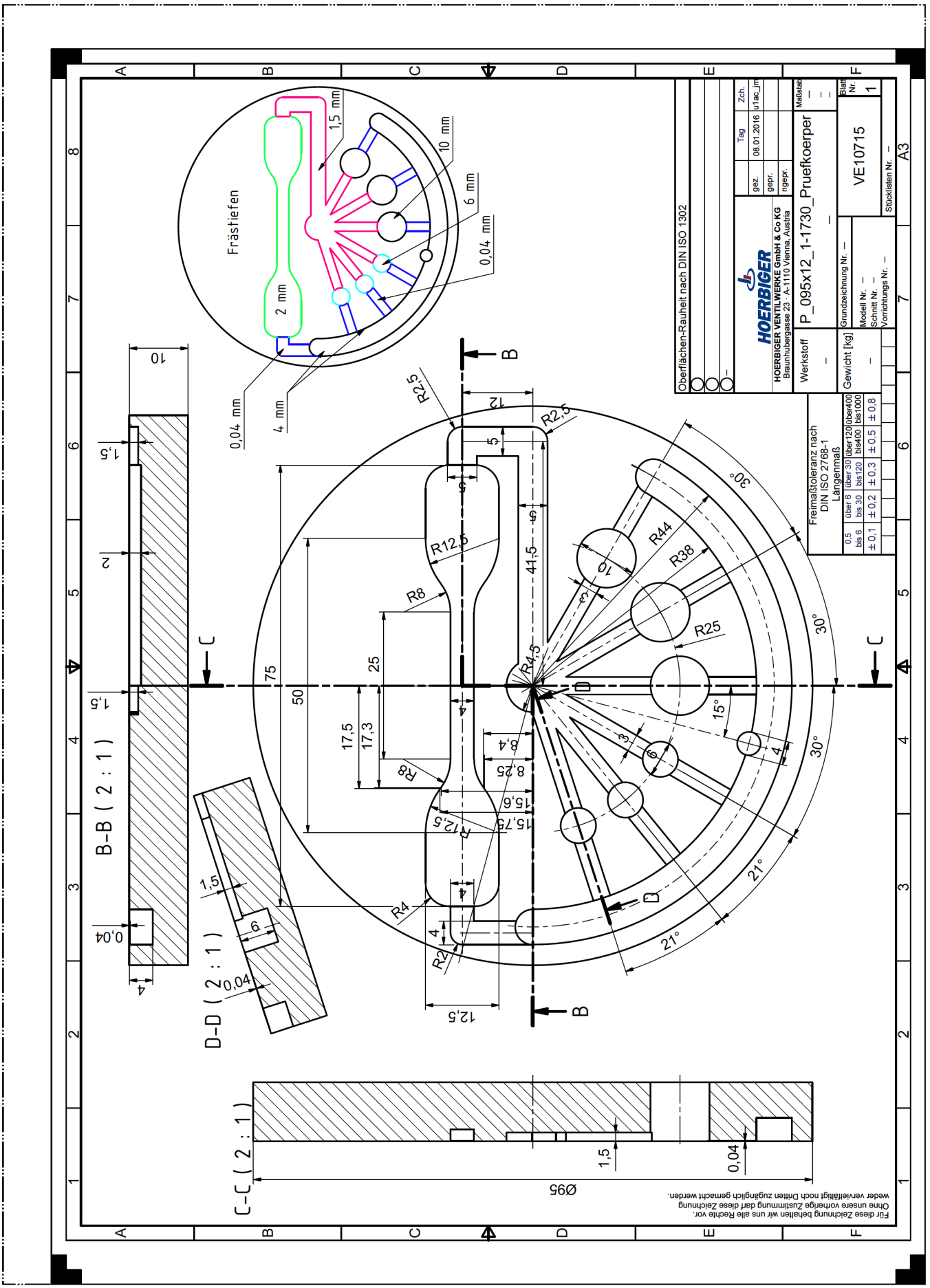
Frästiefen
1,5 mm
10 mm
6 mm
0,04 mm
2 mm
0,04 mm
4 mm
B-B (2 : 1)
D-D (2 : 1)
C-C (2 : 1)
Ø95
R2,5
R12,5
R8
R4,5
R44
R38
R25
R4
R2
30°
21°
15°
HOERBIGER VENTILWERKE GmbH & Co KG
Braunhubergasse 23 · A-1110 Vienna, Austria
P_095x12_1-1730_Pruefkoerper
VE10715
Oberflächen-Rauheit nach DIN ISO 1302
Freimaßtoleranz nach DIN ISO 2768-1 Längenmaß
Für diese Zeichnung behalten wir uns alle Rechte vor.
Ohne unsere vorherige Zustimmung darf diese Zeichnung weder vervielfältigt noch Dritten zugänglich gemacht werden.

7.7 Drawings of new prototypes

Drawing of tangential cut wiper concept

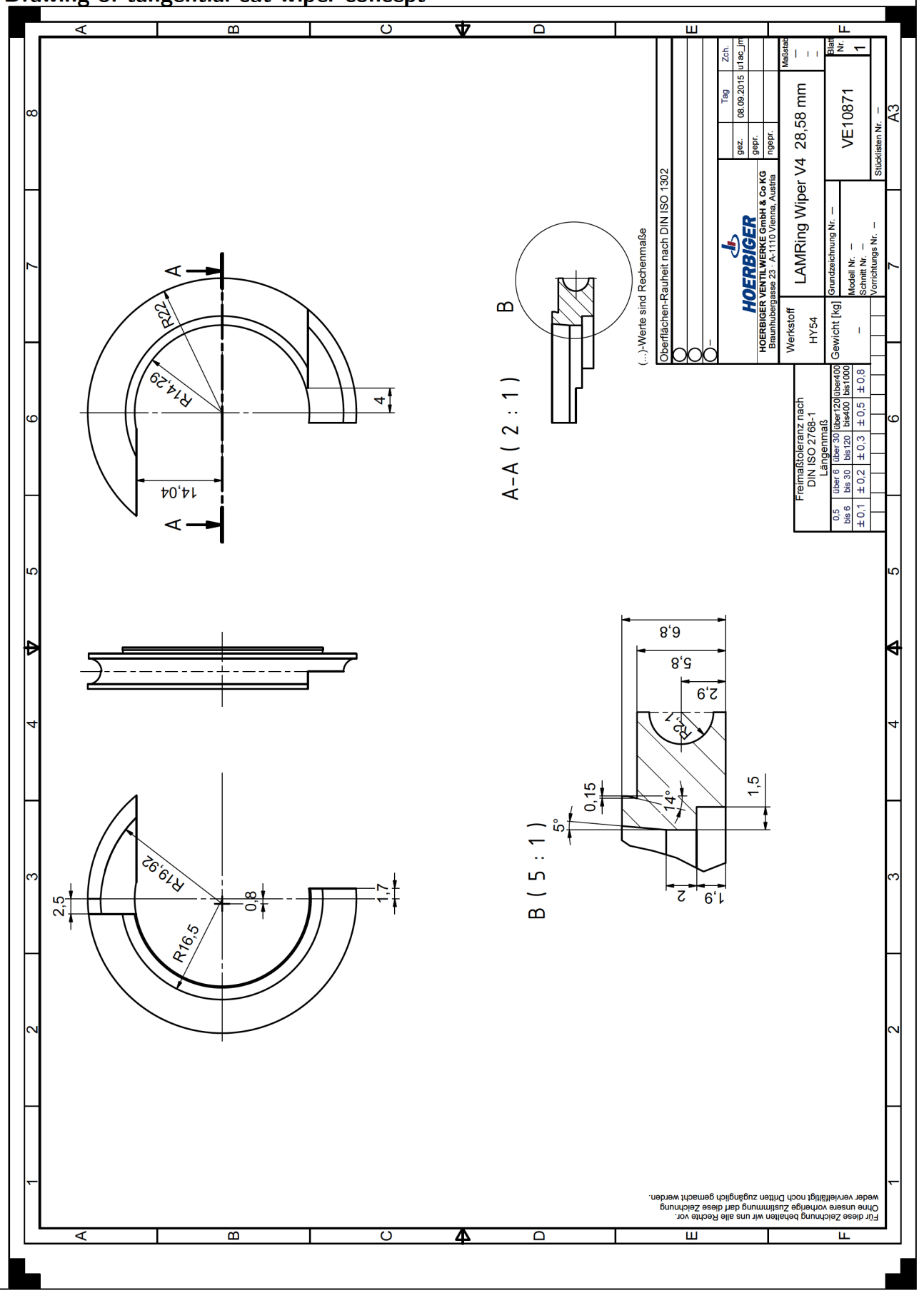

Drawing of gas tight cut wiper concept

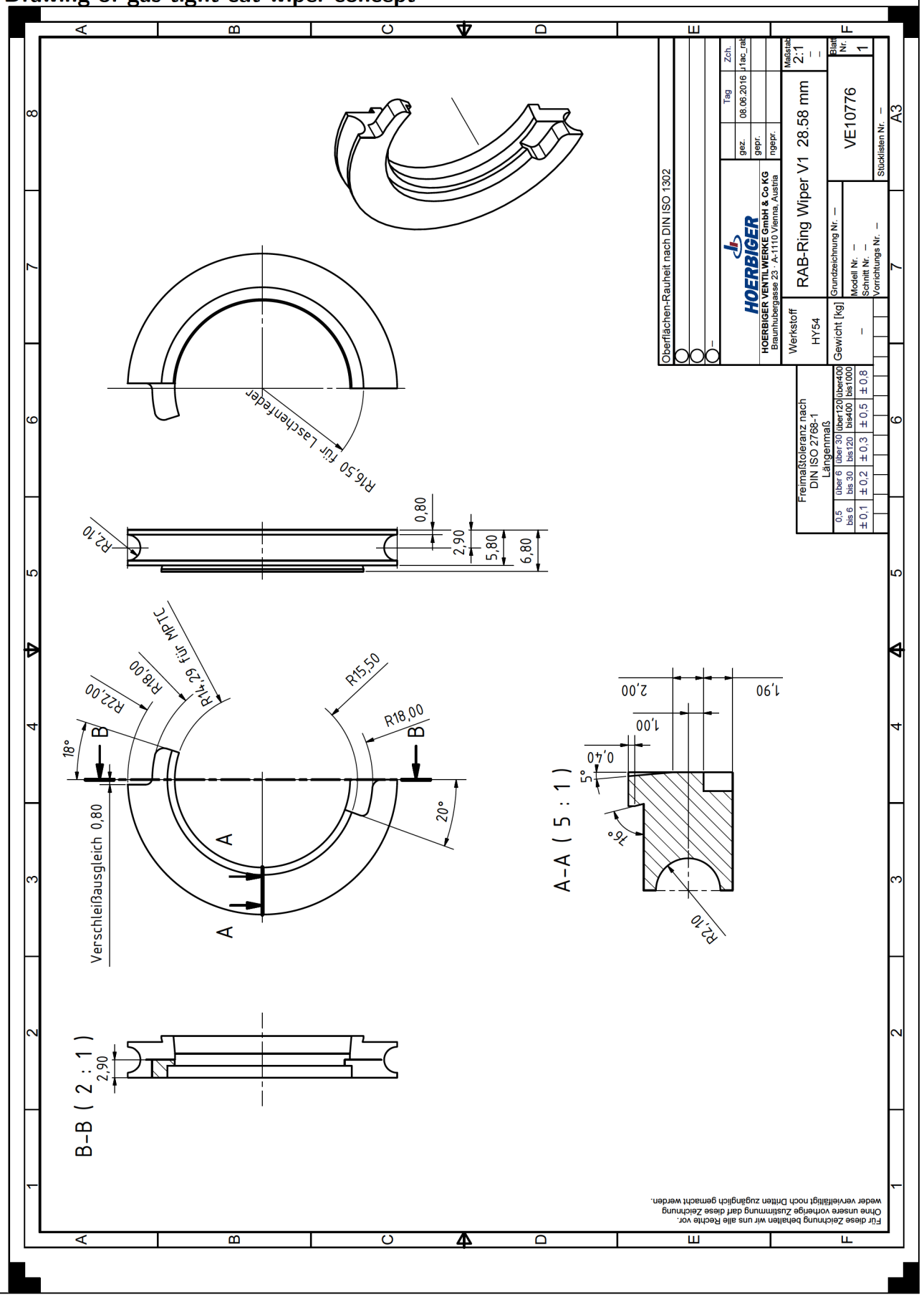

Drawing of radial wiper concept with additional wiping edge

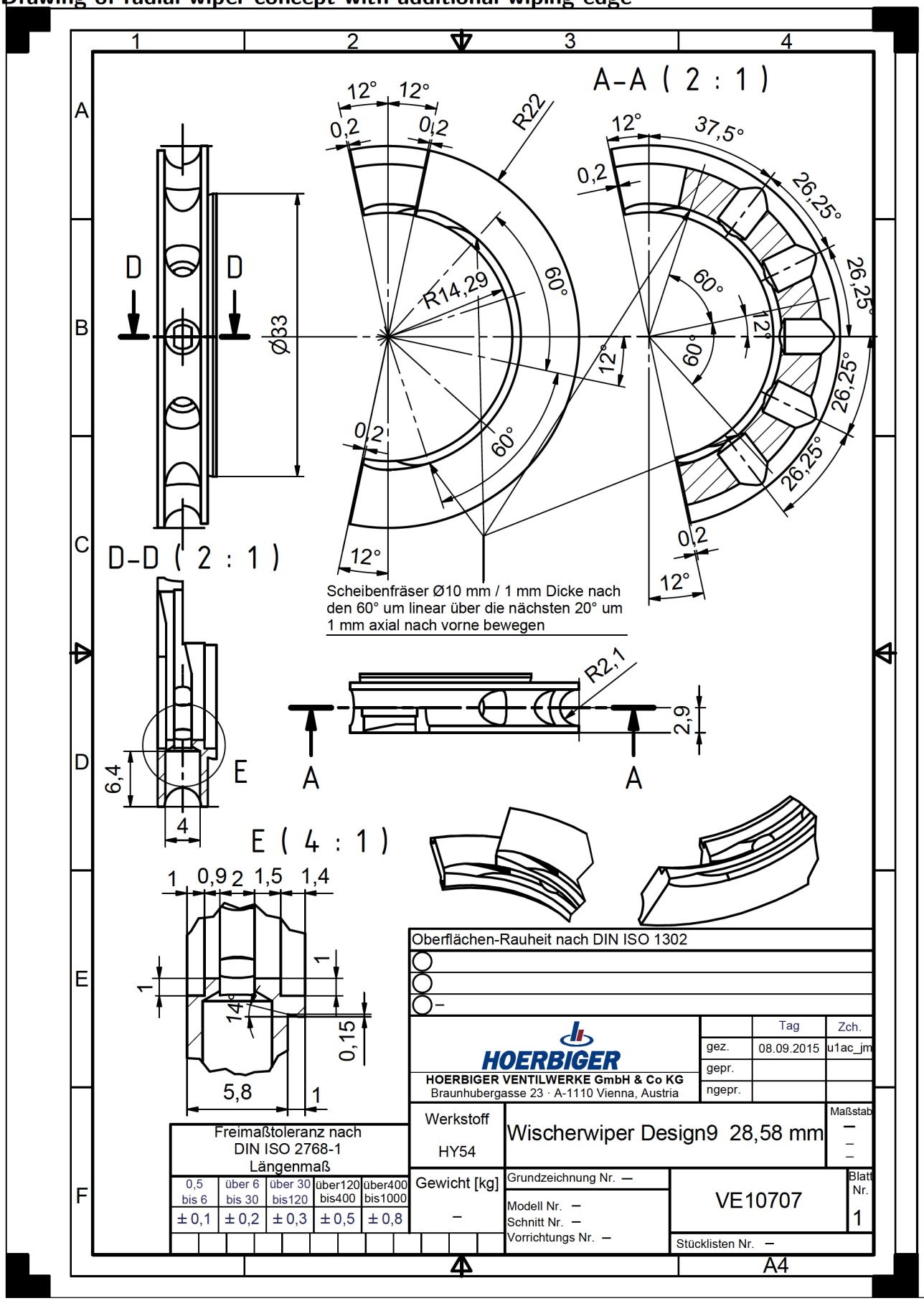

Drawing of radial cut concept with multiple wiping edges

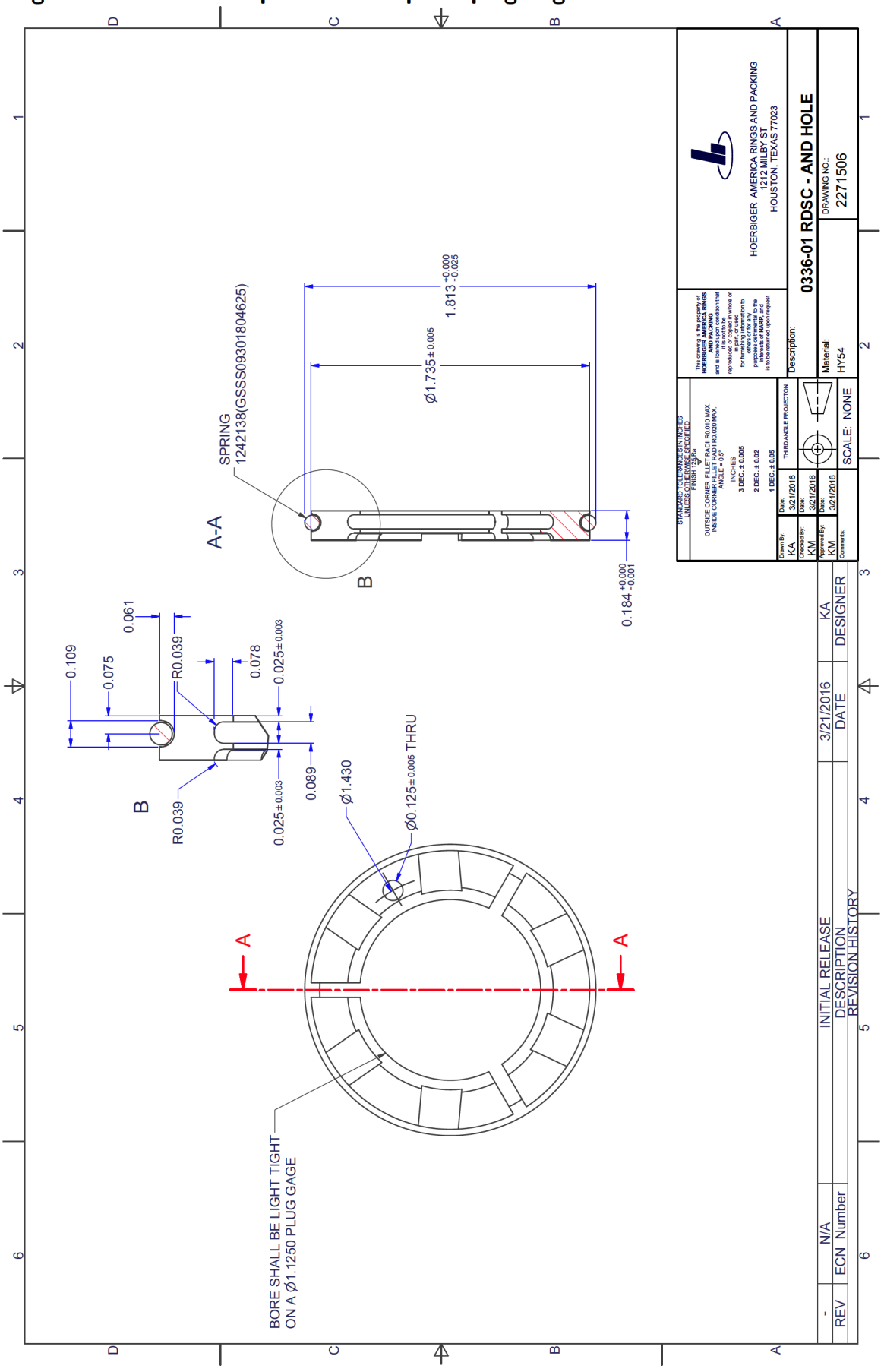

Drawing of uncut wiper concept

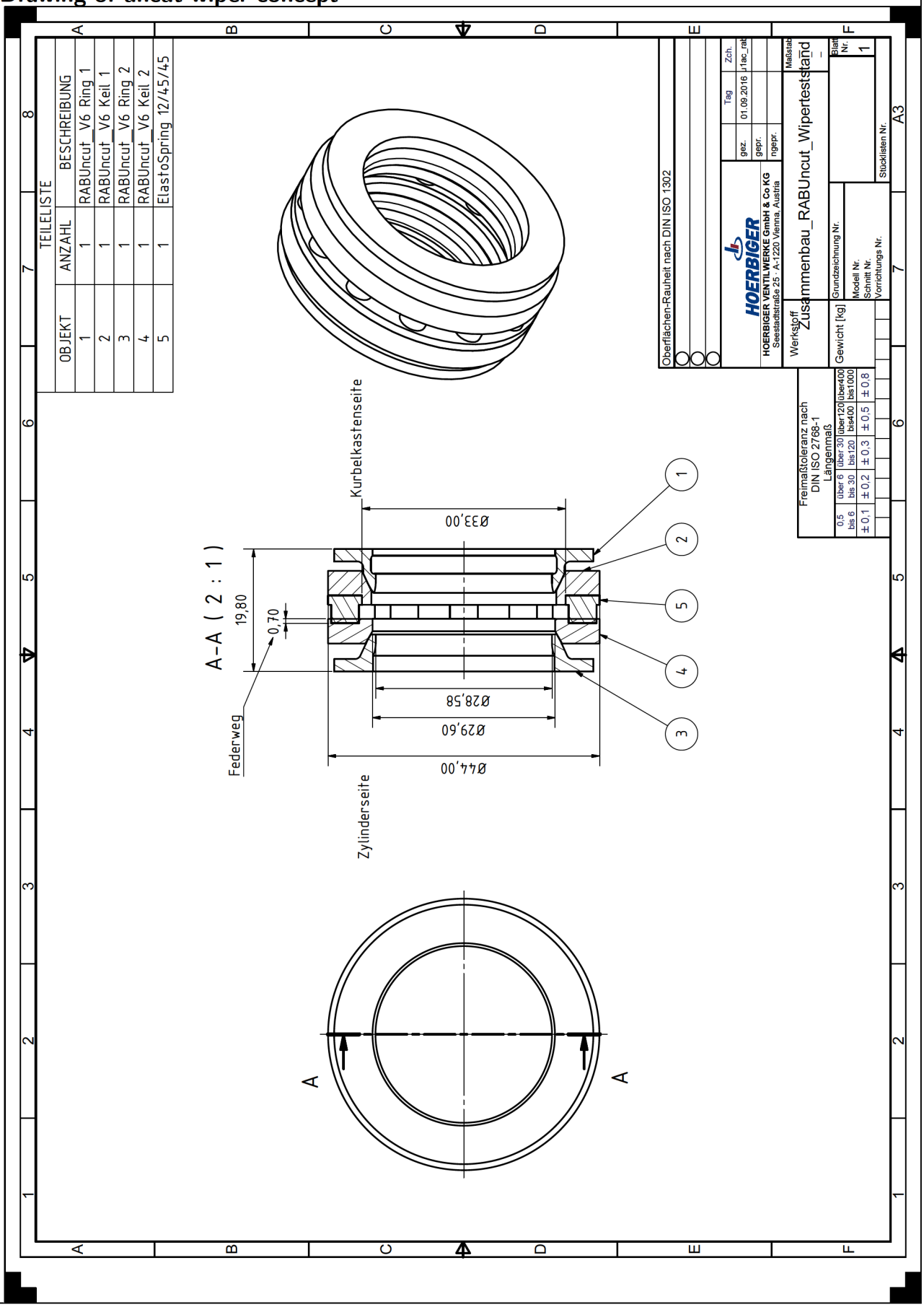

7.8 Data sheets

Ideas and solutions in rubber compounding

KRAIBURG

TECHNISCHES DATENBLATT
TECHNICAL DATA SHEET

Mischung	***Compound:***	**VT6AHZ**			
Basispolymer, Farbe	***Base polymer, colour***	**HNBR, schwarz *(black)***			
Vulkanisationsbed.	*Vulcanisation conditions*	Probekörper			
		Test specimen	Stab S2 *Dumbbell*	15 Min / min	170°C
Temperbedingungen	*Post curing conditions*			3 Std. / h	175°C
Prüfmerkmale	***Properties***		**Einheiten** ***Units***	**Soll – Werte** ***Desired val.***	**Ist – Werte** ***Actual value***
Reißfestigkeit	*Tensile strength*	DIN 53504	MPa		12,0
Reißdehnung	*Elongation at break*	DIN 53504	%		331
Härte	*Hardness*	DIN 53505	Shore A		62
Rückprallelastizität	*Rebound resilience*	DIN 53512	%		44
Weiterreißwiderstand	*Tear strength*	DIN ISO 34-1 A	N/mm		5,0
Dichte	*Specific gravity*	DIN 53479	g /cm^3		1,18
Druckverformungsrest	*Compression set* 24 h 150°C	DIN ISO 815	%		16,0
Beständigkeit gegen Heißluft	***Resistance against hot air***	**DIN 53508**		**Zeit : 7 Tage** ***Time: days***	**Temp.150 °C**
Reißfestigkeit	*Tensile strength*	DIN 53504	MPa		12,5
Reißdehnung	*Elongation at break*	DIN 53504	%		306
Härteänderung	*Hardness change*	DIN 53505	Shore A		+ 3
Rheologische Daten	***Rheological properties***				
Mooney-Viskosität (ML1+4; 100°C)	*Mooney viscosity (ML1+4; 100°C)*	DIN 53523	ME		87
Rheometer Monsanto 2000 E	Rheometer Monsanto 2000 E	DIN 53529		Zeit: 12 min Time: min	Temp.170°C
Drehmomentminimum	*Minimum torque*		dNm		2,10
t10	*t10*		min		1,30
t90	*t90*		min		9,20
Drehmomentmaximum	*Maximum torque*		dNm		15,20

Datum *Date:* *17.12.2015* *RS*

KRAIBURG GROUP
Gummiwerk KRAIBURG GmbH & Co. KG
Teplitzer Str. 20
84478 Waldkraiburg / Germany
Tel. + 49 (0) 8638 / 61- 0
Fax + 49 (0) 8638 / 61- 310
info@kraiburg.de
www.kraiburg-rubber-compounds.com
Handelsregister Traunstein HRA 8626
PhG.: Gummiwerk KRAIBURG Verwaltungs GmbH
Handelsregister Traunstein HRB 16108
Sitz Waldkraiburg, GF: Helmut Esefeld

Ideas and solutions in rubber compounding

KRAIBURG

Gummiwerk KRAIBURG GmbH & Co. KG - Teplitzer Str. 20 - D-84478 Waldkraiburg

HOERBIGER Ventilwerke GmbH & C
Braunhubergasse 23
1110 Wien
ÖSTERREICH

23.02.2016

ABNAHMEPRÜFZEUGNIS 3.1 nach EN 10204

Mischung: VT6AHZ

Auftrag: 754932 **Freigabe:** 23.02.2016
Lot-Nr.: 206433 **Ihre Best. Nr.:** JM/82830/RAT53230

Prüfmerkmal	Einheit	Mittel.	Std.abw.
Dichte, DIN EN ISO 1183-1	g/cm³	1,183	0,000
Härte Shore A, DIN ISO 7619-1	Shore A	60	0,00
Vulkametrie ML, DIN 53529	dNm	1,770	0,000
Vulkametrie T10, DIN 53529	Minuten	0,410	0,000
Vulkametrie T90, DIN 53529	Minuten	2,210	0,000
Vulkametrie MH, DIN 53529	dNm	16,710	0,000

Prüfparameter Rheometrie

Prüfzeit: 6 [Min]
Prüftemperatur: 190 [°C]

Prüflabor / Werksachverständiger

Diese Bescheinigung wurde durch ein EDV-System erstellt und ist ohne Unterschrift gültig. Die Daten des Berichts beziehen sich auf den Zustand direkt nach der Herstellung. Das Zertifikat entbindet den Käufer nicht von der Prüfung der erhaltenen Ware auf ihre Eignung und korrekte Qualität bezogen auf die spezifische Anwendung. Lager und Transportbedingungen können die Eigenschaften des Materials beeinflussen. Dieses Produkt ist nur für die Verarbeitung/Verwendung im gewerblichen Bereich vorgesehen.

Gummiwerk KRAIBURG
GmbH & Co. KG
Teplitzer Straße 20
D-84478 Waldkraiburg/Germany

Fon +49 (0) 8638 / 61-0
Fax +49 (0) 8638 / 61-310
info@kraiburg-rubber-compounds.com
www.kraiburg-rubber-compounds.com

Handelsregister Traunstein HRA 8626
PhG.: Gummiwerk KRAIBURG Verwaltungs GmbH
Handelsregister Traunstein HRB 16108
Sitz Waldkraiburg, GF: Helmut Esefeld

Ideas and solutions in rubber compounding

TECHNISCHES DATENBLATT
TECHNICAL DATA SHEET

Mischung	***Compound:***	**VA6BKZ**			
Basispolymer, Farbe	***Base polymer, colour***	**FPM, schwarz *(black)***			
Vulkanisationsbed.	*Vulcanisation conditions*	Probekörper			
		Test specimen	Stab S2 *Dumbbell*	15 Min / min	170°C
Temperbedingungen	*Post curing conditions*			6 Std. / h	225°C
Prüfmerkmale	***Properties***		**Einheiten** ***Units***	**Soll – Werte** ***Desired val.***	**Ist – Werte** ***Actual value***
Reißfestigkeit	*Tensile strength*	DIN 53504	MPa		9,9
Reißdehnung	*Elongation at break*	DIN 53504	%		283
Spannungswert 100%	*Modulus 100%*	DIN 53504	MPa		2,1
Härte	*Hardness*	DIN ISO 7619-1	Shore A		59
Rückprallelastizität	*Rebound resilience*	DIN 53512	%		6
Weiterreißwiderstand	*Tear strength*	DIN ISO 34-1 A	N/mm		4,7
Dichte	*Specific gravity*	DIN EN ISO 1183-1	g /cm^3		1,83
Druckverformungsrest	*Compression set* 24 h 175°C	DIN ISO 815	%		8,4
Beständigkeit gegen Heißluft	***Resistance against hot air***	**DIN 53508**		**Zeit : 7 Tage** ***Time: days***	**Temp.225 °C**
Reißfestigkeit	*Tensile strength*	DIN 53504	MPa		12,1
Reißdehnung	*Elongation at break*	DIN 53504	%		263
Härteänderung	*Hardness change*	DIN ISO 7619-1	Shore A		+3
Rheologische Daten	***Rheological properties***				
Mooney-Viskosität (ML1+4; 100°C)	*Mooney viscosity (ML1+4; 100°C)*	DIN 53523	ME		90
Rheometer Monsanto 2000 E	*Rheometer Monsanto 2000 E*	DIN 53529		Zeit: 6 min Time: min	Temp.180°C
Drehmomentminimum	*Minimum torque*		dNm		0,66
t10	*t10*		min		2,03
t90	*t90*		min		4,23
Drehmomentmaximum	*Maximum torque*		dNm		13,40

Datum *Date:* 23.08.2016 AT

KRAIBURG GROUP
Gummiwerk KRAIBURG GmbH & Co. KG
Teplitzer Str. 20
84478 Waldkraiburg / Germany
Tel. + 49 (0) 8638 / 61- 0
Fax + 49 (0) 8638 / 61- 310
info@kraiburg.de
www.kraiburg-rubber-compounds.com
Handelsregister Traunstein HRA 8626
PhG.: Gummiwerk KRAIBURG Verwaltungs GmbH
Handelsregister Traunstein HRB 16108
Sitz Waldkraiburg, GF: Helmut Esefeld

Ideas and solutions in rubber compounding

KRAIBURG

Gummiwerk KRAIBURG GmbH & Co. KG - Teplitzer Str. 20 - D-84478 Waldkraiburg

HOERBIGER Ventilwerke GmbH & C
Braunhubergasse 23
1110 Wien
ÖSTERREICH

23.02.2016

ABNAHMEPRÜFZEUGNIS 3.1 nach EN 10204

Mischung: VA6BKZ

Auftrag: 754932 **Freigabe:** 23.02.2016
Lot-Nr.: 206491 **Ihre Best. Nr.:** JM/82830/RAT53230

Prüfmerkmal	Einheit	Mittel.	Std.abw.
Dichte, DIN EN ISO 1183-1	g/cm³	1,821	0,000
Härte Shore A, DIN ISO 7619-1	Shore A	59	0,00
Vulkametrie ML, DIN 53529	dNm	0,820	0,000
Vulkametrie T10, DIN 53529	Minuten	2,110	0,000
Vulkametrie T90, DIN 53529	Minuten	4,230	0,000
Vulkametrie MH, DIN 53529	dNm	14,490	0,000

Prüfparameter Rheometrie

Prüfzeit: 6 [Min]
Prüftemperatur: 180 [°C]

Prüflabor / Werksachverständiger

Diese Bescheinigung wurde durch ein EDV-System erstellt und ist ohne Unterschrift gültig. Die Daten des Berichts beziehen sich auf den Zustand direkt nach der Herstellung. Das Zertifikat entbindet den Käufer nicht von der Prüfung der erhaltenen Ware auf ihre Eignung und korrekte Qualität bezogen auf die spezifische Anwendung. Lager und Transportbedingungen können die Eigenschaften des Materials beeinflussen. Dieses Produkt ist nur für die Verarbeitung/Verwendung im gewerblichen Bereich vorgesehen.

Gummiwerk KRAIBURG
GmbH & Co. KG
Teplitzer Straße 20
D-84478 Waldkraiburg/Germany

Fon +49 (0) 8638 / 61-0
Fax +49 (0) 8638 / 61-310
info@kraiburg-rubber-compounds.com
www.kraiburg-rubber-compounds.com

Handelsregister Traunstein HRA 8626
PhG.: Gummiwerk KRAIBURG Verwaltungs GmbH
Handelsregister Traunstein HRB 16108
Sitz Waldkraiburg, GF: Helmut Esefeld